Universiteit Antwerpen

Faculteit Wetenschappen

Departement Natuurkunde
Theorie van Quantum Systemen en Complexe Systemen

Ultracold Gases as a Quantum Simulator for the Polaron

Ultrakoude Gassen als een Kwantum Simulator voor het Polaron

Proefschrift voorgelegd tot het behalen van de graad van doctor in de wetenschappen: fysica aan de Universiteit Antwerpen te verdedigen door Wim Casteels.

Promotors: prof. dr. J. Tempère and prof. dr. J. T. Devreese
Antwerpen, April 22, 2013

Ph.D. Jury:

- Prof. dr. J. Tempere (Universiteit Antwerpen).
- Prof. dr. J. T. Devreese (Universiteit Antwerpen).
- Prof. dr. S. Van Doorslaer (Universiteit Antwerpen).
- Prof. dr. D. Lamoen (Universiteit Antwerpen).
- Prof. dr. B. Partoens (Universiteit Antwerpen)
- Prof. dr. E. Timmermans (Los Alamos National Laboratory, New Mexico, U.S.A.).
- Prof. Dr. J. Ryckebusch (Universiteit Gent, Belgium).

Acknowledgements:

This work is supported financially by the BOF-UA, the FWO-V under projects No. G.0180.09N, No. G.0115.06, No. G.0356.06, No. G.0370.09N, and No. G.0119.12N and the WOG Belgium under project No. WO.033.09N. Discussions with A. Widera, M. Oberthaler, E. Timmermans, J. Ryckebusch, T. Van Cauteren, S. Knoop, J. Hecker-Denschlag, M. Wouters, N. Spethmann, K. Van Houcke, F. Kindermann and J. Vlietinck are gratefully acknowledged. Also the artwork of visual artist Kasper De Vos titled "De Fysikus" for the cover of this thesis is much appreciated.

Contents

Chapter 1

Introduction

The work presented in this thesis is situated at the intersection of two communities in modern physics: solid state physics and ultracold atomic gases. The basic idea dates back to a paper of Feynman in 1982 where he introduced the notion of a universal quantum simulator [1]. He speculated on the design of a machine that is governed by the laws of quantum mechanics and that can be used to simulate other quantum systems. Nowadays ultracold gases have repeatedly revealed themselves as successful quantum simulators of many-body theories that were developed in the context of solid state physics [2].

We will consider a specific condensed matter system that can be quantum simulated with ultracold gases: the Fröhlich polaron. The main scheme is to apply the well-established theoretical methods from solid state physics to the context of ultracold gases. Hopefully in the end this mechanism can be reversed, allowing us to learn more about the solid state polaron from experiments on ultracold gases. We start with a short introduction to the relevant concepts from the two fields. Then we show how these two fields can merge together which shall bring us to the main topic of this thesis: the polaron consisting of an impurity atom in a Bose-Einstein condensate.

1.1 Ultracold gases and Bose-Einstein condensation*

One of the most intriguing phenomena related to ultracold gases is Bose-Einstein condensation. The idea dates back to a paper of Einstein in 1924 [6] where he generalized a result of Bose [7] concerning the quantum statistics of a gas of identically, non-interacting bosons. In this paper a phase transition was predicted when the gas is cooled below a critical temperature. This transition corresponds to the occupation of a single quantum state by a macroscopic fraction of the bosons. Because the required temperatures are very low (typically $1 - 100$ nK) it took until 1995 for the development of the advanced experimental techniques needed for the first experimental realization in atomic gases [8–10]. In Fig. 1.1 the velocity distribution

*We refer the interested reader to standard textbooks as for example Refs. [3–5] for more details on the introduced concepts related to ultracold atomic gases.

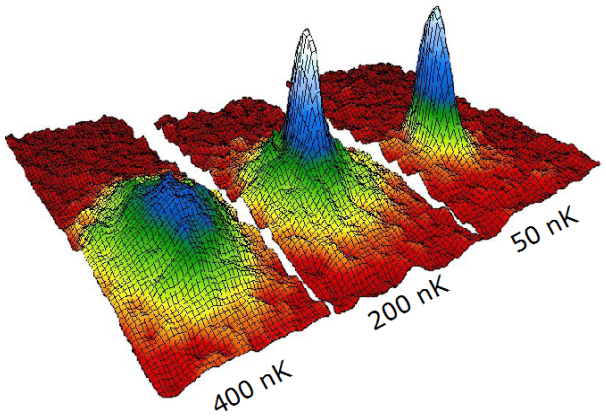

Figure 1.1: The velocity distribution of Rb atoms at different temperatures. The atoms exhibit a Maxwell distribution at 400 nK but at 200 nK a macroscopic fraction of the atoms occupies the state corresponding to velocity zero and at 50 nK nearly all atoms are in this state. (The data corresponds to the experiment of Ref. [8].)

is presented of a gas of Rb atoms at different temperatures which shows the phase transition to a Bose-Einstein condensate.

After the first realization of a Bose-Einstein condensate many other experiments followed which resulted in the application of these systems as quantum simulators for many-body theories [2]. There are multiple advantages of using ultracold gases for this purpose. The systems are for example highly controllable, which is in stark contrast with typical solid state systems where one has to deal with the undesirable effects of defects, impurities, dislocations and other irregularities. Also many properties of the experimental system are externally tunable such as the atom density, the interparticle interactions and the geometry of the system.

1.1.1 Interatomic interactions and Feshbach resonances

Since ultracold gases are typically very dilute (atomic densities are of the order $10^{13} - 10^{15}/\mathrm{cm}^3$) it is usually sufficient to consider only two-body interactions. As the typical temperatures are very low s-wave scattering theory is applicable. The interatomic interactions can then be approximated by s-wave contact interactions for which the interatomic potential is given by:

$$V\left(\vec{r}_1 - \vec{r}_2\right) = g\delta\left(\vec{r}_1 - \vec{r}_2\right), \tag{1.1}$$

with $\vec{r}_1$ and $\vec{r}_2$ the position vectors of the atoms and g the interaction strength. The Lippmann-Schwinger equation gives a relation between the interaction strength g and the scattering matrix $T\left(E\right)$, with E the kinetic energy of the scattering event. Up to second order in g the Lippmann-Schwinger equation can be written as:

$$T\left(E\right) = g + g^2 \sum_{\vec{k}} \frac{1}{E - \frac{\left(\hbar\vec{k}\right)^2}{2m_r}}, \tag{1.2}$$

where m_r is the reduced mass. The Born approximation corresponds to retaining only the first term of the right-hand side of (1.2). In 3 dimensions the scattering

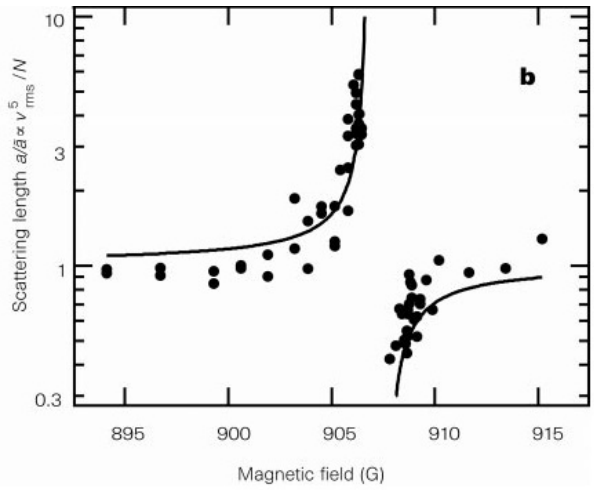

Figure 1.2: Feshbach resonance of the scattering length of Na atoms as a function of an external magnetic field. The dots are the experimental points and the solid line is equation (1.5). (From Ref. [11].)

matrix is independent of E and given by:

$$T = \frac{2\pi\hbar^2 a}{m_r V}, \tag{1.3}$$

with a the scattering length which is an experimentally measurable quantity and V the volume. Taking the low energy limit $E \to 0$ of Eq. (1.2) in 3 dimensions results in:

$$\frac{2\pi\hbar^2 a}{m_r V} = g - g^2 \sum_{\vec{k}} \frac{2m_r}{(\hbar k)^2}. \tag{1.4}$$

If an external magnetic field with strength B is considered, the scattering length can exhibit a resonant behavior as a function of B. The physical origin of these resonances is a coupling between the channel of the incident particles and a channel with a quasi-stationary bound state. If the magnetic moment of the bound state is different from the magnetic moment of the colliding atoms the energy difference can be tuned with a magnetic field. This results in a resonance of the scattering length as a function of B of the form:

$$a = a_{\mathrm{bg}} \left(1 + \frac{\Delta B}{B - B_0} \right), \tag{1.5}$$

with a_{bg} the background scattering length, ΔB the width of the resonance and B_0 the location of the resonance. In Fig. 1.2 a measurement is presented of a Feshbach resonance in a gas of Na atoms [11]. Nowadays Feshbach resonances are considered a standard tool in experiments to tune the strength of the interatomic interactions.

1.1.2 Optical potentials

Another powerful tool in the context of ultracold gases relies on the interaction of atoms with light. If atoms are irradiated with a non-resonant laser the oscillating

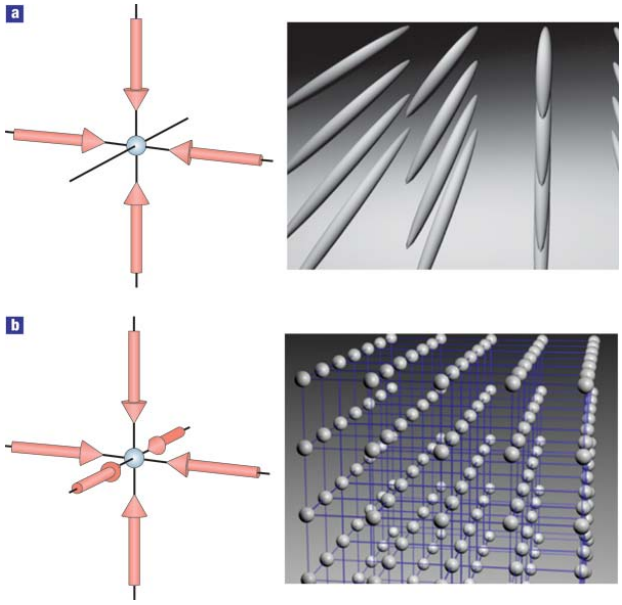

Figure 1.3: Optical lattice potentials formed by superimposing two or three orthogonal standing waves. (a) For a 2D optical lattice, the atoms are confined to an array of tightly confining 1D potential tubes. (b) In the 3D case, the optical lattice can be approximated by a 3D simple cubic array of tightly confining harmonic oscillator potentials at each lattice site. (From Ref. [12].)

electric field induces a dipole moment. The interaction between the electric field and the induced dipole leads to an effective potential for the atoms, commonly known as an optical potential. If multiple laser beams interfere to form standing waves one, two and three dimensional periodic potentials can be created, which are denoted as "optical lattices" [12] (see Fig. 1.3 for a schematic presentation of optical lattice potentials). This can be used to create effectively low-dimensional systems. The system is then confined in one, two or three directions with a confinement length that is much smaller than all other length scales. These systems can be described by a low-dimensional theory with effective interaction strengths that depend on the confinement length. This allows tuning of the effective interaction strength by varying the confinement strength which results in confinement-induced resonances that have been studied theoretically [13–17] and experimentally [18–22].

1.1.3 Bogoliubov approximation

We now discuss the Bogoliubov approximation which is used for the microscopic description of Bose-Einstein condensates. The Hamiltonian of an interacting Bose gas is given by:

$$\widehat{H} = \sum_{\vec{k}} E_{\vec{k}} \widehat{b}^{\dagger}_{\vec{k}} \widehat{b}_{\vec{k}} + \frac{1}{2} \sum_{\vec{k},\vec{k}',\vec{q}} V_{BB}\left(\vec{q}\right) \widehat{b}^{\dagger}_{\vec{k}'-\vec{q}} \widehat{b}^{\dagger}_{\vec{k}+\vec{q}} \widehat{b}_{\vec{k}} \widehat{b}_{\vec{k}'}. \tag{1.6}$$

The operators $\widehat{b}^{\dagger}_{\vec{k}}$, $\widehat{b}_{\vec{k}}$ create, resp. annihilate, a boson with mass m_B, wave number $\vec{k}$, and energy $E_{\vec{k}} = \left(\hbar k\right)^2 / 2m_B - \mu$ where μ is the chemical potential. These

bosons interact, and $V_{BB}(\vec{q})$ is the Fourier transform of the boson-boson interaction potential for which a contact interaction is assumed. This interaction is treated within the Born approximation so that the interaction strength g_{BB} is given by $g_{BB} = 4\pi\hbar^2 a_{BB}/m_B$, with a_{BB} the scattering length.

Within the number representation the creation and annihilation operators act as follows:

$$\widehat{b}^{\dagger}_{\vec{k}} \left|...N_{\vec{k}}...\right\rangle = \sqrt{N_{\vec{k}}+1}\left|...N_{\vec{k}}+1...\right\rangle; \tag{1.7}$$

$$\widehat{b}_{\vec{k}} \left|...N_{\vec{k}}...\right\rangle = \sqrt{N_{\vec{k}}}\left|...N_{\vec{k}}-1...\right\rangle; \tag{1.8}$$

where $N_{\vec{k}}$ denotes the number of bosons with wave number $\vec{k}$. Since we want to consider a Bose Einstein condensate, in which a macroscopic number of bosons occupy the ground state [23], and thus $N_0 \gg 1$, we can use the following approximation:

$$\widehat{b}^{\dagger}_0 \left|N_0...\right\rangle = \sqrt{N_0+1}\left|N_0+1...\right\rangle \approx \sqrt{N_0}\left|N_0...\right\rangle; \tag{1.9}$$

$$\widehat{b}_0 \left|N_0...\right\rangle = \sqrt{N_0}\left|N_0-1...\right\rangle \approx \sqrt{N_0}\left|N_0...\right\rangle. \tag{1.10}$$

Furthermore, compared with $\widehat{b}^{\dagger}_0$ and $\widehat{b}_0$, the action of the creation and annihilation operators for $\vec{k} \neq 0$ is weak ($N_0 \gg N_{\vec{k}}\ \forall \vec{k} \neq 0$). The Bogoliubov approximation amounts for a homogeneous condensate to replacing the operators $\widehat{b}^{\dagger}_0$ and $\widehat{b}_0$ by the number $\sqrt{N_0}$ and keeping only terms up to quadratic order in $\widehat{b}^{\dagger}_{\vec{k}\neq 0}$ or $\widehat{b}_{\vec{k}\neq 0}$. The resulting Hamiltonian is then diagonalized by means of a Bogoliubov transformation [24] (for $\vec{k} \neq 0$):

$$\widehat{b}_{\vec{k}} = u_{\vec{k}}\widehat{\alpha}_{\vec{k}} - v_{\vec{k}}\widehat{\alpha}^{\dagger}_{-\vec{k}}, \tag{1.11}$$

with the functions u_k and v_k given by [25]:

$$u_{\vec{k}} = \frac{1}{2}\left(\sqrt{\frac{E_{\vec{k}}}{\hbar\omega_{\vec{k}}}} + \sqrt{\frac{\hbar\omega_{\vec{k}}}{E_{\vec{k}}}}\right); \tag{1.12}$$

$$v_{\vec{k}} = \frac{1}{2}\left(\sqrt{\frac{\hbar\omega_{\vec{k}}}{E_{\vec{k}}}} - \sqrt{\frac{E_{\vec{k}}}{\hbar\omega_{\vec{k}}}}\right). \tag{1.13}$$

The resulting Hamiltonian, describing a Bose Einstein condensate, is given by:

$$\widehat{H}_{BEC} = E_{GP} + \sum_{\vec{k}\neq 0} \hbar\omega_{\vec{k}}\widehat{\alpha}^{\dagger}_{\vec{k}}\widehat{\alpha}_{\vec{k}}. \tag{1.14}$$

Here, the operators $\widehat{\alpha}^{\dagger}_{\vec{k}}$, $\widehat{\alpha}_{\vec{k}}$ create respectively annihilate a Bogoliubov excitation with wave number $\vec{k}$ and dispersion

$$\omega_{\vec{k}} = \frac{\hbar k}{2m_B\xi}\sqrt{(\xi k)^2 + 2}, \tag{1.15}$$

where $\xi = 1/\sqrt{8\pi a_{BB}N_0/V}$ is the healing length of the condensate, with V the volume. The first term in (1.14) represents the Gross-Pitaevskii energy of the homogeneous condensate [4]:

$$E_{GP} = N_0 E_0 + \frac{N_0^2 g_{BB}}{2} + \frac{1}{2}\sum_{\vec{k}\neq 0} N_0 g_{BB}. \tag{1.16}$$

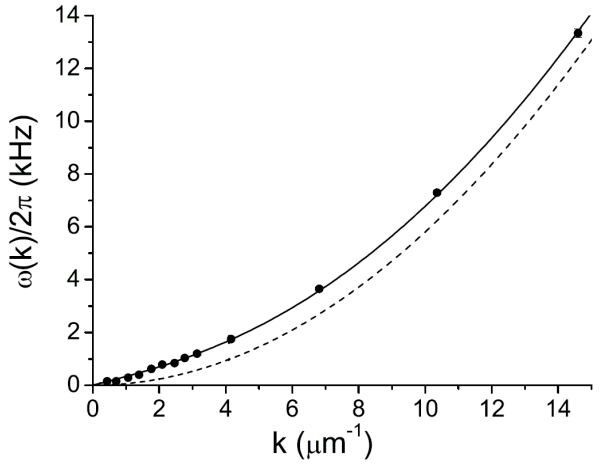

Figure 1.4: The dots give the results of a measurement with Bragg scattering of the excitation spectrum of a Bose-Einstein condensate, the solid line gives the Bogoliubov dispersion (1.15) and the dashed line is the parabolic free particle spectrum. (from Ref. [26].)

This shows that the elementary excitations of a Bose-Einstein condensate are the Bogoliubov excitations described by the Bogoliubov dispersion (1.15). For small k the spectrum is sound-like and for large k it behaves particle-like. In Fig. 1.4 the Bogoliubov dispersion (1.15) is presented together with a measurement of the excitation spectrum of a Bose-Einstein condensate of Rb atoms [26].

1.2 Fröhlich solid state polaron[†]

In the context of solid state physics the polaron describes an electron in an ionic or polar lattice. Because of the negative charge of the electron it will attract the positively charged ions and repel the negatively charged ions (schematically presented in Fig. 1.5). In 1933 the name polaron was coined by Landau [31] for the quasiparticle that consists of the electron together with the surrounding polarization cloud. A distortion of the lattice can be described in terms of lattice vibrations or phonons and in 1954 the polaron Hamiltonian $\widehat{H}_{pol}$ for an electron in a continuum polarizable medium was derived by Fröhlich [32]:

$$\widehat{H}_{pol} = \frac{\widehat{\vec{p}}^{\,2}}{2m} + \sum_{\vec{k}} \hbar\omega_{\vec{k}} \widehat{a}^{\dagger}_{\vec{k}} \widehat{a}_{\vec{k}} + \sum_{\vec{k}} V_{\vec{k}} e^{i\vec{k}.\widehat{\vec{r}}} \left(\widehat{a}_{\vec{k}} + \widehat{a}^{\dagger}_{-\vec{k}} \right). \tag{1.17}$$

This Hamiltonian is suited to describe a large polaron of which the wave function and the corresponding lattice distortion spread over many lattice sites. Because of this the terms large polaron, continuum polaron and Fröhlich polaron are often used interchangeably. The first term represents the kinetic energy of the electron with mass m and momentum (position) operator $\widehat{\vec{p}}$ ($\widehat{\vec{r}}$). The second term gives the energy of the phonons with dispersion $\omega_{\overrightarrow{k}}$ and $\widehat{a}^{\dagger}_{\overrightarrow{k}}$, $\widehat{a}_{\overrightarrow{k}}$ the creation, resp. annihilation,

[†]The interested reader is refered to Refs. [27–29] for more details.

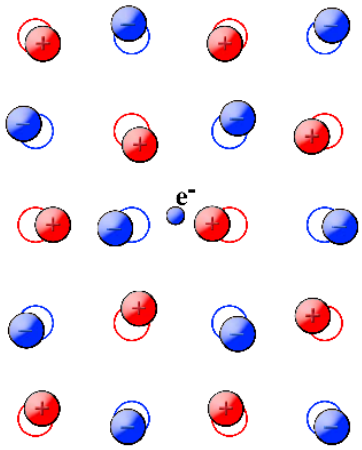

Figure 1.5: Schematic picture of an electron in a charged lattice. Because of the Coulomb interaction the positively charged ions are attracted by the electron while the negatively charged ones are repelled. The polaron is the quasiparticle consisting of the electron and a cloud of lattice distortion. (from Ref. [30].)

operator. The last term represents the polaronic interaction between the electron and the phonons with $V_{\vec{k}}$ the interaction amplitude. For an electron interacting with optical phonons the phonon dispersion $\omega_{\vec{k}}$ and the Fröhlich interaction amplitude $V_{\vec{k}}$ are given by:

$$\omega_{\vec{k}} = \omega_{LO}; \tag{1.18}$$

$$V_{\vec{k}} = -i\frac{\hbar\omega_{LO}}{k}\left(\frac{4\pi\alpha}{V}\right)^{1/2}\left(\frac{\hbar}{2m\omega_{LO}}\right)^{1/4}. \tag{1.19}$$

Here ω_{LO} is used to denote the long-wavelength longitudinal optical phonon frequency and α is the dimensionless polaronic coupling constant:

$$\alpha = \frac{e^2}{\hbar}\sqrt{\frac{m}{2\hbar\omega_{LO}}}\left(\frac{1}{\varepsilon_\infty}-\frac{1}{\varepsilon_0}\right), \tag{1.20}$$

where ε_∞ is the electronic and ε_0 is the static dielectric constant of the polar crystal.

If the dispersion $\omega_{\vec{k}}$ and the interaction amplitude $V_{\vec{k}}$ are kept general, the Hamiltonian (1.17) describes a generic polaron which consists of a particle of mass m, coupled to a bath of bosons with dispersion $\omega_{\vec{k}}$ through the polaronic interaction with amplitude $V_{\vec{k}}$. So far we considered an electron interacting with optical phonons, commonly known as the optical Fröhlich polaron (in this thesis it is denoted as the solid state polaron). The polaron Hamiltonian (1.17) can also be used to describe an electron interacting with acoustical phonons which is known as the acoustopolaron or piezopolaron [33, 34]. Other examples are the ripplopolaron which consists of an electron on a helium film where the role of the phonons is played by the helium surface waves or ripplons [35–40], the plasmaron in which case the phonons are replaced by the plasmons [41–48] and the electronic polaron which describes the interaction with excitons [49–51].

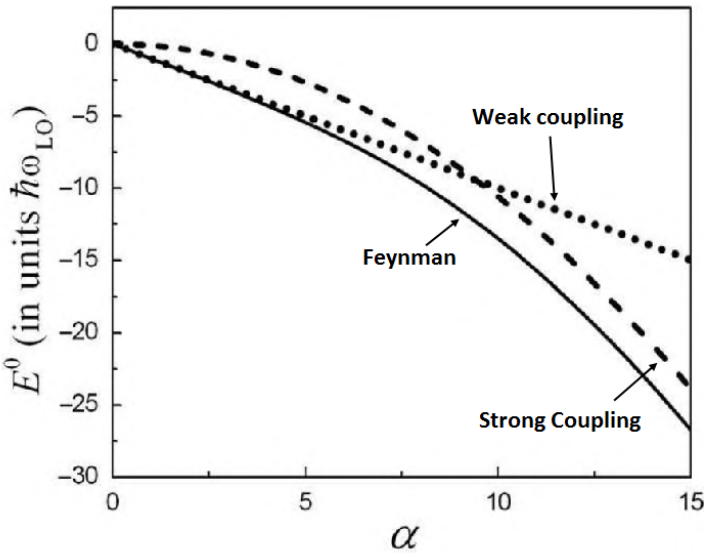

Figure 1.6: The Fröhlich polaron internal energy as a function of the coupling parameter α (1.20) as calculated with the weak coupling formalism, the strong coupling formalism and the Feynman formalism. Note that the Feynman result nicely interpolates between the weak coupling result and the strong coupling result. (from Ref. [27].)

The Fröhlich Hamiltonian (1.17) has resisted analytical diagonalization which made it the subject of many approximation methods developed in the context of many-particle physics. Considering the ground state properties as a function of the coupling parameter α different coupling regimes can be identified. The weak coupling regime ($\alpha \ll 1$) was examined with perturbation theory by Fröhlich [32] and an alternative derivation, based on a canonical transformation, was presented by Lee, Low and Pines [52]. The strong coupling regime ($\alpha \gg 1$) was examined by Bogolubov and Tyablikov with a canonical transformation [53] and by Landau and Pekar with the "displaced phonon operators" [54]. Both formalisms apply a product Ansatz and the variational principle which results in the prediction of a bound state of the electron in the self-induced potential at strong coupling. Feynman developed a superior all-coupling polaron theory using his path integral formalism and the Jensen-Feynman inequality [55]. In Fig. 1.6 a comparison is presented of the polaron internal energy as calculated with these three formalisms as a function of α. This shows that the upper bound as calculated by Feynman nicely interpolates between the results at weak and at strong coupling. In Refs. [56, 57] an exact diagrammatic Monte Carlo technique was developed which is also valid at all coupling and is in good agreement with the Feynman results.

The polaron dynamic response properties have been studied by considering the optical absorption. A perturbative calculation of the optical absorption, valid at weak coupling, was presented by Gurevich, Lang and Firsov [58]. An extension of the strong coupling groundstate treatment to the optical absorption was presented by Kartheuser, Evrard and Devreese [59]. The all-coupling approximation of Feynman was expanded by Feynman, Hellwarth, Iddings and Platzman to derive an expression

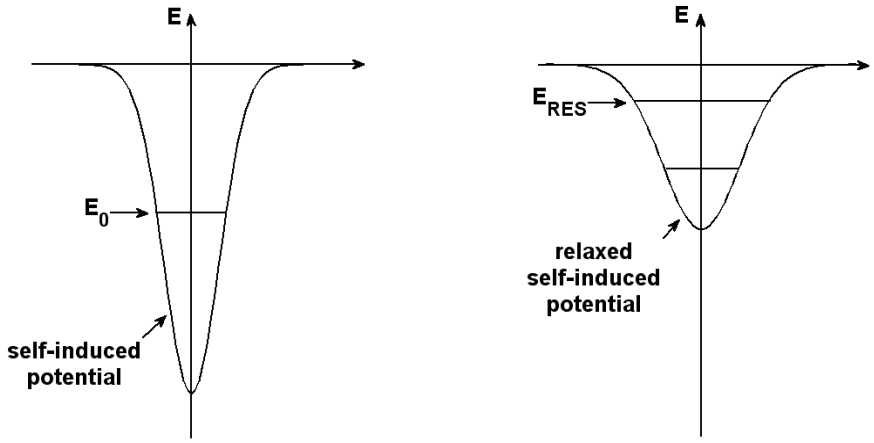

Figure 1.7: Structure of the energy spectrum of a polaron at strong coupling: E_0 is the ground state energy and E_{RES} the energy of the (first) relaxed excited state.

for the polaron mobility [60]. This result was generalised by Devreese, De Sitter and Goovaerts (DSG) to calculate the optical absorption at arbitrary polaronic coupling [61]. This confirmed the existence of the Relaxed Excited State (RES) at strong coupling which was previously predicted within the strong coupling formalism by Kartheuser, Evrard and Devreese in Ref. [59]. The RES corresponds to an excitation of the electron in the self-induced potential that has been adapted (or relaxed) to the new wave function of the electron (see Fig. 1.7 for a schematic picture of the RES). More recently the optical absorption was calculated with the diagrammatic Monte Carlo technique [62] which is compared with the DSG results of Ref. [61] in Fig. 1.8. This shows a good agreement at weak coupling but at intermediate and strong coupling discrepancies appear. In Ref. [61] it was noted that for $\alpha > 7$ the width of the RES-peak in the DSG result violates the Heisenberg uncertainty principle. This was resolved in Ref. [63] with the extended memory function formalism which empirically introduces dissipation. This results in a broader RES-peak and a better agreement with the diagrammatic Monte Carlo results at intermediate coupling. This however does not settle the discrepancies in the optical absorption at strong coupling which are resolved by a strong coupling approach by Klimin and Devreese [27]. This shows the need for a better understanding of the transition to the polaronic strong coupling regime. Furthermore, this could also shed light on the possible role of polaron and bipolarons for unconventional pairing mechanisms for high-temperature superconductivity [64–66].

The polaron has also been studied for other dimensionalities. This resulted in the scaling relations which give a relation between the polaronic properties in different dimensions and predict a significant increase of the effective electron-phonon coupling strength in low-dimensional systems [67–69].

Experimentally, the weak and intermediate coupling regime have been probed, confirming the theoretical results [70, 71]. Unfortunately the polaronic coupling parameter α of the known ionic crystals is too small ($\alpha < 5$) for an experimental study of the optical absorption at strong coupling. Moreover, the continuum approxima-

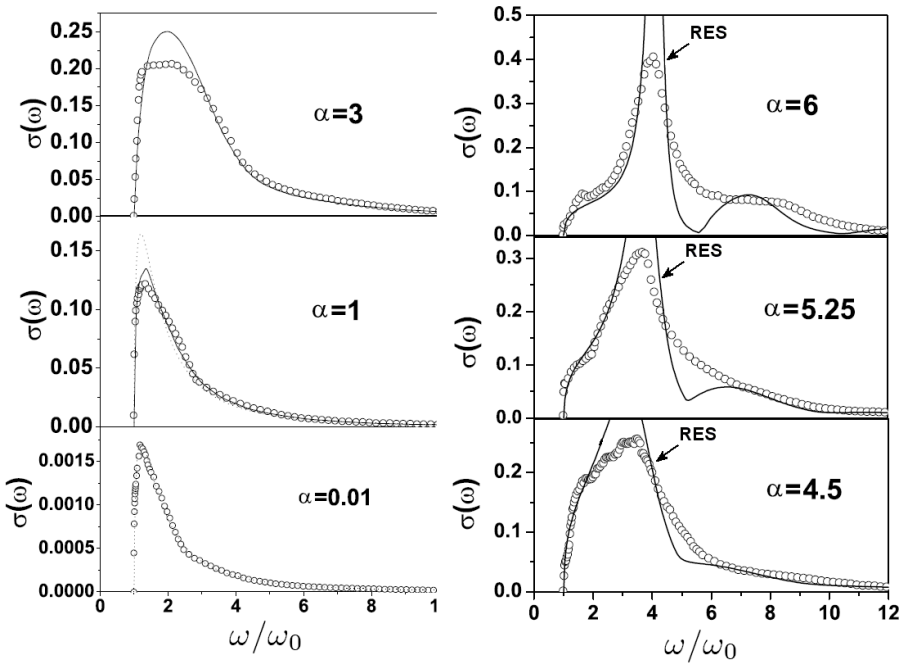

Figure 1.8: The optical absorption of the Fröhlich polaron as a function of the frequency ω of the light. The open circles show the diagrammatic Monte Carlo result, the dotted line is the weak coupling result and the solid line presents the all-coupling DSG result. At strong coupling the spectrum is dominated by the RES peak. The peak to the right of the RES peak (sometimes denoted as the Franck Condon peak) corresponds to a transition to the RES together with the emission of phonons. Note the discrepancies at intermediate and strong polaronic coupling. (From Ref. [62].)

tion is expected to break down at strong coupling and the Frohlich Hamiltonian (1.17) is thus not expected to adequately describe an electron in a charged lattice at strong polaronic coupling.

For N_I electrons the Fröhlich Hamiltonian is

$$\begin{aligned}\widehat{H}_{pol}^{(N_I)} &= \sum_{i}^{N_I} \frac{\widehat{\vec{p}}_i^{\,2}}{2m} + \sum_{\overrightarrow{k}} \hbar\omega_{\overrightarrow{k}} \widehat{a}_{\overrightarrow{k}}^{\dagger} \widehat{a}_{\overrightarrow{k}} + \sum_{i}^{N_I} \sum_{\overrightarrow{k}} V_{\overrightarrow{k}} e^{i\overrightarrow{k}.\widehat{\vec{r}}_i} \left(\widehat{a}_{\overrightarrow{k}} + \widehat{a}_{\overrightarrow{-k}}^{\dagger} \right) \\ &+ \sum_{i<j}^{N_I} U\left(\widehat{\vec{r}}_i - \widehat{\vec{r}}_j \right), \end{aligned} \tag{1.21}$$

with $U(\vec{r})$ the interaction potential between the electrons. An extension of the Feynman all-coupling treatment to two electrons was developed in Ref. [72]. This resulted in the prediction of the formation of a bipolaron, which is a bound state of two electrons, at strong polaronic coupling and weak effective Coulomb repulsion. A consideration of multiple impurities within the strong coupling formalism resulted in the prediction of the possible formation of a multi-polaron [73, 74]. For the weak coupling regime a generalization of the Lee-Low-Pines formalism to many polarons was presented in Ref. [75] and an extension for the dynamic response properties

was derived in Refs. [76, 77]. In Ref. [78] an extension of the all-coupling Feynman treatment was developed for multiple electrons which predicted the formation of a multi-polaron at strong coupling and weak effective Coulomb repulsion.

1.3 Impurities in a condensate

The Hamiltonian of N_I impurity atoms, in the presence of a homogeneous Bose gas is given by [79]:

$$\begin{aligned}\widehat{H} &= \sum_i^{N_I} \frac{\widehat{\vec{p}}^2}{2m_I} + \sum_{\vec{k}} E_{\vec{k}} \widehat{b}^\dagger_{\vec{k}} \widehat{b}_{\vec{k}} + \frac{1}{2} \sum_{\vec{k},\vec{k}',\vec{q}} V_{BB}(\vec{q})\, \widehat{b}^\dagger_{\vec{k}'-\vec{q}} \widehat{b}^\dagger_{\vec{k}+\vec{q}} \widehat{b}_{\vec{k}} \widehat{b}_{\vec{k}'} \\ &\quad + \sum_{\vec{k},,\vec{q}} V_{IB}(\vec{q})\, \widehat{\rho}_{\vec{q}} \widehat{b}^\dagger_{\vec{k}-\vec{q}} \widehat{b}_{\vec{k}} + \sum_{i<j}^{N_I} U\left(\widehat{\vec{r}}_i - \widehat{\vec{r}}_j\right). \end{aligned} \tag{1.22}$$

The second and third terms together correspond to an undisturbed Bose gas, identical to the Hamiltonian (1.6). The first term represents the kinetic energy of the impurity atoms with mass m_I. These are atoms that are distinguishable from the bosons that form the condensate, which in practice means they are either different atoms or atoms in a different hyperfine state. The interaction between the bosonic atoms and the impurity atoms is described by a potential $V_{IB}(\vec{q})$ coupling the boson density to the impurity density $\widehat{\rho}_{\vec{q}}$ which can be expressed as a function of the impurity position operators $\widehat{r}_i$ as

$$\widehat{\rho}_{\vec{q}} = \sum_i^{N_I} e^{-i\vec{q}.\widehat{\vec{r}}_i}. \tag{1.23}$$

For V_{BB} and V_{IB} contact potentials are assumed with interaction strengths g_{BB} and g_{IB}, respectively. As before, the boson-boson interaction is described with the Born approximation: $g_{BB} = 4\pi\hbar^2 a_{BB}/(m_B V)$. For the boson-impurity interaction, the Lippmann-Schwinger equation needs to be treated correctly up to second order, as in expression (1.2), to avoid divergences. The last term in (1.22) represents the interaction between the impurities mutually, with $U(\vec{r})$ the interaction potential.

We now assume that the bosons form a Bose-Einstein condensate and apply the Bogoliubov approximation, as discussed in section 1.1.3. Replacing the operators $\widehat{b}^\dagger_0$ and $\widehat{b}_0$ by the number $\sqrt{N_0}$ gives for the term describing the impurity-boson interaction in the Hamiltonian (1.22):

$$\begin{aligned}\sum_{\vec{k},,\vec{q}} V_{IB}(\vec{q})\, \widehat{\rho}_{\vec{k}} \widehat{b}^\dagger_{\vec{k}-\vec{q}} \widehat{b}_{\vec{k}} &\approx g_{IB} N_0 \widehat{\rho}_{\vec{0}} + \sqrt{N_0} g_{IB} \sum_{\vec{k}\neq\vec{0}} \widehat{\rho}_{\vec{k}} \left(\widehat{b}_{\vec{k}} + \widehat{b}^\dagger_{-\vec{k}}\right) + g_{IB} \sum_{\vec{k},,\vec{q}} \widehat{\rho}_{\vec{q}} \widehat{b}^\dagger_{\vec{k}-\vec{q}} \widehat{b}_{\vec{k}} \\ &\approx g_{IB} N_0 N_I + \sqrt{N_0} g_{IB} \sum_{\vec{k}\neq\vec{0}} \widehat{\rho}_{\vec{k}} \left(\widehat{b}_{\vec{k}} + \widehat{b}^\dagger_{-\vec{k}}\right), \end{aligned} \tag{1.24}$$

where the last term could be neglected since $N_0 \gg 1$. Applying the Bogoliubov

transformation (1.11) gives:

$$\begin{aligned}\sum_{\vec{k},,\vec{q}} V_{IB}\left(\vec{q}\right)\widehat{\rho}_{\vec{q}}\widehat{b}^{\dagger}_{\vec{k}-\vec{q}}\widehat{b}_{\vec{k}} &= g_{IB}N_0N_I+\sqrt{N_0}g_{IB}\sum_{\vec{k}\neq\vec{0}}\widehat{\rho}_{\vec{k}}\left(u_{\vec{k}}-v_{\vec{k}}\right)\left(\widehat{\alpha}_{\vec{k}}+\widehat{\alpha}^{\dagger}_{-\vec{k}}\right)\\ &= g_{IB}N_0N_I+\sqrt{N_0}g_{IB}\sum_{\vec{k}\neq\vec{0}}\sqrt{\frac{E_{\vec{k}}}{\hbar\omega_{\vec{k}}}}\widehat{\rho}_{\vec{k}}\left(\widehat{\alpha}_{\vec{k}}+\widehat{\alpha}^{\dagger}_{-\vec{k}}\right). \quad (1.25)\end{aligned}$$

The first term is the interaction shift due to the impurity and the second term represents the interaction between the impurity and the Bogoliubov excitations. Physically this term describes the absorption or emission of a Bogoliubov excitation by the impurity with the following interaction amplitude:

$$\begin{aligned}V_{\overrightarrow{k}} &= \sqrt{N_0}g_{IB}\sqrt{\frac{E_{\vec{k}}}{\hbar\omega_{\vec{k}}}}\\ &= \sqrt{N_0}g_{IB}\left[\frac{\left(\xi k\right)^2}{\left(\xi k\right)^2+2}\right]. \quad (1.26)\end{aligned}$$

Applying the Bogoliubov approximation also for the second and third term in the Hamiltonian (1.22) (see section 1.1.3) shows that the Bogoliubov approximation transforms the Hamiltonian (1.22) into:

$$\begin{aligned}\widehat{H} &= E_{GP}+g_{IB}N_IN_0+\sum_{i}^{N_I}\frac{\widehat{p}^2}{2m_I}+\sum_{\overrightarrow{k}}\hbar\omega_{\overrightarrow{k}}\widehat{\alpha}^{\dagger}_{\overrightarrow{k}}\widehat{\alpha}_{\overrightarrow{k}}\\ &\quad+\sum_{\overrightarrow{k}}V_{\overrightarrow{k}}\widehat{\rho}_{\vec{k}}\left(\widehat{\alpha}_{\overrightarrow{k}}+\widehat{\alpha}^{\dagger}_{-\overrightarrow{k}}\right)+\sum_{i<j}^{N_I}U\left(\widehat{\vec{r}}_i-\widehat{\vec{r}}_j\right), \quad (1.27)\end{aligned}$$

Note that this Hamiltonian can be mapped onto the N_I-polaron Hamiltonian (1.21). This shows that impurities in a condensate can be understood in terms of polarons where the impurities take the role of the electrons and the phonons are replaced by the Bogoliubov excitations.

As in the case of the solid state polaron different coupling regimes can be distinguished in the ground state properties of a single impurity in a condensate . The weak coupling regime of the BEC-impurity polaron was examined in Refs. [80, 81]. The strong coupling regime with the formation of a bound state of the impurity in the self-induced potential was considered in Refs. [82–88].

In Ref. [89] (and later also in Ref. [90]) the all-coupling Feynman treatment from Ref. [55] was applied for a single impurity in a condensate (this was the main topic of my master-thesis [25]). This description is based on the Jensen-Feynman inequality for the free energy $\mathcal{F}$, which is given by [91, 92]:

$$\mathcal{F}\leq\mathcal{F}_0+\frac{1}{\hbar\beta}\left\langle\mathcal{S}-\mathcal{S}_0\right\rangle_{\mathcal{S}_0}, \quad (1.28)$$

where $\mathcal{S}$ is the action of the system described by the Hamiltonian (1.17) and $\mathcal{S}_0$ is the action of a model system with free energy $\mathcal{F}_0$. In Eq. (1.28) $\beta=\left(k_BT\right)^{-1}$

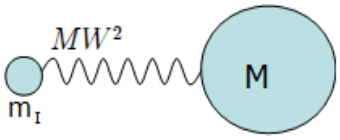

Figure 1.9: The variational model system consisting of the impurity harmonically coupled to a mass M with spring constant MW^2. The eigenfrequency of this system is $\Omega = W\sqrt{1+M/m_I}$.

with T the temperature. Since the Fröhlich Hamiltonian depends quadratically on the Bogoliubov excitation operators the path integration of the degrees of freedom of the Bogoliubov excitations can be done analytically. This results in an effective polaron action which contains retardation effects:

$$\mathcal{S} = \int_0^{\hbar\beta} \frac{m_I}{2}\dot{r}^2(\tau)\,d\tau - \sum_{\vec{k}\neq 0} \frac{\left|V_{\vec{k}}\right|^2}{2\hbar} \int_0^{\hbar\beta} d\tau \int_0^{\hbar\beta} d\sigma \mathcal{G}\left(\vec{k}, |\tau-\sigma|\right) e^{i\vec{k}.[\vec{r}(\tau)-\vec{r}(\sigma)]}, \quad (1.29)$$

with $\mathcal{G}\left(\vec{k}, u\right)$ the Bogoliubov excitation Green's function:

$$\mathcal{G}\left(\vec{k}, u\right) = \frac{\cosh\left[\omega_{\vec{k}}\left(u-\hbar\beta/2\right)\right]}{\sinh\left[\hbar\beta\omega_{\vec{k}}/2\right]}. \quad (1.30)$$

This shows that the influence of the Bogoliubov excitations on the impurities can be described with a retarded interaction, mediated by the Bogoliubov excitations Green's function. Feynman introduced a variational model system in Ref. [55] to model the polaron which is schematically presented in Fig. 1.9 and consists of the impurity harmonically coupled to a fictitious particle with mass M with spring constant MW^2. The action of the model system is:

$$\mathcal{S}_0 = \int_0^{\hbar\beta} \left[\frac{m_I}{2}\dot{r}^2(\tau) + \frac{M}{2}\dot{Q}^2(\tau) + \frac{MW^2}{2}\left[\vec{r}(\tau) - \vec{Q}(\tau)\right]\right] d\tau, \quad (1.31)$$

with $\vec{Q}$ the coordinate of the fictitious particle. The model system action (1.31) depends quadratically on the fictitious particle coordinates, allowing to eliminate the degrees of freedom of the fictitious particle and to rewrite the action of the model system as:

$$\begin{aligned}\mathcal{S}_0 \;=\; & \int_0^{\hbar\beta} \frac{m_I}{2}\dot{r}^2(\tau)\,d\tau \\ & + \frac{MW^3}{8}\int_0^{\hbar\beta} d\tau \int_0^{\hbar\beta} d\sigma \frac{\cosh\left[W\left(|\tau-\sigma| - \hbar\beta/2\right)\right]}{\sinh\left[\hbar\beta W/2\right]}\left[\vec{r}(\tau)-\vec{r}(\sigma)\right]^2 \quad (1.32)\end{aligned}$$

Since the modelsystem action (1.31) also depends quadratically on the impurity coordinates the path integral is exactly solvable and the free energy of the model-system $\mathcal{F}_0$ can be calculated. Introducing the polaron action (1.29) and the action

of the model system (1.32) in the Jensen-Feynman inequality (1.28) results in the following upper bound for the free energy of the polaron:

$$\begin{aligned}\mathcal{F} \leq & \frac{3}{\beta}\left\{\ln\left[2\sinh\left(\frac{\beta\hbar\Omega}{2}\right)\right]-\ln\left[2\sinh\left(\frac{\beta\hbar W}{2}\right)\right]\right\} \\ & -\frac{1}{\beta}\ln\left[V\left(\frac{m_I+M}{2\pi\hbar^2\beta}\right)^{3/2}\right]-\frac{3}{2\beta}\frac{M}{m_I+M}\left[\frac{\hbar\beta\Omega}{2}\coth\left[\frac{\hbar\beta\Omega}{2}\right]-1\right] \\ & -\sum_{\vec{k}}\frac{\left|V_{\vec{k}}\right|^2}{\hbar}\int_0^{\hbar\beta/2}du\mathcal{G}\left(\vec{k},u\right)\mathcal{M}_{M,\Omega}\left(\vec{k},u\right), \end{aligned} \tag{1.33}$$

with $\mathcal{M}_{M,\Omega}\left(\vec{k},u\right)$ the memory function:

$$\mathcal{M}_{M,\Omega}\left(\vec{k},u\right)=e^{-\frac{\hbar k^2}{2(m_I+M)}\left(u-\frac{u^2}{\hbar\beta}-\frac{M}{m_I}\frac{\cosh[\Omega\hbar\beta/2]-\cosh[\Omega(\hbar\beta/2-u)]}{\Omega\cosh[\Omega\hbar\beta/2]}\right)},$$

and $\Omega = W\sqrt{1+M/m_I}$. The parameters M and W (or equivalently M and Ω) can now be used as variational parameters to minimize expression (1.33).

Introducing the first Born approximation for the impurity-boson interaction strength: $g_{IB} = 2\pi\hbar^2 a_{IB}/m_r V$, with a_{IB} the impurity-boson scattering length, and rewriting the definition of the healing length ξ as $N_0 = V/\left(\xi^2 8\pi a_{BB}\right)$ shows that the modulus squared of the interaction amplitude is proportional to a dimensionless parameter α, which we denote as the polaronic coupling parameter:

$$\left|V_{\vec{k}}\right|^2 \propto \alpha,$$

with:

$$\alpha = \frac{a_{IB}^2}{\xi a_{BB}}. \tag{1.34}$$

Note that α can be tuned with an external magnetic field through a Feshbach resonance (1.5). This is not possible for the solid state polaron and makes this system a good candidate to probe the polaronic strong coupling regime. The resulting radius and the effective mass of the polaron are presented in Fig. 1.10 as a function of α. This shows that the two coupling regimes cross over at a critical coupling parameter $\alpha_c \approx 3$ in the zero temperature limit. The weak coupling regime is characterized by a small increase of the mass and a large radius which corresponds to a quasifree polaron. The strong coupling regime exhibits a large increase of the mass and a small size which indicates the formation of a bound state of the impurity in the self-induced potential.

At the moment there are multiple ongoing experiments that are promising to probe the polaronic properties of an impurity in a Bose-Einstein condensate. For now, however, a measurement of polaronic features of an impurity atom in a BEC remains elusive. We now discuss a few of these recent experiments.

The experimental lab "Synthetic Quantum Systems" at the university of Heidelberg in Germany considers the experimental realization of a Li-6 impurity in a Na condensate [93]. In the absence of a magnetic field the intraspecies scattering length is $a_{\mathrm{Na}} = 2.89$ nm [94] and the interspecies scattering length is $a_{\text{Li-Na}} = -3.86$

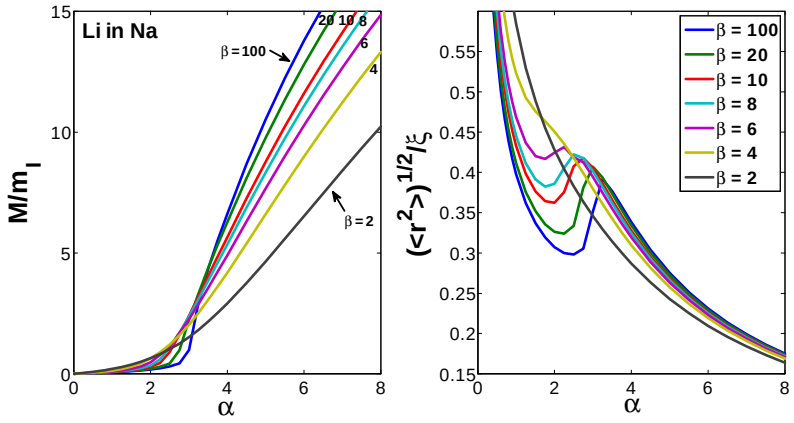

Figure 1.10: The effective mass ($m^* \approx m_I + M$) and the radius (estimated by the root mean square of the reduced coordinate of the model system) of the polaron are presented as a function of the polaronic coupling parameter α at different temperatures T ($\beta = \hbar^2/\left(m_I \xi^2 k_B T\right)$) for a Li impurity in a Na condensate. (From Ref. [89].)

nm [95]. A typical density for the condensed Na atoms is: $n_0 \approx 10^{14}$ cm^{-3}. Introducing these parameters gives for the coupling parameter $\alpha \approx 0.014$ which is in the weak polaronic coupling regime. In Ref. [95] 26 interspecies Feshbach resonances are measured for this system with calculated widths of the order of mG. This is of the same order as the magnetic field fluctuations which demonstrates the difficulty of using these resonances to tune α. Another possibility to increase α is to use intraspecies Feshbach resonances to lower $a_{\rm Na}$. These have been reported in Ref. [94] with widths of the order of 1G. A possible difficulty in this case is the disappearance of the Bogoliubov modes if $a_{\rm Na} \to 0$. Another possibility is to use a Li-7 impurity in a Na condensate for which broad interspecies Feshbach resonances of the order of 1G are predicted [95].

The experimental lab "Quantum Physics with Single Atoms and Quantum Gases" at the university of Kaiserslautern in Germany has reported the immersion of a Cs impurity in an ultracold Rb gas [96,97]. In this case the Rb density is typically of the order $n_0 \approx 10^{13}$ cm^{-3}, the background intraspecies scattering length is $a_{\rm Rb} = 4.76$ nm [98] and the background interspecies scattering length is $a_{\rm Rb\text{-}Cs} = 34$ nm [99]. This results in $\alpha \approx 0.27$ which shows that without the use of an external magnetic field this system is also in the weak coupling regime. In Ref. [99] the Cs-Rb scattering properties are examined which reveals a broad interspecies Feshbach resonances (with width $\Delta B = 4.2$ G) at 790 G that is useful to tune the scattering length $a_{\rm Rb\text{-}Cs}$.

During recent years we have had contacts with the two previously mentioned experimental groups who provided us with the necessary data to calculate the polaronic coupling strengths for their respective experimental configurations. However, there have been also other reports on experimental setups that are promising to probe polaronic effects. For example, in Refs. [100–102] the introduction of a single ion in a condensate is presented and Ref. [103] reports on the realization of a

K atom in a Rb condensate in a one dimensional geometry. There are also multiple experiments with binary mixtures with broad interspecies Feshbach resonances (see for example Refs. [99, 104, 105]) which is interesting to probe the many-polaron character.

There is also some interest in the polaronic properties of impurities in an optical lattice in the presence of an ultra cold bosonic gas. If the optical lattice is sufficiently strong the motion of the impurity is described in terms of hopping between the different lattice sites. This system can be interpreted in terms of a small or Holstein polaron which consists of an electron in a polar or ionic lattice of which the radius of the wave function is of the order of the lattice constant that can tunnel between the different lattice sites [106]. Theoretical studies of impurities in an optical lattice immersed in a BEC have been presented in Refs. [107–110] and in Ref. [111] the experimental immersion of a single fermion and a coherent bosonic field in an optical lattice is reported. In this context there have been experimental measurements of polaronic effects in ultracold binary mixtures loaded in an optical lattice [112, 113]. In Ref. [114] it is shown that ultracold polar molecules trapped in an optical lattices can be used to quantum simulate a generalization of the polaron where a modulation of the distance between the lattice sites by the phonons is incorporated, described by the Su-Schrieffer-Heeger polaron model [115]. Furthermore, a remarkable agreement has been presented between the theoretical prediction and the experimental measurement of the spectral function of the Fermi-polaron which consists of an impurity atom in an ultracold Fermi gas [116–118].

We also have a collaboration with the group "Theoretical Nuclear Physics and Statistical Physics" from Ghent University in Belgium. They are developing an application of the diagrammatic Monte Carlo technique for the BEC-impurity polaron. Recently they used this technique to calculate the equation of state of a unitary Fermi gas which is in good agreement with an experimental measurement [119].

The hybrid system consisting of impurities in an ultra cold bosonic gas has multiple other interesting applications besides the quantum simulation of the polaron. An example is to use it as a cooling technique for the impurities which brings them to very low temperatures that are not attainable by standard cooling mechanisms [97]. This is interesting from the perspective of quantum information since under the appropriate conditions the internal state of the impurities remains unchanged which allows a non-destructive cooling of qubits [120–122]. Also in the context of quantum information a single impurity can be used as a switch for the transport of a 1D condensate, resulting in a single atom transistor [123]. The impurity can also be used to probe properties of the ultracold bosons. For example the decoherence of the Bose-Einstein condensate can be non-destructively probed by the impurity [124]. In a one dimensional set-up the observation of the impurity dynamics can be used to measure the atomic Luttinger parameters of the Bose gas directly [125]. Furthermore, a single impurity allows a study of the interactions between the impurity and the bosons and the possibility of molecule formation without the interference of other impurities [97, 126].

Throughout this thesis the results will be presented in polaronic units which are listed in Table 1.1. Since the results will be frequently applied to the system of a Li-6 impurity in a Na condensate, which allows a comparison with the results of

	unit	unit for Li-6 in Na
length	ξ	450 nm
mass	m_I	1.0×10^{-26} kg
wave number	ξ^{-1}	2.22 μm^{-1}
momentum	$\hbar\xi^{-1}$	1.47×10^{-27} $\frac{\text{kg.m}}{\text{s}}$
frequency	$\frac{\hbar}{m_I\xi^2}$	52 kHz
energy	$\frac{\hbar^2}{m_I\xi^2}$	5.5×10^{-30} J
time	$\left(\frac{\hbar}{m_I\xi^2}\right)^{-1}$	19 μs
temperature	$\frac{\hbar^2}{k_B m_I\xi^2}$	397 nK
β $(= (k_B T)^{-1})$	$\left(\frac{\hbar^2}{m_I\xi^2}\right)^{-1}$	1.8×10^{29} J^{-1}

Table 1.1: Overview of the polaronic units together with the value in SI units for a Li-6 impurity in a Na condensate.

Ref. [89], we also give the SI values of the polaronic units for this system to give an idea of the typical magnitudes of the considered effects. The ratio of the impurity and boson masses for this system is $m_{\text{Na}}/m_{\text{Li-6}} = 3.8221$.

1.4 Outline

In chapter 2 the dynamic response properties of a single impurity in a Bose-Einstein condensate are considered. Since the impurity is not charged this can not be studied by considering the optical absorption as for the solid state polaron. We show that Bragg spectroscopy is a suitable experimental probe. This means we have to consider a finite momentum exchange, which is negligible for optical absorption. The typical polaronic features such as the Drude-like background, the Bogoliubov peak, the relaxed excited states and the Franck-Condon peaks are identified for an impurity in a condensate. Because of the rather complex nature of these response calculations we present in chapter 3 a simplified analysis of the polaronic excitation structure that is valid in the strong coupling regime. This allows an estimation of the transition frequencies for the relaxed excited states.

This was for a single impurity and in chapter 4 we consider a few impurities in a condensate. For the case of two impurities an extension of the Feynman all-coupling approach is applied. At strong coupling this results in the prediction of the formation of a bipolaron which is a bound state of the two impurities. Also the typical polaronic properties are investigated such as the bipolaron radius and the effective mass. We also develop a strong coupling description which is valid for multiple impurities and predicts the formation of a multi-polaron at strong coupling.

In chapter 5 the possibility of reduced dimensions is considered. This results in larger amplitudes of the polaronic properties and the transition to the strong coupling regime occurs at lower coupling. These observations show that experimentally the consideration of reduced dimensions can facilitate the detection of the polaron and the realization of the strong coupling regime. Furthermore, one can use confinement-induced resonances to tune the coupling parameter.

Chapter 6 is devoted to the many-polaron description of a gas of impurities together with a Bose-Einstein condensate at weak coupling. This is relevant since the first experimental measurements are expected to be in this regime. The ground state properties and the response of the system to Bragg spectroscopy are derived. This is then applied for ultracold fermionic and bosonic impurities.

Finally, in chapter 7, the possibility of a charged impurity is considered. Because of the greater range of the ion-boson interaction the system is expected to be in the strong coupling regime. On the other hand this also results in a larger depletion of the condensate in the vicinity of the ion which may compromise the use of the Bogoliubov approximation and thus the mapping onto the polaron. The allowed values for the system parameters are determined such that the system exhibits strong coupling polaronic features.

Chapter 2

Response of the BEC-impurity polaron to Bragg spectroscopy*

In this chapter the dynamic response of the polaronic system consisting of a single impurity in a Bose-Einstein condensate is investigated. For the solid state polaron the optical absorption was derived in Ref. [61]. Since the impurity is neutral we have to consider a different experiment for the response. We show that Bragg spectroscopy is a suitable probe for the polaronic response properties. We will closely follow an alternative derivation for the optical absorption with the Mori-Zwanzig projection operator formalism, presented in Ref. [127]. The main innovation is that we have to consider a finite momentum exchange for Bragg spectroscopy which is negligible for the optical absorption. The polaronic mass sum rule from Ref. [128] is applied as a consistency check for the resulting spectra.

2.1 Bragg spectroscopy

Bragg spectroscopy is a well-established experimental technique that has been applied for example to measure the excitation spectrum and the structure factor of a Bose-Einstein condensate [26, 129] (see also Fig. 1.4). It is realized by irradiating the considered system with two laser beams with wave vectors $\overrightarrow{k}_1$ and $\overrightarrow{k}_2$ and frequencies ω_1 and ω_2. An atom can then undergo a stimulated scattering event by absorbing a photon from beam 1 and emitting it in beam 2. During this process it gains a momentum $\hbar\overrightarrow{k} = \hbar\overrightarrow{k}_1 - \hbar\overrightarrow{k}_2$ and energy $\hbar\omega = \hbar\omega_1 - \hbar\omega_2$. See Fig. 2.1 for a schematic picture of a typical experimental set-up. The response of the system N_{Bragg} is then determined by measuring the total exchanged momentum to the system as a function of ω and $\vec{k}$ by performing a time-of-flight experiment. Within linear-response theory, this number is proportional to the imaginary part of the density-density correlation $\chi\left(\omega, \vec{k}\right)$ [4]:

$$N_{Bragg} = \frac{2}{\hbar}\left(\frac{V}{2}\right)^2 \tau \,\mathrm{Im}\,\chi\left(\omega, \vec{k}\right) \tag{2.1}$$

*The results from this chapter are published in W. Casteels, J. Tempere and J. T. Devreese - *Response of the polaron system consisting of an impurity in a Bose-Einstein condensate to Bragg spectroscopy* - Phys. Rev. A **83**, 033631 (2011).

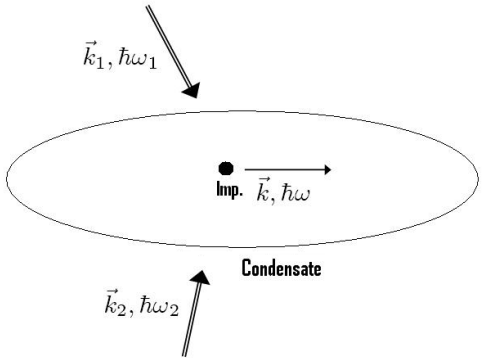

Figure 2.1: Schematical presentation of the experimental set-up for Bragg spectroscopy. The impurity gains a momentum $\hbar\overrightarrow{k} = \hbar\overrightarrow{k}_1 - \hbar\overrightarrow{k}_2$ and energy $\hbar\omega = \hbar\omega_1 - \hbar\omega_2$ by absorbing a photon from beam 1 and emitting a photon to beam 2.

with τ the duration of the pulse and V the amplitude of the laser induced potential:

$$V = -\frac{\alpha E_0^2}{4}, \tag{2.2}$$

with E_0 the amplitude of the lasers and α the polarizability of the atoms. By adjusting the average laser frequency α can be made large for the impurity and small for the bosons. The density-density correlation for the impurity is given by

$$\chi\left(\omega, \vec{k}\right) = \frac{i}{\hbar}\int_0^\infty dt e^{i\omega t}\left\langle\left[\widehat{\rho}_{\vec{k}}\left(t\right), \widehat{\rho}_{\vec{k}}^\dagger\right]\right\rangle, \tag{2.3}$$

with $\widehat{\rho}_{\vec{q}}$ the impurity density (1.23). With $\langle ...\rangle$ the expectation value over the Gibbs ensemble is denoted:

$$\left\langle\widehat{O}\right\rangle = \frac{\mathrm{tr}\left[e^{-\beta\widehat{H}}\widehat{O}\right]}{\mathrm{tr}\left[e^{-\beta\widehat{H}}\right]},$$

where β is the inverse temperature T: $\beta = 1/\left(k_B T\right)$ and $\widehat{H}$ the Hamiltonian of the system.

2.2 Mori formalism for the density-density correlation

Here we present a calculation of the density-density correlation (2.3) within the Mori-Zwanzig projection operator formalism from Refs. [130, 131]. For the density-density correlation the usual definition of the Mori projection operator has to be adjusted, as demonstrated in Ref. [132]. We will closely follow the derivation for the polaronic optical absorption from Refs. [29, 127]. We start by rewriting the

density-density correlation (2.3) by means of a partial integration:

$$\begin{aligned}\chi\left(\omega,\vec{k}\right) &= \frac{1}{\hbar\omega}\int_0^\infty d\left(e^{i\omega t}\right)\left\langle\left[\widehat{\rho}_{\vec{k}}\left(0\right),\widehat{\rho}_{\vec{k}}^{\dagger}\left(-t\right)\right]\right\rangle \\ &= \frac{1}{\hbar\omega}\left[e^{i\omega t}\left\langle\left[\widehat{\rho}_{\vec{k}}\left(0\right),\widehat{\rho}_{\vec{k}}^{\dagger}\left(-t\right)\right]\right\rangle\right]_{t=0}^{t=\infty} - \frac{1}{\hbar\omega}\int_0^\infty dt e^{i\omega t}\left\langle\left[\widehat{\rho}_{\vec{k}}\left(0\right),\dot{\widehat{\rho}}_{\vec{k}}^{\dagger}\left(-t\right)\right]\right\rangle \\ &= -\frac{1}{\hbar\omega}\int_0^\infty dt e^{i\omega t}\left\langle\left[\widehat{\rho}_{\vec{k}}\left(t\right),\dot{\widehat{\rho}}_{\vec{k}}^{\dagger}\left(0\right)\right]\right\rangle. \end{aligned} \tag{2.4}$$

We used the general property of a correlation that it becomes zero in the limit $t\rightarrow\infty$ and:

$$\begin{aligned}\left\langle\widehat{A}\left(t\right)\widehat{B}\left(0\right)\right\rangle &= \left\langle e^{i\widehat{H}t/\hbar}\widehat{A}e^{-i\widehat{H}t/\hbar}\widehat{B}\right\rangle \\ &= \frac{\mathrm{tr}\left[e^{-\beta\widehat{H}}e^{i\widehat{H}t/\hbar}\widehat{A}e^{-i\widehat{H}t/\hbar}\widehat{B}\right]}{\mathrm{tr}\left[e^{-\beta\widehat{H}}\right]} \\ &= \frac{\mathrm{tr}\left[e^{i\widehat{H}t/\hbar}e^{-\beta\widehat{H}}\widehat{A}e^{-i\widehat{H}t/\hbar}\widehat{B}\right]}{\mathrm{tr}\left[e^{-\beta\widehat{H}}\right]} \\ &= \frac{\mathrm{tr}\left[e^{-\beta\widehat{H}}\widehat{A}e^{-i\widehat{H}t/\hbar}\widehat{B}e^{i\widehat{H}t/\hbar}\right]}{\mathrm{tr}\left[e^{-\beta\widehat{H}}\right]} \\ &= \left\langle\widehat{A}\left(0\right)B\left(-t\right)\right\rangle, \end{aligned} \tag{2.5}$$

where the cyclic invariance of the trace was used. The Heisenberg equation of motion for the density is:

$$\frac{\partial\widehat{\rho}_{\vec{k}}\left(t\right)}{\partial t} = \frac{i}{\hbar}\left[\widehat{H},\widehat{\rho}_{\vec{k}}\left(t\right)\right] = i\widehat{L}\widehat{\rho}_{\vec{k}}\left(t\right), \tag{2.6}$$

which is the definition of the Liouville operator $\widehat{L}$. The formal solution of the differential equation (2.6) is:

$$\widehat{\rho}_{\vec{k}}\left(t\right) = e^{i\widehat{L}t}\widehat{\rho}_{\vec{k}} = e^{i\widehat{H}t/\hbar}\widehat{\rho}_{\vec{k}}e^{-i\widehat{H}t/\hbar}, \tag{2.7}$$

with $\widehat{\rho}_{\vec{k}} = \widehat{\rho}_{\vec{k}}\left(0\right)$. We now rewrite (2.4) as (to have a convergent integral we introduce $z=\omega+i\delta$, with δ a positive infinitesimal):

$$\begin{aligned}\chi\left(z,\vec{k}\right) &= -\frac{1}{\hbar z}\int_0^\infty dt e^{izt}\left\langle\left[e^{i\widehat{L}t}\widehat{\rho}_{\vec{k}},\dot{\widehat{\rho}}_{\vec{k}}^{\dagger}\right]\right\rangle \\ &= \frac{i}{\hbar z}\left\langle\left[\frac{1}{z+\widehat{L}}\widehat{\rho}_{\vec{k}},\dot{\widehat{\rho}}_{\vec{k}}^{\dagger}\right]\right\rangle. \end{aligned} \tag{2.8}$$

We now introduce the Mori projection operator $\widehat{P}$ as [132]

$$\widehat{P}\widehat{O} = \frac{\left\langle\left[\widehat{O},\dot{\widehat{\rho}}_{\vec{k}}^{\dagger}\right]\right\rangle}{\left\langle\left[\widehat{\rho}_{\vec{k}},\dot{\widehat{\rho}}_{\vec{k}}^{\dagger}\right]\right\rangle}\widehat{\rho}_{\vec{k}}. \tag{2.9}$$

It can easily verified that this is a projection operator (with $\widehat{Q} = 1 - \widehat{P}$):

$$\widehat{P}^2 = \widehat{P}; \quad \widehat{Q}^2 = \widehat{Q}; \qquad \widehat{Q}\widehat{P} = \widehat{P}\widehat{Q} = 0. \tag{2.10}$$

We can now use the identity $\widehat{L} = \widehat{L}\widehat{Q} + \widehat{L}\widehat{P}$ to write the correlation function (2.8) as

$$\begin{aligned}
\chi\left(z,\vec{k}\right) &= \frac{i}{\hbar z}\left\langle\left[\frac{1}{z+\widehat{L}}\widehat{\rho}_{\vec{k}},\widehat{\dot{\rho}}_{\vec{k}}^{\dagger}\right]\right\rangle \\
&= \frac{i}{\hbar z}\left\langle\left[\frac{1}{z+\widehat{L}\widehat{Q}+\widehat{L}\widehat{P}}\widehat{\rho}_{\vec{k}},\widehat{\dot{\rho}}_{\vec{k}}^{\dagger}\right]\right\rangle \\
&= \frac{i}{\hbar z}\left\langle\left[\frac{1}{z+\widehat{L}\widehat{Q}}\widehat{\rho}_{\vec{k}} - \frac{1}{z+\widehat{L}\widehat{Q}}\widehat{L}\widehat{P}\frac{1}{z+\widehat{L}}\widehat{\rho}_{\vec{k}},\widehat{\dot{\rho}}_{\vec{k}}^{\dagger}\right]\right\rangle,
\end{aligned} \tag{2.11}$$

where the following algebraic identity was used:

$$\frac{1}{a+b} = \frac{1}{a} - \frac{1}{a}b\frac{1}{a+b}. \tag{2.12}$$

Furthermore, since $\widehat{Q}\widehat{\rho}_{\vec{k}} = 0$, we can write the first term of (2.11) as:

$$\begin{aligned}
\frac{1}{z+\widehat{L}\widehat{Q}}\widehat{\rho}_{\vec{k}} &= \left(\frac{1}{z} - \frac{1}{z^2}\widehat{L}\widehat{Q} + \frac{1}{z^3}\widehat{L}\widehat{Q}\widehat{L}\widehat{Q} - ...\right)\widehat{\rho}_{\vec{k}} \\
&= \frac{1}{z}\widehat{\rho}_{\vec{k}}.
\end{aligned} \tag{2.13}$$

This means (2.11) becomes:

$$\chi\left(z,\vec{k}\right) = \frac{i}{\hbar z^2}\left\langle\left[\widehat{\rho}_{\vec{k}},\widehat{\dot{\rho}}_{\vec{k}}^{\dagger}\right]\right\rangle - \frac{i}{\hbar z}\left\langle\left[\frac{1}{z+\widehat{L}\widehat{Q}}\widehat{L}\widehat{P}\frac{1}{z+\widehat{L}}\widehat{\rho}_{\vec{k}},\widehat{\dot{\rho}}_{\vec{k}}^{\dagger}\right]\right\rangle. \tag{2.14}$$

In the second term we use the definition of the projection operator:

$$\begin{aligned}
\frac{i}{\hbar z}\widehat{P}\left(\frac{1}{z+\widehat{L}}\widehat{\rho}_{\vec{k}}\right) &= \frac{i}{\hbar z}\frac{1}{\varphi}\left\langle\left[\frac{1}{z+\widehat{L}}\widehat{\rho}_{\vec{k}},\widehat{\dot{\rho}}_{\vec{k}}^{\dagger}\right]\right\rangle\widehat{\rho}_{\vec{k}} \\
&= \frac{1}{\varphi}\chi\left(z,\vec{k}\right)\widehat{\rho}_{\vec{k}},
\end{aligned} \tag{2.15}$$

where we introduced $\varphi = \left\langle\left[\widehat{\rho}_{\vec{k}},\widehat{\dot{\rho}}_{\vec{k}}^{\dagger}\right]\right\rangle$. This gives for the correlation function (2.14):

$$\begin{aligned}
z^2\chi\left(z,\vec{k}\right) &= i\frac{\varphi}{\hbar} - \frac{z}{\varphi}\left\langle\left[\frac{z}{z+\widehat{L}\widehat{Q}}\widehat{L}\widehat{\rho}_{\vec{k}},\widehat{\dot{\rho}}_{\vec{k}}^{\dagger}\right]\right\rangle\chi\left(z,\vec{k}\right) \\
&= i\frac{\varphi}{\hbar} - \frac{z}{\varphi}\left\langle\left[\frac{z+\widehat{L}\widehat{Q}-\widehat{L}\widehat{Q}}{z+\widehat{L}\widehat{Q}}\widehat{L}\widehat{\rho}_{\vec{k}},\widehat{\dot{\rho}}_{\vec{k}}^{\dagger}\right]\right\rangle\chi\left(z,\vec{k}\right) \\
&= i\frac{\varphi}{\hbar} - \frac{z}{\varphi}\left\langle\left[\widehat{L}\widehat{\rho}_{\vec{k}},\widehat{\dot{\rho}}_{\vec{k}}^{\dagger}\right]\right\rangle\chi\left(z,\vec{k}\right) \\
&\quad + \frac{z}{\varphi}\left\langle\left[\frac{\widehat{L}\widehat{Q}}{z+\widehat{L}\widehat{Q}}\widehat{L}\widehat{\rho}_{\vec{k}},\widehat{\dot{\rho}}_{\vec{k}}^{\dagger}\right]\right\rangle\chi\left(z,\vec{k}\right).
\end{aligned} \tag{2.16}$$

We now introduce the following notation:

$$O\left(z,\vec{k}\right) = \frac{z}{\varphi}\left\langle\left[\widehat{L\rho}_{\vec{k}},\widehat{\dot{\rho}}_{\vec{k}}^{\dagger}\right]\right\rangle; \tag{2.17}$$

$$\Sigma\left(z,\vec{k}\right) = \frac{z}{\varphi}\left\langle\left[\frac{\widehat{L}\widehat{Q}}{z+\widehat{L}\widehat{Q}}\widehat{L\rho}_{\vec{k}},\widehat{\dot{\rho}}_{\vec{k}}^{\dagger}\right]\right\rangle. \tag{2.18}$$

The correlation function $\chi\left(\omega,\vec{k}\right)$ then becomes:

$$\chi\left(z,\vec{k}\right) = i\frac{\varphi}{\hbar}\frac{1}{z^2+O\left(z,\vec{k}\right)-\Sigma\left(z,\vec{k}\right)}. \tag{2.19}$$

To rewrite $\Sigma\left(\omega,\vec{k}\right)$ we use the following identity:

$$\begin{aligned}
\left\langle\left[\left(\widehat{L}\widehat{A}\right),\widehat{B}^{\dagger}\right]\right\rangle &= \frac{1}{\hbar}\left\langle\left[\left(\widehat{H}\widehat{A}-\widehat{A}\widehat{H}\right),\widehat{B}^{\dagger}\right]\right\rangle \\
&= \frac{1}{\hbar}\left\langle\left(\widehat{H}\widehat{A}-\widehat{A}\widehat{H}\right)\widehat{B}^{\dagger}-\widehat{B}^{\dagger}\left(\widehat{H}\widehat{A}-\widehat{A}\widehat{H}\right)\right\rangle \\
&= \frac{1}{\hbar}\left\langle\widehat{A}\widehat{B}^{\dagger}\widehat{H}-\widehat{A}\widehat{H}\widehat{B}^{\dagger}-\widehat{B}^{\dagger}\widehat{H}\widehat{A}+\widehat{H}\widehat{B}^{\dagger}\widehat{A}\right\rangle \\
&= \frac{1}{\hbar}\left\langle\widehat{A}\left(\widehat{H}\widehat{B}-\widehat{B}\widehat{H}\right)^{\dagger}-\left(\widehat{H}\widehat{B}-\widehat{B}\widehat{H}\right)^{\dagger}\widehat{A}\right\rangle \\
&= \left\langle\left[\widehat{A},\left(\widehat{L}\widehat{B}\right)^{\dagger}\right]\right\rangle,
\end{aligned} \tag{2.20}$$

which gives:

$$\Sigma\left(z,\vec{k}\right) = \frac{z}{\varphi}\left\langle\left[\widehat{Q}\frac{1}{z+\widehat{L}\widehat{Q}}\widehat{L\rho}_{\vec{k}},\left(\widehat{L\dot{\rho}}_{\vec{k}}\right)^{\dagger}\right]\right\rangle. \tag{2.21}$$

Another identity we will use is:

$$\begin{aligned}
\widehat{Q}\frac{1}{1-\widehat{L}\widehat{Q}} &= \widehat{Q}\left(1+\widehat{L}\widehat{Q}+\left(\widehat{L}\widehat{Q}\right)^2+...\right) \\
&= \left(\widehat{Q}+\widehat{Q}\widehat{L}\widehat{Q}+\widehat{Q}\left(\widehat{L}\widehat{Q}\right)^2+...\right) \\
&= \left(1+\widehat{Q}\widehat{L}\widehat{Q}+\left(\widehat{Q}\widehat{L}\widehat{Q}\right)^2+...\right)\widehat{Q} \\
&= \frac{1}{1-\widehat{Q}\widehat{L}\widehat{Q}}\widehat{Q}.
\end{aligned} \tag{2.22}$$

This gives for $\Sigma\left(z,\vec{k}\right)$ (with the new Liouville operator $\widehat{\mathcal{L}}$=$\widehat{Q}\widehat{L}\widehat{Q}$):

$$\begin{aligned}
\Sigma\left(z,\vec{k}\right) &= \frac{z}{\varphi}\left\langle\left[\frac{1}{z+\widehat{\mathcal{L}}}\widehat{L\rho}_{\vec{k}},\left(\widehat{L\dot{\rho}}_{\vec{k}}\right)^{\dagger}\right]\right\rangle \\
&= -\frac{iz}{\varphi}\int_0^{\infty}dte^{izt}\left\langle\left[e^{i\widehat{\mathcal{L}}t}\widehat{L\rho}_{\vec{k}},\left(\widehat{L\dot{\rho}}_{\vec{k}}\right)^{\dagger}\right]\right\rangle \\
&= -\frac{1}{\varphi}\int_0^{\infty}d\left(e^{izt}\right)\left\langle\left[e^{i\widehat{\mathcal{L}}t}\widehat{L\rho}_{\vec{k}},\left(\widehat{L\dot{\rho}}_{\vec{k}}\right)^{\dagger}\right]\right\rangle \\
&= -\frac{1}{\varphi}\left[e^{izt}\left\langle\left[e^{i\widehat{\mathcal{L}}t}\widehat{L\rho}_{\vec{k}},\left(\widehat{L\dot{\rho}}_{\vec{k}}\right)^{\dagger}\right]\right\rangle\right]_{t=0}^{t=\infty} \\
&\quad +\frac{1}{\varphi}\int_0^{\infty}dte^{izt}\left\langle\left[i\widehat{\mathcal{L}}e^{i\widehat{\mathcal{L}}t}\widehat{L\rho}_{\vec{k}},\left(\widehat{L\dot{\rho}}_{\vec{k}}\right)^{\dagger}\right]\right\rangle \\
&= \frac{1}{\varphi}\left\langle\left[\widehat{L}\rho_{\vec{k}},\left(\widehat{L}\dot{\rho}_{\vec{k}}\right)^{\dagger}\right]\right\rangle \\
&\quad +\frac{i}{\varphi}\int_0^{\infty}dte^{izt}\left\langle\left[e^{i\widehat{\mathcal{L}}t}\widehat{L\dot{\rho}}_{\vec{k}},\left(\widehat{L\dot{\rho}}_{\vec{k}}\right)^{\dagger}\right]\right\rangle. \qquad (2.23)
\end{aligned}$$

Introducing the operator $\widehat{\mathcal{B}}_{\vec{k}}=\widehat{L\dot{\rho}}_{\vec{k}}$ allows us to write:

$$\Sigma\left(z,\vec{k}\right)=\frac{1}{\varphi}\left\langle\left[\widehat{L\rho}_{\vec{k}},\left(\widehat{L\dot{\rho}}_{\vec{k}}\right)^{\dagger}\right]\right\rangle+\frac{1}{\varphi}\int_0^{\infty}dte^{izt}\left\langle\left[\widehat{\mathcal{B}}_{\vec{k}}\left(t\right),\widehat{\mathcal{B}}_{\vec{k}}^{\dagger}\right]\right\rangle. \qquad (2.24)$$

Note that the time evolution of the operator $\widehat{\mathcal{B}}_{\vec{k}}$ is governed by the new Liouville operator $\widehat{\mathcal{L}}$. The first term we can write as:

$$\begin{aligned}
\frac{1}{\varphi}\left\langle\left[\widehat{L\rho}_{\vec{k}},\left(\widehat{L\dot{\rho}}_{\vec{k}}\right)^{\dagger}\right]\right\rangle &= -\frac{i}{\varphi}\left\langle\left[\frac{1}{\widehat{\mathcal{L}}}\widehat{\mathcal{L}\dot{\rho}}_{\vec{k}},\left(\widehat{L\dot{\rho}}_{\vec{k}}\right)^{\dagger}\right]\right\rangle \\
&= -\frac{i}{\varphi}\left\langle\left[\frac{1}{\widehat{\mathcal{L}}}\widehat{\mathcal{B}}_{\vec{k}},\widehat{\mathcal{B}}_{\vec{k}}^{\dagger}\right]\right\rangle \\
&= -\frac{1}{\varphi}\int_0^{\infty}dt\left\langle\left[e^{i\widehat{\mathcal{L}}t}\widehat{\mathcal{B}}_{\vec{k}},\widehat{\mathcal{B}}_{\vec{k}}^{\dagger}\right]\right\rangle \\
&= -\frac{1}{\varphi}\int_0^{\infty}dt\left\langle\left[\widehat{\mathcal{B}}_{\vec{k}}\left(t\right),\widehat{\mathcal{B}}_{\vec{k}}^{\dagger}\right]\right\rangle. \qquad (2.25)
\end{aligned}$$

So we find for the memory function:

$$\Sigma\left(z,\vec{k}\right)=-\frac{1}{\varphi}\int_0^{\infty}dt\left(1-e^{izt}\right)\left\langle\left[\widehat{\mathcal{B}}_{\vec{k}}\left(t\right),\widehat{\mathcal{B}}_{\vec{k}}^{\dagger}\right]\right\rangle. \qquad (2.26)$$

2.3 Density-density correlation for the Fröhlich polaron Hamiltonian

Here we calculate the functions from the previous section for the Fröhlich Hamiltonian (1.17), similar to the derivation presented in Refs. [29, 127]. We will use the

continuity equation which can be written as: $\widehat{\dot{\rho}}_{\vec{k}} = i\vec{k}.\widehat{\vec{j}}_{\vec{k}}$, with $\widehat{\vec{j}}_{\vec{k}}$ the current operator. For the calculation of the commutators we consider the different quantities as a function of the creation, resp. annihilation, operators $\widehat{c}^{\dagger}_{\vec{k}}$, $\widehat{c}_{\vec{k}}$ of the impurity with wave vector $\vec{k}$. This gives:

$$\widehat{\rho}_{\vec{q}} = \sum_{\vec{k}} \widehat{c}^{\dagger}_{\vec{k}+\vec{q}}\widehat{c}_{\vec{k}}; \tag{2.27}$$

$$\widehat{\vec{j}}_{\vec{q}} = \sum_{\vec{k}} \left(\vec{k}+\frac{\vec{q}}{2}\right)\widehat{c}^{\dagger}_{\vec{k}+\vec{q}}\widehat{c}_{\vec{k}}; \tag{2.28}$$

$$\widehat{H}_{pol} = \sum_{\vec{k}} \frac{\hbar^2 k^2}{2m_I}\widehat{c}^{\dagger}_{\vec{k}}\widehat{c}_{\vec{k}} + \sum_{\overrightarrow{k}} \hbar\omega_{\overrightarrow{k}}\widehat{\alpha}^{\dagger}_{\overrightarrow{k}}\widehat{\alpha}_{\overrightarrow{k}} + \sum_{\overrightarrow{k},\vec{q}} V_{\overrightarrow{k}}\widehat{c}^{\dagger}_{\vec{q}+\vec{k}}\widehat{c}_{\vec{q}}\left(\widehat{\alpha}_{\overrightarrow{k}} + \widehat{\alpha}^{\dagger}_{\overrightarrow{-k}}\right). \tag{2.29}$$

We start with the expectation value of the density-density commutator:

$$\begin{aligned}
\left[\widehat{\rho}_{\vec{q}_1}, \widehat{\rho}_{\vec{q}_2}\right] &= \sum_{\vec{k},\vec{k}'} \left[\widehat{c}^{\dagger}_{\vec{k}+\vec{q}_1}\widehat{c}_{\vec{k}}, \widehat{c}^{\dagger}_{\vec{k}'+\vec{q}_2}\widehat{c}_{\vec{k}'}\right] \\
&= \sum_{\vec{k},\vec{k}'} \left(\widehat{c}^{\dagger}_{\vec{k}+\vec{q}_1}\widehat{c}_{\vec{k}}\widehat{c}^{\dagger}_{\vec{k}'+\vec{q}_2}\widehat{c}_{\vec{k}'} - \widehat{c}^{\dagger}_{\vec{k}'+\vec{q}_2}\widehat{c}_{\vec{k}'}\widehat{c}^{\dagger}_{\vec{k}+\vec{q}}\widehat{c}_{\vec{k}}\right) \\
&= \sum_{\vec{k},\vec{k}'} \left[\widehat{c}^{\dagger}_{\vec{k}+\vec{q}_1}\widehat{c}_{\vec{k}}\widehat{c}^{\dagger}_{\vec{k}'+\vec{q}_2}\widehat{c}_{\vec{k}'} \pm \widehat{c}^{\dagger}_{\vec{k}'+\vec{q}_2}\widehat{c}^{\dagger}_{\vec{k}+\vec{q}_1}\widehat{c}_{\vec{k}'}\widehat{c}_{\vec{k}} - \widehat{c}^{\dagger}_{\vec{k}'+\vec{q}_2}\widehat{c}_{\vec{k}}\delta_{\vec{k}+\vec{q}_1,\vec{k}'}\right] \\
&= \sum_{\vec{k},\vec{k}'} \Big[\widehat{c}^{\dagger}_{\vec{k}+\vec{q}_1}\widehat{c}_{\vec{k}}\widehat{c}^{\dagger}_{\vec{k}'+\vec{q}_2}\widehat{c}_{\vec{k}'} - \widehat{c}^{\dagger}_{\vec{k}+\vec{q}_1}\widehat{c}_{\vec{k}}\widehat{c}^{\dagger}_{\vec{k}'+\vec{q}_2}\widehat{c}_{\vec{k}'} \\
&\quad + \widehat{c}^{\dagger}_{\vec{k}+\vec{q}_1}\widehat{c}_{\vec{k}'}\delta_{\vec{k},\vec{k}'+\vec{q}_2} - \widehat{c}^{\dagger}_{\vec{k}'+\vec{q}_2}\widehat{c}_{\vec{k}}\delta_{\vec{k}+\vec{q}_1,\vec{k}'}\Big] \\
&= \sum_{\vec{k}} \left(\widehat{c}^{\dagger}_{\vec{k}+\vec{q}_2+\vec{q}_1}\widehat{c}_{\vec{k}} - \widehat{c}^{\dagger}_{\vec{k}+\vec{q}_1+\vec{q}_2}\widehat{c}_{\vec{k}}\right) \\
&= 0.
\end{aligned} \tag{2.30}$$

During the calculation we had to distinguish between fermionic impurities or bosonic impurities for the sign, the result however does not depend on the nature of the impurity. The density-current commutator gives:

$$\begin{aligned}
\left[\rho_{\vec{q}_1}, \vec{j}_{\vec{q}_2}\right] &= \frac{\hbar}{m}\sum_{\vec{k},\vec{k}'} \left(\vec{k}'+\frac{\vec{q}_2}{2}\right)\left[\widehat{c}^{\dagger}_{\vec{k}+\vec{q}_1}\widehat{c}_{\vec{k}}, \widehat{c}^{\dagger}_{\vec{k}'+\vec{q}_2}\widehat{c}_{\vec{k}'}\right] \\
&= \frac{\hbar}{m}\sum_{\vec{k},\vec{k}'} \vec{k}'\left[\widehat{c}^{\dagger}_{\vec{k}+\vec{q}_1}\widehat{c}_{\vec{k}}, \widehat{c}^{\dagger}_{\vec{k}'+\vec{q}_2}\widehat{c}_{\vec{k}'}\right] + \frac{\hbar}{m}\frac{\vec{q}_2}{2}\left[\widehat{\rho}_{\vec{q}_1}, \widehat{\rho}_{\vec{q}_2}\right] \\
&= \frac{\hbar}{m}\sum_{\vec{k},\vec{k}'} \vec{k}'\left[\widehat{c}^{\dagger}_{\vec{k}+\vec{q}_1}\widehat{c}_{\vec{k}'}\delta_{\vec{k},\vec{k}'+\vec{q}_2} - \widehat{c}^{\dagger}_{\vec{k}'+\vec{q}_2}\widehat{c}_{\vec{k}}\delta_{\vec{k}+\vec{q}_1,\vec{k}'}\right] \\
&= \frac{\hbar}{m}\sum_{\vec{k}} \left[\vec{k}\widehat{c}^{\dagger}_{\vec{k}-\vec{q}_2+\vec{q}_1}\widehat{c}_{\vec{k}} - \left(\vec{k}+\vec{q}_1\right)\widehat{c}^{\dagger}_{\vec{k}+\vec{q}_1+\vec{q}_2}\widehat{c}_{\vec{k}}\right] \\
&= -\frac{\hbar}{m}\vec{q}_1\widehat{\rho}_{\vec{q}_1+\vec{q}_2}.
\end{aligned} \tag{2.31}$$

This can be used to calculate φ (note from (2.28) that $\widehat{\vec{j}}^{\dagger}_{\vec{q}} = \widehat{\vec{j}}_{-\vec{q}}$):

$$\begin{aligned}
\varphi &= \left\langle \left[\widehat{\rho}_{\vec{k}}, \widehat{\dot{\rho}}^{\dagger}_{\vec{k}} \right] \right\rangle \\
&= -i\vec{k}. \left\langle \left[\widehat{\rho}_{\vec{k}}, \widehat{\vec{j}}^{\dagger}_{\vec{k}} \right] \right\rangle \\
&= i\frac{\hbar}{m} k^2 \left\langle \widehat{\rho}_0 \right\rangle \\
&= i\frac{\hbar k^2}{m_I} N_I, \qquad (2.32)
\end{aligned}$$

With N_I the number of impurities which we consider one: $N_I = 1$. We also need the current-current commutator:

$$\begin{aligned}
\left[\widehat{\vec{j}}_{\vec{q}_1}, \widehat{\vec{j}}_{\vec{q}_2} \right] &= \left(\frac{\hbar}{m}\right)^2 \sum_{\vec{k},\vec{k}'} \left(\vec{k} + \frac{\vec{q}_1}{2}\right) \left(\vec{k}' + \frac{\vec{q}_2}{2}\right) \left[\widehat{c}^{\dagger}_{\vec{k}+\vec{q}_1} \widehat{c}_{\vec{k}}, \widehat{c}^{\dagger}_{\vec{k}'+\vec{q}_2} \widehat{c}_{\vec{k}'} \right] \\
&= \left(\frac{\hbar}{m}\right)^2 \sum_{\vec{k},\vec{k}'} \left(\vec{k} + \frac{\vec{q}_1}{2}\right) \left(\vec{k}' + \frac{\vec{q}_2}{2}\right) \left[\widehat{c}^{\dagger}_{\vec{k}+\vec{q}_1} \widehat{c}_{\vec{k}'} \delta_{\vec{k},\vec{k}'+\vec{q}_2} - \widehat{c}^{\dagger}_{\vec{k}'+\vec{q}_2} \widehat{c}_{\vec{k}} \delta_{\vec{k}+\vec{q}_1,\vec{k}'} \right] \\
&= \left(\frac{\hbar}{m}\right)^2 \sum_{\vec{k}} \left[\left(\vec{k} + \vec{q}_2 + \frac{\vec{q}_1}{2}\right) \left(\vec{k} + \frac{\vec{q}_2}{2}\right) \right. \\
&\quad \left. - \left(\vec{k} + \frac{\vec{q}_1}{2}\right) \left(\vec{k} + \vec{q}_1 + \frac{\vec{q}_2}{2}\right) \right] \widehat{c}^{\dagger}_{\vec{k}+\vec{q}_1+\vec{q}_2} \widehat{c}_{\vec{k}} \\
&= -\left(\frac{\hbar}{m}\right)^2 \sum_{\vec{k}} \left[\vec{k}. (\vec{q}_1 - \vec{q}_2) + \frac{q_2^2}{2} - \frac{q_1^2}{2} \right] \widehat{c}^{\dagger}_{\vec{k}+\vec{q}_1+\vec{q}_2} \widehat{c}_{\vec{k}}. \qquad (2.33)
\end{aligned}$$

This can be used to calculate $O\left(z, \vec{k}\right)$:

$$\begin{aligned}
O\left(z, \vec{k}\right) &= \frac{z}{\varphi} \left\langle \left[\widehat{L\rho}_{\vec{k}}, \widehat{\dot{\rho}}^{\dagger}_{\vec{k}} \right] \right\rangle \\
&= -i\frac{z}{\varphi} \left\langle \left[\widehat{\dot{\rho}}_{\vec{k}}, \widehat{\dot{\rho}}^{\dagger}_{\vec{k}} \right] \right\rangle \\
&= -i\frac{z}{\varphi} \left\langle \left[\vec{k}.\widehat{\vec{j}}_{\vec{k}}, \vec{k}.\widehat{\vec{j}}_{-\vec{k}} \right] \right\rangle \\
&= 2i\frac{z}{\varphi} \frac{\hbar k^2}{m_I^2} \vec{k}. \left\langle \widehat{\vec{p}} \right\rangle \\
&= 0, \qquad (2.34)
\end{aligned}$$

with $\widehat{\vec{p}} = \sum_{\vec{k}} \hbar\vec{k} \widehat{c}^{\dagger}_{\vec{k}} \widehat{c}_{\vec{k}}$ the momentum operator of the impurity of which the expectation value gives zero since the unperturbed system is at rest. We also need the commutator of the current operator with the Hamiltonian, only the interaction term results in a non-vanishing commutator and gives:

$$\begin{aligned}
\left[\widehat{H}, \widehat{\vec{j}}_{\vec{k}} \right] &= \sum_{\vec{q}} V_{\vec{q}} \left(\widehat{\alpha}_{\vec{q}} + \widehat{\alpha}^{\dagger}_{-\vec{q}} \right) \left[\widehat{\rho}_{\vec{q}}, \widehat{\vec{j}}_{\vec{k}} \right] \\
&= -\frac{\hbar}{m} \sum_{\vec{q}} V_{\vec{q}} \left(\widehat{\alpha}_{\vec{q}} + \widehat{\alpha}^{\dagger}_{-\vec{q}} \right) \vec{q} \widehat{\rho}_{\vec{q}+\vec{k}} \qquad (2.35)
\end{aligned}$$

This leads to the following expression for the $\widehat{\mathcal{B}}_{\vec{k}}$ operator:

$$\begin{aligned}\widehat{\mathcal{B}}_{\vec{k}} &= \widehat{L}\widehat{\dot{\rho}}_{\vec{k}} \\ &= i\vec{k}.\widehat{L}\widehat{\vec{j}}_{\vec{k}} \\ &= \frac{i\vec{k}}{\hbar}.\left[\widehat{H},\widehat{\vec{j}}_{\vec{k}}\right] \\ &= -\frac{i}{m_I}\vec{k}.\sum_{\vec{q}} V_{\vec{q}}\left(\widehat{\alpha}_{\vec{q}}+\widehat{\alpha}^{\dagger}_{-\vec{q}}\right)\vec{q}\widehat{\rho}_{\vec{k}+\vec{q}}. \end{aligned} \tag{2.36}$$

Using this in the expression for the memory function (2.26) leads to

$$\begin{aligned}\Sigma\left(\omega,\vec{k}\right) &= \frac{i}{\hbar m_I}\sum_{\vec{q}\neq 0}|V_{\vec{q}}|^2\frac{\left(\vec{k}.\vec{q}\right)^2}{k^2}\int_0^{\infty}dt\left(1-e^{i\omega t}\right) \\ &\quad\times\left\langle\left[\left(\widehat{\alpha}_{\vec{q}}(t)+\widehat{\alpha}^{\dagger}_{-\vec{q}}(t)\right)\widehat{\rho}_{\vec{k}+\vec{q}}(t)\,,\left(\widehat{\alpha}^{\dagger}_{\vec{q}}+\widehat{\alpha}_{-\vec{q}}\right)\widehat{\rho}^{\dagger}_{\vec{k}+\vec{q}}\right]\right\rangle. \end{aligned} \tag{2.37}$$

Note that the time dependence of the operators is determined by the new Liouville operator $\widehat{\mathcal{L}}$ for which we do not have an analytical expression.

2.3.1 Feynman-Hellwarth-Iddings-Platzman approximation

To proceed in the calculation of the density-density correlation function (2.19) we now apply an approximation in the expression for the memory function (2.37). We use the Feynman-Hellwarth-Iddings-Platzman approximation from Ref. [60] of which it was shown in Refs. [29, 127] that in the present formalism it corresponds to the replacement of the new Liouville operator $\widehat{\mathcal{L}}$ by the sum of the Liouville operator of the free Bogoliubov excitations $\widehat{L}_{bos}$ and the Liouville operator of the Feynman model system $\widehat{L}_F$: $\mathcal{L}\rightarrow\widehat{L}_{bos}+\widehat{L}_F$, this gives:

$$\begin{aligned}&\left\langle\left[\left(\widehat{\alpha}_{\vec{q}}(t)+\widehat{\alpha}^{\dagger}_{-\vec{q}}(t)\right)\widehat{\rho}_{\vec{k}+\vec{q}}(t)\,,\left(\widehat{\alpha}^{\dagger}_{\vec{q}}+\widehat{\alpha}_{-\vec{q}}\right)\widehat{\rho}^{\dagger}_{\vec{k}+\vec{q}}\right]\right\rangle \\ \rightarrow\quad&\left\langle\left(\widehat{\alpha}_{\vec{q}}(t)+\widehat{\alpha}^{\dagger}_{-\vec{q}}(t)\right)\left(\widehat{\alpha}^{\dagger}_{\vec{q}}+\widehat{\alpha}_{-\vec{q}}\right)\right\rangle_{bos}\left\langle\widehat{\rho}_{\vec{k}+\vec{q}}(t)\,\widehat{\rho}^{\dagger}_{\vec{k}+\vec{q}}\right\rangle_F \\ &-\left\langle\left(\widehat{\alpha}^{\dagger}_{\vec{q}}+c_{-\vec{q}}\right)\left(\widehat{\alpha}_{\vec{q}}(t)+\widehat{\alpha}^{\dagger}_{-\vec{q}}(t)\right)\right\rangle_{bos}\left\langle\widehat{\rho}^{\dagger}_{\vec{k}+\vec{q}}\widehat{\rho}_{\vec{k}+\vec{q}}(t)\right\rangle_F \end{aligned} \tag{2.38}$$

We can now calculate the expectation values , we start with the expectation values with respect to the free Bogoliubov excitations:

$$\begin{aligned}
\left\langle \left(\widehat{\alpha}_{\vec{q}}(t)+\widehat{\alpha}^{\dagger}_{-\vec{q}}(t)\right)\left(\widehat{\alpha}^{\dagger}_{\vec{q}}+\widehat{\alpha}_{-\vec{q}}\right)\right\rangle_{bos} &= \left\langle \widehat{\alpha}_{\vec{q}}(t)\,\widehat{\alpha}^{\dagger}_{\vec{q}}\right\rangle_{bos}+\left\langle \widehat{\alpha}^{\dagger}_{-\vec{q}}(t)\,\widehat{\alpha}_{-\vec{q}}\right\rangle_{bos} \\
&= e^{-i\omega_{\vec{q}}t}\left\langle \widehat{\alpha}_{\vec{q}}\widehat{\alpha}^{\dagger}_{\vec{q}}\right\rangle_{bos}+e^{i\omega_{\vec{q}}t}\left\langle \widehat{\alpha}^{\dagger}_{-\vec{q}}\widehat{\alpha}_{-\vec{q}}\right\rangle_{bos} \\
&= e^{-i\omega_{\vec{q}}t}\left(n_{\vec{q}}+1\right)+e^{i\omega_{\vec{q}}t}n_{\vec{q}} \\
&= e^{-i\omega_{\vec{q}}t}+2\cos\left(\omega_{\vec{q}}t\right)n_{\vec{q}}; \qquad (2.39) \\
\left\langle \left(\widehat{\alpha}^{\dagger}_{\vec{q}}+\widehat{\alpha}_{-\vec{q}}\right)\left(\widehat{\alpha}_{\vec{q}}(t)+\widehat{\alpha}^{\dagger}_{-\vec{q}}(t)\right)\right\rangle_{bos} &= \left\langle \widehat{\alpha}^{\dagger}_{\vec{q}}\widehat{\alpha}_{\vec{q}}(t)\right\rangle_{bos}+\left\langle \widehat{\alpha}^{\dagger}_{-\vec{q}}\widehat{\alpha}_{-\vec{q}}(t)\right\rangle_{bos} \\
&= e^{-i\omega_{\vec{q}}t}\left\langle \widehat{\alpha}^{\dagger}_{\vec{q}}\widehat{\alpha}_{\vec{q}}\right\rangle_{bos}+e^{i\omega_{\vec{q}}t}\left\langle \widehat{\alpha}^{\dagger}_{-\vec{q}}\widehat{\alpha}_{-\vec{q}}\right\rangle_{bos} \\
&= e^{-i\omega_{\vec{q}}t}n_{\vec{q}}+e^{i\omega_{\vec{q}}t}\left(n_{\vec{q}}+1\right) \\
&= e^{i\omega_{\vec{q}}t}+2\cos\left(\omega_{\vec{q}}t\right)n_{\vec{q}}. \qquad (2.40)
\end{aligned}$$

Here $\omega_{\vec{q}}$ is the dispersion of the bosons (we also used $\omega_{\vec{q}}=\omega_{-\vec{q}}$) and $n_{\vec{q}}$ is the Bose-Einstein distribution: $n_{\vec{q}}=\left(\exp\left[\beta\omega_{\vec{q}}\right]-1\right)^{-1}$. Within the Feynman model system the density-density correlation is given by [133]

$$\left\langle \widehat{\rho}^{\dagger}_{\vec{q}}\widehat{\rho}_{\vec{q}}(t)\right\rangle=\left\langle \widehat{\rho}_{\vec{q}}(-t)\,\widehat{\rho}^{\dagger}_{\vec{q}}(0)\right\rangle=\exp\left(-q^{2}D\left(t\right)\right), \qquad (2.41)$$

with

$$\begin{aligned}
D\left(t\right) &= \frac{t^{2}}{2\beta\left(m_{I}+M\right)}-i\frac{\hbar}{2\left(m_{I}+M\right)}t \\
&\quad+\frac{\hbar M}{2m_{I}\Omega(m_{I}+M)}\left(1-\exp\left(i\Omega t\right)+4\sin^{2}\left(\frac{\Omega t}{2}\right)n\left(\Omega\right)\right). \qquad (2.42)
\end{aligned}$$

The resulting expression for the memory function (2.37) is

$$\begin{aligned}
\Sigma\left(\omega,\vec{k}\right) &= \frac{2}{\hbar m_{I}}\sum_{\vec{q}\neq 0}\left|V_{\vec{q}}\right|^{2}\frac{\left(\vec{k}.\vec{q}\right)^{2}}{k^{2}}\int_{0}^{\infty}dt\left(1-e^{i\omega t}\right) \\
&\quad\times\mathrm{Im}\left\{\left[e^{i\omega_{\vec{q}}t}+2\cos\left(\omega_{\vec{q}}t\right)n_{\vec{q}}\right]\exp\left[-\left(\vec{k}+\vec{q}\right)^{2}D\left(t\right)\right]\right\}. \qquad (2.43)
\end{aligned}$$

2.3.2 Extended memory function formalism

In Ref. [61] it was noted that for the solid state polaron the linewidth of the RES-peaks as calculated with the Feyman-Hellwarth-Iddings-Platzman approximation violates the Heisenberg uncertainty relation for $\alpha > 7$. This can be resolved by using the extended memory function formalism, as presented in Ref. [63], where dissipation was considered by introducing a finite lifetime τ for the eigenstates of the Feynman model system. This corresponds to replacing the term $\exp\left(-i\Omega t\right)$ in equation (2.42) by $\left(1+it/\tau\right)^{-\Omega\tau}$. The original expression is retrieved in the limit $\tau\rightarrow\infty$.

2.3.3 Second representation for the imaginary part of the memory function

The integrals in the memory function (2.43) can not be calculated analytically and further calculations have to be done numerically. Expression (2.43) is however not convenient for numerical calculations because of slow convergence. This is especially troublesome for the imaginary part of $\Sigma\left(\omega,\vec{k}\right)$ and because of this we will use another representation for the imaginary part of the memory function [127]:

$$\begin{aligned}\mathrm{Im}\left[\Sigma\left(\omega,\vec{k}\right)\right] &= -\frac{\pi}{\hbar m_I}\left(\frac{\beta\left(m_I+M\right)}{2\pi}\right)^{1/2}\left(1-e^{-\hbar\beta\omega}\right)\\ &\sum_{\vec{q}\neq 0}\sum_{n,n'}^{\infty}\left|V_{\vec{q}}\right|^2 e^{-\left(\vec{k}+\vec{q}\right)^2 a^2(\beta)}\frac{\left(\vec{k}.\vec{q}\right)^2}{k^2}B\left(\beta,n,n'\right)\left|\vec{k}+\vec{q}\right|^{2(n+n')-1}\\ &\left[n_{\vec{q}}e^{-\frac{\beta\left(M+m_I\right)A^{-}_{n-n'}(\omega)^2}{2\left(\vec{k}+\vec{q}\right)^2}}+\left(1+n_{\vec{q}}\right)e^{-\frac{\beta\left(M+m_I\right)A^{+}_{n-n'}(\omega)^2}{2\left(\vec{k}+\vec{q}\right)^2}}\right]; \quad (2.44)\end{aligned}$$

where the following notation was used:

$$a^2\left(\beta\right) = \frac{\hbar M}{2m_I\Omega(m_I+M)}\coth\left[\frac{\hbar\beta\Omega}{2}\right]; \quad (2.45)$$

$$B\left(\beta,n,n'\right) = \frac{1}{n!}\frac{1}{n'!}\left[a^2\left(1+n\left(\Omega\right)\right)\right]^n\left[a^2 n\left(\Omega\right)\right]^{n'}; \quad (2.46)$$

$$A^{\pm}_n\left(\omega\right) = \pm\omega_{\vec{q}}+\frac{\hbar\left(\vec{k}+\vec{q}\right)^2}{2\left(m_I+M\right)}+n\Omega-\omega. \quad (2.47)$$

The real part of the memory function can also be rewritten within this representation which leads to an extensive function which does not offer a computational advantage. For this reason we use the real part of expression (2.43) for the numerical calculations.

2.3.4 Third representation for the memory function

Here the memory function (2.43) is rewritten in a yet another representation, more suited for numerical calculations. The advantage of this representation is that it also yields a more convenient expression for the real part. This was not the case with the representation of the previous section. The derivation is based on the treatment of the optical absorption of the solid state polaron, as presented in Refs. [61, 127]. We start by rewriting $D\left(t\right)$ (2.42):

$$\begin{aligned}D\left(t\right) &= \frac{t^2}{2\beta\left(m_I+M\right)}-i\frac{\hbar}{2\left(m_I+M\right)}t\\ &+\frac{\hbar M}{2m_I\Omega\left(m_I+M\right)}\left\{\coth\left(\frac{\hbar\beta\Omega}{2}\right)-\left[1+n\left(\Omega\right)\right]e^{i\Omega t}-n\left(\Omega\right)e^{-i\Omega t}\right\}, \quad (2.48)\end{aligned}$$

which allows us to write

$$e^{-k^2 D(t)} = e^{-a^2(\beta)k^2} \sum_{n,n'} k^{2(n+n')} B\left(\beta, n, n'\right) e^{-\frac{k^2 t^2}{2\beta\left(m_I+M\right)} + it\left[\frac{k^2\hbar}{2\left(m_I+M\right)} + \Omega(n-n')\right]}, \quad (2.49)$$

with the functions $a\left(\beta\right)$ and $B\left(\beta, n, n'\right)$ as defined in (2.45) and (2.46), respectively. Using (2.49) in the expression for the memory function (2.43) leads to

$$\begin{aligned}\Sigma\left(\omega, \vec{k}\right) = \frac{2}{m_I N\hbar} \sum_{n,n'=0}^{\infty} \sum_{\vec{q}\neq 0} \left|V_{\vec{q}}\right|^2 \frac{\left(\vec{k}.\vec{q}\right)^2}{k^2} \left|\vec{k}+\vec{q}\right|^{2(n+n')} B\left(\beta, n, n'\right) \\ \times e^{-a^2(\beta)\left(\vec{k}+\vec{q}\right)^2} \int_0^{\infty} dt \left(1 - e^{i\omega t}\right) \mathrm{Im}\left\{\left[1 + n\left(\omega_{\vec{q}}\right)\right] e^{-\frac{\left(\vec{k}+\vec{q}\right)^2}{2\beta\left(m_I+M\right)} t^2 + iA^+_{n-n'}t} \right. \\ \left. + n\left(\omega_{\vec{q}}\right) e^{-\frac{\left(\vec{k}+\vec{q}\right)^2}{2\beta\left(m_I+M\right)} t^2 + iA^-_{n-n'}t}\right\}, \end{aligned} \quad (2.50)$$

with $A^{\pm}_n = A^{\pm}_n\left(0\right)$. We now consider the imaginary and the real part of the memory function separately. Taking the imaginary part of (2.50) results in:

$$\begin{aligned}\mathrm{Im}\left[\Sigma\left(\omega, \vec{k}\right)\right] = -\frac{2}{m_I N\hbar} \sum_{n,n'=0}^{\infty} \sum_{\vec{q}\neq 0} \left|V_{\vec{q}}\right|^2 \frac{\left(\vec{k}.\vec{q}\right)^2}{k^2} \left(\vec{k}+\vec{q}\right)^{2(n+n')} B\left(\beta, n, n'\right) \\ \times e^{-a^2(\beta)\left(\vec{k}+\vec{q}\right)^2} \mathrm{Im}\left(\int_0^{\infty} dt \sin\left(\omega t\right) \left\{\left[1 + n\left(\omega_{\vec{q}}\right)\right] e^{-\frac{\left(\vec{k}+\vec{q}\right)^2}{2\beta\left(m_I+M\right)} t^2 + iA^+_{n-n'}t} \right.\right. \\ \left.\left. + n\left(\omega_{\vec{q}}\right) e^{-\frac{\left(\vec{k}+\vec{q}\right)^2}{2\beta\left(m_I+M\right)} t^2 + iA^-_{n-n'}t}\right\}\right). \end{aligned} \quad (2.51)$$

For the time integration we have (with $C^2 = \frac{\left(\vec{k}+\vec{q}\right)^2}{2\beta\left(m_I+M\right)}$):

$$\begin{aligned}&\int_0^{\infty} dt \sin\left(\omega t\right) \left\{\left[1 + n\left(\omega_{\vec{q}}\right)\right] e^{-C^2t^2 + iA^+_{n-n'}t} + n\left(\omega_{\vec{q}}\right) e^{-C^2t^2 + iA^-_{n-n'}t}\right\} \\ &= \frac{1}{2iC} \left\{\left[1 + n\left(\omega_{\vec{q}}\right)\right] \left[\frac{\sqrt{\pi}}{2} e^{-\frac{\left(A^+_{n-n'}+\omega\right)^2}{4C^2}} + iF\left(\frac{A^+_{n-n'}+\omega}{2C}\right) - \frac{\sqrt{\pi}}{2} e^{-\frac{\left(A^+_{n-n'}-\omega\right)^2}{4C^2}} \right.\right. \\ &\left. - iF\left(\frac{A^+_{n-n'}-\omega}{2C}\right)\right] + n\left(\omega_{\vec{q}}\right) \left[\frac{\sqrt{\pi}}{2} e^{-\frac{\left(A^-_{n-n'}+\omega\right)^2}{4C^2}} + iF\left(\frac{A^-_{n-n'}+\omega}{2C}\right) \right. \\ &\left.\left. - \frac{\sqrt{\pi}}{2} e^{-\frac{\left(A^-_{n-n'}-\omega\right)^2}{4C^2}} - iF\left(\frac{A^-_{n-n'}-\omega}{2C}\right)\right]\right\}, \end{aligned} \quad (2.52)$$

where the Dawson function $F\left(x\right)$ was introduced:

$$\begin{aligned}F\left(x\right) &= e^{-x^2} \int_0^x e^{y^2} dy \\ &= \frac{1}{2}\sqrt{\pi} e^{-x^2} \mathrm{erfi}\left(x\right), \end{aligned} \quad (2.53)$$

where erfi(x) is the imaginary error function: erfi$(x) = -i\,\mathrm{erf}\,(ix)$, with erf (x) the error function. This results in the following expression for the imaginary part of the memory function:

$$\begin{aligned}\mathrm{Im}\left[\Sigma\left(\omega,\vec{k}\right)\right] = \frac{\sqrt{2\pi\beta\left(m_I+M\right)}}{2m_I N\hbar}\sum_{n,n'=0}^{\infty}\sum_{\vec{q}\neq 0}|V_{\vec{q}}|^2\,\frac{\left(\vec{k}.\vec{q}\right)^2}{k^2}\left(\vec{k}+\vec{q}\right)^{2(n+n')-1}\\ \times B\left(\beta,n,n'\right)e^{-a^2(\beta)\left(\vec{k}+\vec{q}\right)^2}\\ \times\left\{\left[1+n\left(\omega_{\vec{q}}\right)\right]\left[e^{-\frac{\beta\left(m_I+M\right)\left(A^+_{n-n'}+\omega\right)^2}{2\left(\vec{k}+\vec{q}\right)^2}}-e^{-\frac{\beta\left(m_I+M\right)\left(A^+_{n-n'}-\omega\right)^2}{2\left(\vec{k}+\vec{q}\right)^2}}\right]\right.\\ \left.+n\left(\omega_{\vec{q}}\right)\left[e^{-\frac{\beta\left(m_I+M\right)\left(A^-_{n-n'}+\omega\right)^2}{2\left(\vec{k}+\vec{q}\right)^2}}-e^{-\frac{\beta\left(m_I+M\right)\left(A^-_{n-n'}-\omega\right)^2}{2\left(\vec{k}+\vec{q}\right)^2}}\right]\right\}. \qquad (2.54)\end{aligned}$$

The real part of (2.50) is

$$\begin{aligned}\mathrm{Re}\left[\Sigma\left(\omega,\vec{k}\right)\right] = \frac{2}{m_I N\hbar}\sum_{n,n'=0}^{\infty}\sum_{\vec{q}\neq 0}|V_{\vec{q}}|^2\,\frac{\left(\vec{k}.\vec{q}\right)^2}{k^2}\left(\vec{k}+\vec{q}\right)^{2(n+n')}B\left(\beta,n,n'\right)\\ \times e^{-a^2(\beta)\left(\vec{k}+\vec{q}\right)^2}\,\mathrm{Im}\left(\int_0^{\infty}dt\left[1-\cos\left(\omega t\right)\right]\left\{\left[1+n\left(\omega_{\vec{q}}\right)\right]\right.\right.\\ \left.\left.\times e^{-\frac{\left(\vec{k}+\vec{q}\right)^2}{2\beta\left(m_I+M\right)}t^2+iA^+_{n-n'}t}+n\left(\omega_{\vec{q}}\right)e^{-\frac{\left(\vec{k}+\vec{q}\right)^2}{2\beta\left(m_I+M\right)}t^2+iA^-_{n-n'}t}\right\}\right). \qquad (2.55)\end{aligned}$$

In this case the time-integration is

$$\begin{aligned}\int_0^{\infty}dt\left[1-\cos\left(\omega t\right)\right]\left\{\left[1+n\left(\omega_{\vec{q}}\right)\right]e^{-C^2t^2+iA^+_{n-n'}t}+n\left(\omega_{\vec{q}}\right)e^{-C^2t^2+iA^-_{n-n'}t}\right\}\\ =\frac{1}{2C}\left\{\left[1+n\left(\omega_{\vec{q}}\right)\right]\left[\sqrt{\pi}e^{-\frac{\left(A^+_{n-n'}\right)^2}{4C^2}}+2iF\left(\frac{A^+_{n-n'}+\omega}{2C}\right)-\frac{\sqrt{\pi}}{2}e^{-\frac{\left(A^+_{n-n'}+\omega\right)^2}{4C^2}}\right.\right.\\ \left.-iF\left(\frac{A^+_{n-n'}+\omega}{2C}\right)-\frac{\sqrt{\pi}}{2}e^{-\frac{\left(A^+_{n-n'}+\omega\right)^2}{4C^2}}-iF\left(\frac{A^+_{n-n'}-\omega}{2C}\right)\right]\\ +n\left(\omega_{\vec{q}}\right)\left[\sqrt{\pi}e^{-\frac{\left(A^-_{n-n'}\right)^2}{4C^2}}+2iF\left(\frac{A^-_{n-n'}+\omega}{2C}\right)-\frac{\sqrt{\pi}}{2}e^{-\frac{\left(A^-_{n-n'}+\omega\right)^2}{4C^2}}\right.\\ \left.\left.-iF\left(\frac{A^-_{n-n'}+\omega}{2C}\right)-\frac{\sqrt{\pi}}{2}e^{-\frac{\left(A^-_{n-n'}+\omega\right)^2}{4C^2}}-iF\left(\frac{A^-_{n-n'}-\omega}{2C}\right)\right]\right\}. \qquad (2.56)\end{aligned}$$

This results in the following expression for the real part of the memory function:

$$
\begin{aligned}
&\mathrm{Re}\left[\Sigma\left(\omega,\vec{k}\right)\right] \\
&= \frac{\sqrt{2\beta\left(m_I+M\right)}}{m_I N\hbar}\sum_{n,n'=0}^{\infty}\sum_{\vec{q}\neq 0}\left|V_{\vec{q}}\right|^2\frac{\left(\vec{k}.\vec{q}\right)^2}{k^2}\left(\vec{k}+\vec{q}\right)^{2(n+n')-1}B\left(\beta,n,n'\right) \\
&e^{-a^2(\beta)\left(\vec{k}+\vec{q}\right)^2}\left(\left(1+n\left(\omega_{\vec{q}}\right)\right)\left\{2F\left[\frac{\sqrt{2\beta\left(m_I+M\right)}A^+_{n-n'}}{2\left|\vec{k}+\vec{q}\right|}\right]\right.\right. \\
&-F\left[\frac{\sqrt{2\beta\left(m_I+M\right)}\left(A^+_{n-n'}+\omega\right)}{2\left|\vec{k}+\vec{q}\right|}\right]-F\left[\frac{\sqrt{2\beta\left(m_I+M\right)}\left(A^+_{n-n'}-\omega\right)}{2\left|\vec{k}+\vec{q}\right|}\right]\Bigg\} \\
&+n\left(\omega_{\vec{q}}\right)\left\{2F\left[\frac{\sqrt{2\beta\left(m_I+M\right)}A^-_{n-n'}}{2\left|\vec{k}+\vec{q}\right|}\right]-F\left[\frac{\sqrt{2\beta\left(m_I+M\right)}\left(A^-_{n-n'}+\omega\right)}{2\left|\vec{k}+\vec{q}\right|}\right]\right. \\
&\left.\left.-F\left[\frac{\sqrt{2\beta\left(m_I+M\right)}\left(A^-_{n-n'}-\omega\right)}{2\left|\vec{k}+\vec{q}\right|}\right]\right\}\right). \qquad (2.57)
\end{aligned}
$$

Expressions (2.54) and (2.57) are well-suited for numerical calculations.

2.4 Optical absorption and link with the solid state polaron

If a charged polaron is considered (as for example in the case of the solid state polaron) the optical absorption can be calculated. Since the momentum of the photon is negligible we need to take the limit $\vec{k}\to 0$, this gives for the memory function:

$$
\begin{aligned}
\Sigma\left(\omega,\vec{k}\to 0\right) &= \frac{2}{3m\hbar}\sum_{\vec{q}}q^2\left|V_{\vec{q}}\right|^2\int_0^{\infty}dt\left(1-e^{i\omega t}\right) \\
&\quad\times\mathrm{Im}\left\{\left[e^{i\omega_{\vec{q}}t}+2\cos\left(\omega_{\vec{q}}t\right)n_{\vec{q}}\right]e^{-k^2D(t)}\right\} \\
&= \omega\Sigma\left(\omega\right) \qquad (2.58)
\end{aligned}
$$

with $\Sigma\left(\omega\right)$ as defined in Ref. [127]. The optical absorption is given by the real part of the optical conductivity $\sigma\left(\omega\right)$ which within the Kubo formalism can be written as a current-current correlation:

$$
\begin{aligned}
\mathrm{Re}\left[\sigma\left(\omega\right)\right] &= \mathrm{Re}\left[i\frac{e^2}{Vm\omega}+\frac{1}{\hbar\omega}\int_0^{\infty}dte^{i\omega t}\left\langle\left[\widehat{j}_x\left(t\right),\widehat{j}_x\right]\right\rangle\right] \\
&= \mathrm{Im}\left[\frac{i}{\hbar\omega}\int_0^{\infty}dte^{i\omega t}\left\langle\left[\widehat{j}_{\vec{k}=0}\left(t\right),\widehat{j}^{\dagger}_{\vec{k}=0}\right]\right\rangle\right], \qquad (2.59)
\end{aligned}
$$

with e the charge of the polaron. Applying two partial integrations leads to the following relation between the density-density correlation (2.3) and the current-current correlation:

$$\chi\left(\vec{k},\omega\right)=-\frac{i}{\hbar e^{2}\omega^{2}}\int_{0}^{\infty}dte^{i\omega t}\left\langle\left[\vec{k}.\widehat{j}_{\vec{k}}\left(t\right),\vec{k}.\widehat{j}_{\vec{k}}^{\dagger}\right]\right\rangle. \tag{2.60}$$

This allows us to write

$$\begin{aligned}\mathrm{Re}\left[\sigma\left(\omega\right)\right] &= \lim_{\vec{k}\rightarrow0}\mathrm{Im}\left[\frac{\omega e^{2}}{k^{2}}\chi\left(\omega,\vec{k}\right)\right]\\ &= \mathrm{Im}\left[\frac{e^{2}}{m_{I}}\frac{1}{\omega-\Sigma\left(\omega\right)}\right],\end{aligned} \tag{2.61}$$

which is the same result as was derived for the solid state polaron in Refs. [60, 61].

2.5 Response of the BEC-impurity polaron

The response of the system to Bragg spectroscopy (2.1) is proportional to the imaginary part of the density-density correlation (2.19), this gives [61]:

$$\mathrm{Im}\left[\chi\left(\vec{k},\omega\right)\right]=-\frac{k^{2}}{m_{I}}\frac{\mathrm{Im}\left[\Sigma\left(\omega,\vec{k}\right)\right]}{\left(\omega^{2}-\mathrm{Re}\left[\Sigma\left(\omega,\vec{k}\right)\right]\right)^{2}+\left(\mathrm{Im}\left[\Sigma\left(\omega,\vec{k}\right)\right]\right)^{2}}, \tag{2.62}$$

where we have used (2.34). We now introduce the interaction amplitude (1.26) for an impurity in a condensate, this gives for the memory function (2.43) (in the polaronic units of table 1.1):

$$\begin{aligned}\Sigma\left(\omega,\vec{k}\right) &= \frac{\alpha}{8\pi^{2}}\left(\frac{m_{B}+1}{m_{B}}\right)^{2}\int d\vec{q}\frac{q}{\sqrt{q+2}}\frac{\left(\vec{k}.\vec{q}\right)^{2}}{k^{2}}\int_{0}^{\infty}dt\left(1-e^{i\omega t}\right)\\ &\quad\times\mathrm{Im}\left\{\left[e^{i\omega_{\vec{q}}t}+2\cos\left(\omega_{\vec{q}}t\right)n_{\vec{q}}\right]\exp\left[-\left(\vec{k}+\vec{q}\right)^{2}D\left(t\right)\right]\right\},\end{aligned} \tag{2.63}$$

where $\omega_{\vec{k}}$ is the Bogoliubov dispersion (1.15).

2.5.1 Response at weak coupling

At weak polaronic coupling ($\alpha, V_{\vec{q}}\rightarrow0$) the memory function $\Sigma\left(\omega,\vec{k}\right)$ becomes small and the Bragg response (2.62) can be written as:

$$\mathrm{Im}\left[\chi^{W}\left(\omega,\vec{k}\right)\right]=-\frac{k^{2}}{m_{I}\omega^{4}}\mathrm{Im}\left[\Sigma^{W}\left(\omega,\vec{k}\right)\right]. \tag{2.64}$$

In the weak coupling limit the variational parameter M tends to zero and the imaginary part of the self energy (2.54) becomes:

$$\begin{aligned}\mathrm{Im}\left[\Sigma\left(\omega,\vec{k}\right)\right] = \sqrt{\frac{\pi\beta}{2\hbar^2 m_I}}\sum_{\vec{q}\neq 0}|V_{\vec{q}}|^2\,\frac{\left(\vec{k}.\vec{q}\right)^2}{k^2}\left|\vec{k}+\vec{q}\right|^{-1}\\ \times\left\{\left[1+n\left(\omega_{\vec{q}}\right)\right]\left[e^{-\frac{\beta m_I\left(A^+ +\omega\right)^2}{2\left(\vec{k}+\vec{q}\right)^2}}-e^{-\frac{\beta m_I\left(A^+ -\omega\right)^2}{2\left(\vec{k}+\vec{q}\right)^2}}\right]\right.\\ \left.+n\left(\omega_{\vec{q}}\right)\left[e^{-\frac{\beta m_I\left(A^- +\omega\right)^2}{2\left(\vec{k}+\vec{q}\right)^2}}-e^{-\frac{\beta m_I\left(A^- -\omega\right)^2}{2\left(\vec{k}+\vec{q}\right)^2}}\right]\right\},\end{aligned} \tag{2.65}$$

with:

$$A^{\pm} = \pm\omega_{\vec{q}} + \frac{\hbar\left(\vec{k}+\vec{q}\right)^2}{2m_I}. \tag{2.66}$$

Weak coupling calculation

We now present another derivation of the imaginary part of the density-density correlation of the Fröhlich polaron, valid at weak coupling. After four partial integrations the density-density correlation (2.3) can be written as (see section 6.1.2):

$$\begin{aligned}\chi\left(\omega,\vec{k}\right) &= \frac{i}{\hbar\omega^4}\frac{1}{m^2}\sum_{\vec{q}}|V_{\vec{q}}|^2\left(\vec{k}.\vec{q}\right)^2 \\ &\quad\times\int_0^\infty dt e^{i\omega t}\left\langle\left[\left(\widehat{\alpha}_{\vec{q}}(t)+\widehat{\alpha}^\dagger_{-\vec{q}}(t)\right)\widehat{\rho}_{\vec{k}+\vec{q}}(t)\,,\left(\widehat{\alpha}^\dagger_{\vec{q}}+\widehat{\alpha}_{-\vec{q}}\right)\widehat{\rho}^\dagger_{\vec{k}+\vec{q}}\right]\right\rangle.\end{aligned} \tag{2.67}$$

This expression is proportional to $|V_{\vec{q}}|^2$ and the lowest order polaronic effects are thus captured by calculating the expectation value with respect to the unperturbed system of a free impurity and a free gas of Bogoliubov excitations. This gives:

$$\begin{aligned}&\left\langle\left[\left(\widehat{\alpha}_{\vec{q}}(t)+\widehat{\alpha}^\dagger_{-\vec{q}}(t)\right)\widehat{\rho}_{\vec{k}+\vec{q}}(t)\,,\left(\widehat{\alpha}^\dagger_{\vec{q}}+\widehat{\alpha}_{-\vec{q}}\right)\widehat{\rho}^\dagger_{\vec{k}+\vec{q}}\right]\right\rangle_0 \\ =\;&\left\langle\left(\widehat{\alpha}_{\vec{q}}(t)+\widehat{\alpha}^\dagger_{-\vec{q}}(t)\right)\left(\widehat{\alpha}^\dagger_{\vec{q}}+\widehat{\alpha}_{-\vec{q}}\right)\right\rangle_0\left\langle\widehat{\rho}_{\vec{k}+\vec{q}}(t)\,\widehat{\rho}^\dagger_{\vec{k}+\vec{q}}\right\rangle_0 \\ &-\left\langle\left(\widehat{\alpha}^\dagger_{\vec{q}}+\widehat{\alpha}_{-\vec{q}}\right)\left(\widehat{\alpha}_{\vec{q}}(t)+\widehat{\alpha}^\dagger_{-\vec{q}}(t)\right)\right\rangle_0\left\langle\widehat{\rho}^\dagger_{\vec{k}+\vec{q}}\widehat{\rho}_{\vec{k}+\vec{q}}(t)\right\rangle_0 \\ =\;&\left(\left\langle\widehat{\alpha}_{\vec{q}}(t)\,\widehat{\alpha}^\dagger_{\vec{q}}\right\rangle_0+\left\langle\widehat{\alpha}^\dagger_{-\vec{q}}(t)\,\widehat{\alpha}_{-\vec{q}}\right\rangle_0\right)\left\langle\widehat{\rho}_{\vec{k}+\vec{q}}(t)\,\widehat{\rho}^\dagger_{\vec{k}+\vec{q}}\right\rangle_0 \\ &-\left(\left\langle\widehat{\alpha}^\dagger_{\vec{q}}\widehat{\alpha}_{\vec{q}}(t)\right\rangle_0+\left\langle\widehat{\alpha}_{-\vec{q}}\widehat{\alpha}^\dagger_{-\vec{q}}(t)\right\rangle_0\right)\left\langle\widehat{\rho}^\dagger_{\vec{k}+\vec{q}}\widehat{\rho}_{\vec{k}+\vec{q}}(t)\right\rangle_0 \\ =\;&\left(e^{-i\omega_{\vec{q}}t}\left(1+n\left(\omega_{\vec{q}}\right)\right)+e^{i\omega_{\vec{q}}t}n\left(\omega_{\vec{q}}\right)\right)\left\langle\widehat{\rho}_{\vec{k}+\vec{q}}(t)\,\widehat{\rho}^\dagger_{\vec{k}+\vec{q}}\right\rangle_0 \\ &-\left(e^{-i\omega_{\vec{q}}t}n\left(\omega_{\vec{q}}\right)+e^{i\omega_{\vec{q}}t}\left(1+n\left(\omega_{\vec{q}}\right)\right)\right)\left\langle\widehat{\rho}^\dagger_{\vec{k}+\vec{q}}\widehat{\rho}_{\vec{k}+\vec{q}}(t)\right\rangle_0.\end{aligned} \tag{2.68}$$

For a free impurity we have:

$$\begin{aligned}\left\langle \widehat{\rho}_{\vec{k}+\vec{q}}(t)\,\widehat{\rho}^{\dagger}_{\vec{k}+\vec{q}}\right\rangle_0 &= \left(\left\langle \widehat{\rho}^{\dagger}_{\vec{k}+\vec{q}}\widehat{\rho}_{\vec{k}+\vec{q}}(t)\right\rangle_0\right)^* \\ &= \exp\left(-i\frac{\hbar k^2}{2m_I}t-\frac{k^2t^2}{2m_I\beta}\right). \end{aligned} \tag{2.69}$$

This gives (with $A^{\pm}$ as defined in (2.66)):

$$\begin{aligned}\chi\left(\omega,\vec{k}\right) &= \frac{i}{\hbar\omega^4}\frac{1}{m^2}\sum_{\vec{q}}|V_{\vec{q}}|^2\left(\vec{k}.\vec{q}\right)^2 \\ &\quad\times\int_0^{\infty}dt\left\{n\left(\omega_{\vec{q}}\right)\left[e^{i\left(\omega-A^-\right)t-\frac{\left(\vec{k}+\vec{q}\right)^2t^2}{2m_I\beta}}-e^{i\left(\omega+A^-\right)t-\frac{\left(\vec{k}+\vec{q}\right)^2t^2}{2m_I\beta}}\right]\right. \\ &\quad\left.+\left(1+n\left(\omega_{\vec{q}}\right)\right)\left[e^{i\left(\omega-A^+\right)t-\frac{\left(\vec{k}+\vec{q}\right)^2t^2}{2m_I\beta}}-e^{i\left(\omega+A^+\right)t-\frac{\left(\vec{k}+\vec{q}\right)^2t^2}{2m_I\beta}}\right]\right\}. \end{aligned} \tag{2.70}$$

Taking the imaginary part of expression (2.70) and performing the t-integral gives:

$$\begin{aligned}\mathrm{Im}\left[\chi\left(\omega,\vec{k}\right)\right] &= -\frac{k^2}{m_I\omega^4}\sqrt{\frac{\beta\pi}{2\hbar^2m_I}}\sum_{\vec{q}}|V_{\vec{q}}|\,\frac{\left(\vec{k}.\vec{q}\right)^2}{k^2}\left|\vec{k}+\vec{q}\right|^{-1} \\ &\quad\times\left\{\left(n\left(\omega_{\vec{q}}\right)\left[e^{-\frac{\beta m_I\left(\omega+A^-\right)^2}{2\left(\vec{k}+\vec{q}\right)^2}}-e^{-\frac{\beta m_I\left(\omega-A^-\right)^2}{2\left(\vec{k}+\vec{q}\right)^2}}\right]\right.\right. \\ &\quad\left.\left.+\left(1+n\left(\omega_{\vec{q}}\right)\right)\left[e^{-\frac{\beta m_I\left(\omega+A^+\right)^2}{2\left(\vec{k}+\vec{q}\right)^2}}-e^{-\frac{\beta m_I\left(\omega-A^+\right)^2}{2\left(\vec{k}+\vec{q}\right)^2}}\right]\right\}. \end{aligned} \tag{2.71}$$

This result coincides with the weak coupling limit from above. Furthermore, in the limit of vanishing momentum exchange $\vec{k}\to 0$ this becomes the weak coupling result obtained in the framework of Gurevich, Lang and Firsov [58, 134].

2.6 Mass sum rule

In the context of the solid state polaron it was shown that the f-sum rule for the optical absorption of the polaron at temperature zero can be written as [128]:

$$\frac{\pi e^2}{2m^*}+\int_{\omega_{LO}}^{\infty}d\omega\,\mathrm{Re}\left[\sigma\left(\omega\right)\right]=\frac{\pi e^2}{2m}. \tag{2.72}$$

This gives a relation between the absorption spectrum and the effective mass m^* of the polaron. This sum rule has been used to experimentally determine the effective mass [135, 136].

For the density-density correlation (2.3) the f-sum rule is [4]:

$$\int_0^{\infty}d\omega\omega\,\mathrm{Im}\left[\chi\left(\vec{k},\omega\right)\right]=\pi\frac{k^2}{2m}. \tag{2.73}$$

The imaginary part of the density-density correlation (2.62) can be written as [61]:

$$\mathrm{Im}\left[\chi\left(\vec{k},\omega\right)\right]=-\frac{k^2}{m_I}\frac{1}{\mathrm{Im}\left[\Sigma\left(\omega,\vec{k}\right)\right]}\frac{1}{\left(\frac{\omega}{\mathrm{Im}\left[\Sigma\left(\omega,\vec{k}\right)\right]}\right)^2\omega^2\left[\left(1-\frac{\mathrm{Re}\left[\Sigma\left(\omega,\vec{k}\right)\right]}{\omega^2}\right)\right]^2+1}. \tag{2.74}$$

At small ω the imaginary part of (2.43) is linear in ω and the real part quadratic, resulting in the following behavior at small ω:

$$\lim_{\omega\to 0}\left[\omega\,\mathrm{Im}\left[\chi\left(\vec{k},\omega\right)\right]\right]=\frac{k^2}{m_I}\frac{\tau^D\left(\alpha,\vec{k}\right)}{\tau^D\left(\alpha,\vec{k}\right)^2\omega^2\left(m^D\left(\alpha,\vec{k}\right)/m_I\right)^2+1}, \tag{2.75}$$

where we used the following definitions:

$$\frac{1}{\tau^D\left(\alpha,\vec{k}\right)} = \lim_{\omega\to 0}\frac{\mathrm{Im}\left[\Sigma\left(\omega,\vec{k}\right)\right]}{\omega}; \tag{2.76}$$

$$m^D\left(\alpha,\vec{k}\right) = \lim_{\omega\to 0}\left(1-\frac{\mathrm{Re}\left[\Sigma\left(\omega,\vec{k}\right)\right]}{\omega^2}\right)m_I. \tag{2.77}$$

The small ω behavior of (2.74) corresponds to a Drude-like background which is a consequence of the incoherent scattering of the polaron with thermal Bogoliubov excitations. For the solid state polaron the Drude-like background is also present in the optical absorption spectra and is discussed in Ref. [137]. Considering only this Drude-like background the integration gives:

$$\begin{aligned}\int_0^\infty d\omega\lim_{\omega\to 0}\left[\omega\,\mathrm{Im}\left[\chi\left(\vec{k},\omega\right)\right]\right] &= \int_0^\infty d\omega\frac{k^2}{m_I}\frac{\tau^D\left(\alpha,\vec{k}\right)}{\tau^D\left(\alpha,\vec{k}\right)^2\omega^2\left(m^D\left(\alpha,\vec{k}\right)/m_I\right)^2+1}\\ &= \pi\frac{k^2}{2m^D\left(\alpha,\vec{k}\right)}.\end{aligned} \tag{2.78}$$

This suggests that $m^D\left(\alpha,\vec{k}\right)$ can be interpreted as a mass and $\tau^D\left(\alpha,\vec{k}\right)$ as a relaxation time related to the scattering with thermal excitations. The temperature zero limit gives:

$$\lim_{\beta\to\infty}\tau^D\left(\alpha,\vec{k}\right)=0, \tag{2.79}$$

showing that the Drude-like contribution reduces to a δ-peak. At zero temperature and in the limit $\vec{k}\to 0$ the "Drude mass" becomes

$$\lim_{\substack{\beta\to\infty\\ \vec{k}\to 0}} m^D\left(\alpha,\vec{k}\right)=m_I-\sum_{\vec{q}\neq 0}\frac{\left|V_{\vec{q}}\right|^2}{\hbar}q_x^2\int_0^\infty dt\;t^2\,\mathrm{Im}\left\{e^{i\omega_{\vec{q}}t}\exp\left[-q^2D\left(t\right)\right]\right\}. \tag{2.80}$$

This is the same expression as found by Feynman within the path integral formalism for the effective mass of the polaron [55] which is another motivation to consider

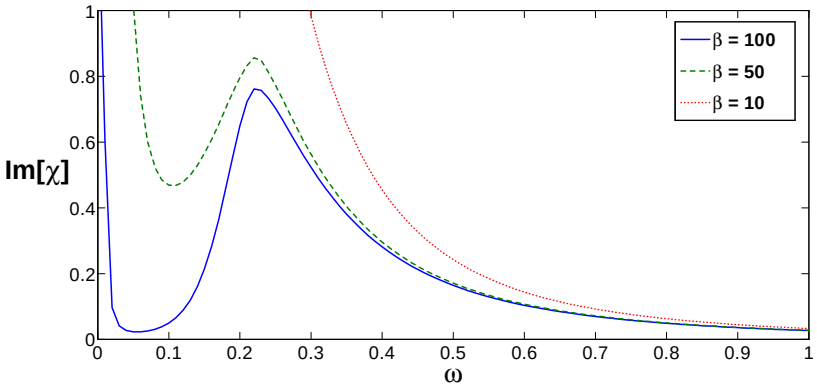

Figure 2.2: The Bragg response (2.62) of the polaron system consisting of a Li-6 impurity in a Na condensate in the weak coupling regime ($\alpha = 0.1$) with momentum exchange $k = 1$ at different temperatures ($\beta = (k_B T)^{-1}$).

$m^D\left(\alpha, \vec{k}\right)$ as an effective mass. At relatively small temperatures the Drude peak is narrow and the f-sum rule can be applied as a consistency check for our results, we will use (similar to expression 2.72 from Ref. [128]):

$$\pi \frac{k^2}{2m^D\left(\alpha, \vec{k}\right)} + \int_{\varepsilon}^{\infty} d\omega \omega \, \mathrm{Im}\left[\chi\left(\vec{k}, \omega\right)\right] = \pi \frac{k^2}{2m_I}, \tag{2.81}$$

where ε is a real parameter that has to be chosen such as to exclude the Drude peak from the integral, while keeping al other contributions to the spectrum.

2.7 Results and discussion

In this section we apply the developed formalism for a Li-6 impurity in a Na condensate in three dimensions, all results are presented in the polaronic units of table 1.1.

In Fig. 2.2 the Bragg response (2.62) is presented as a function of the transferred energy ω at different temperatures and for a momentum exchange $k = 1$ in the weak coupling regime ($\alpha = 0.1$). At relatively low temperature ($\beta = 100$) a peak can be distinguished that represents the emission of Bogoliubov excitations. We shall denote this peak as the Bogoliubov peak. The Drude-like background at $\omega \to 0$ is also clearly present. At higher temperatures the Drude peak broadens resulting in a larger overlap with the Bogoliubov emission peak which is indistinguishable at $\beta = 10$. For $\beta = 100$ the two contributions can be distinguished which allows us to make a suitable choice for ε in (2.81) and to apply the mass sum rule from Ref. [128] as a consistency check.

The dependence of the spectrum on the exchanged momentum k is presented in Fig. 2.3 at weak coupling and at $\beta = 100$. For larger momentum exchange the Bogoliubov peak broadens and is shifted to higher frequencies. The inset of Fig. 2.3 shows the frequency $\omega_{\max}(k)$ corresponding to the maximum of the Bogoliubov

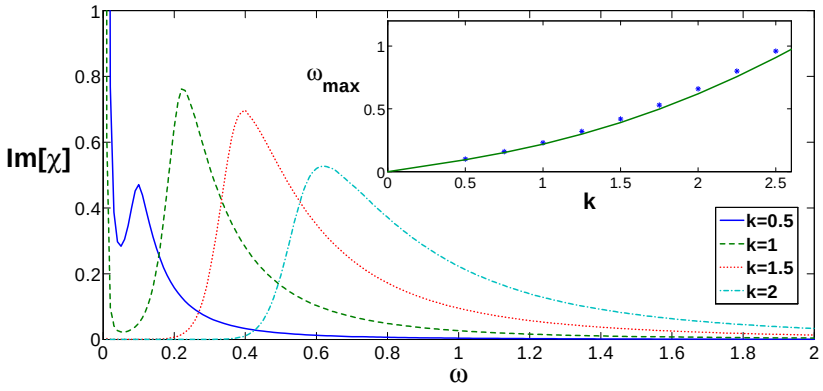

Figure 2.3: The Bragg response (2.62) of the polaron consisting of a Li-6 impurity in a Na condensate in the weak polaronic coupling regime ($\alpha = 0.1$) at temperature $\beta = 100$ for different momentum exchanges k. The inset shows the frequency of the maximum of the Bogoliubov peak as a function of the exchanged momentum k (markers) together with a least square fit to the Bogoliubov spectrum (2.82).

peak together with a least squares fit to the Bogoliubov spectrum:

$$\omega = \frac{k}{2m}\sqrt{k^2+2}, \tag{2.82}$$

with m the fitting parameter which results in $m = 3.9534$ which is in fair agreement with the mass of the condensate atoms ($m_B = 3.8221$). This shift according to the Bogoliubov dispersion is plausible since the peak corresponds to the emission of Bogoliubov excitations.

In Fig. 2.4, the high frequency tail of the Bragg spectrum is presented at different coupling strengths α and at $\beta = 100$ and $k = 1$. In the strong coupling regime a secondary peak appears which is absent in the weak coupling regime. This feature is well-known from the solid state Fröhlich polaron and corresponds to a transition to the Relaxed Excited State (RES) [59]. This resonance appears at a frequency ω_{RES} such that $\omega_{RES}^2 = \mathrm{Re}\left[\Sigma\left(\omega_{RES}, \vec{k}\right)\right]$ with the supplementary condition $\mathrm{Im}\left[\Sigma\left(\omega_{RES}, \vec{k}\right)\right] \ll 1$. It is clear from (2.62) that these conditions cause a peak in the spectrum. Physically it corresponds to a transition of the impurity from the ground state to an excitation in the self-induced potential which has been relaxed consistent with the new excited wave function of the impurity (as schematically presented in Fig. 1.7). The coupling strength where the relaxed excited state appears is around $\alpha \approx 4$. This is in agreement with the prediction in [89] that for a BEC-impurity the transition between the weak and the strong coupling regime occurs around $\alpha_c \approx 3$ for $\beta \to \infty$. In the strong coupling regime other peaks are present which are indicated for $\alpha = 8$ in the inset of Fig. 2.4. These are the Franck-Condon (FC) peaks and correspond to a transition to the RES together with the emission of Bogoliubov excitations. They are also present in the optical absorption spectrum of the acoustopolaron [138].

The dependence of the RES peak on the exchanged momentum k is shown in Fig. 2.5. The inset shows the frequency of the maximum of the RES peaks as a

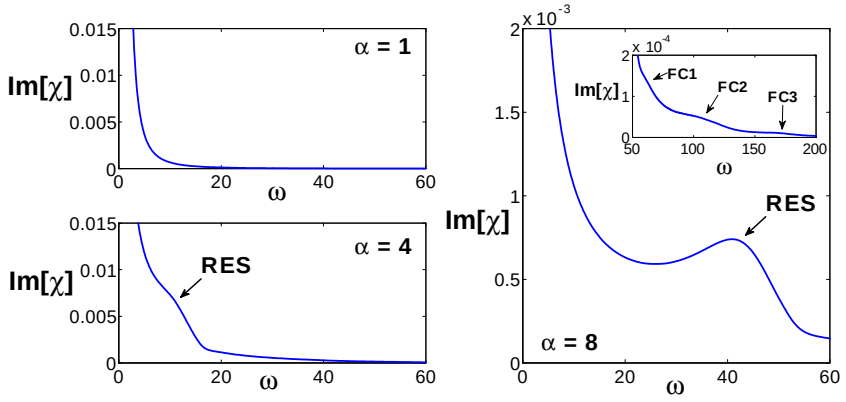

Figure 2.4: The Bragg response (2.62) of the polaron consisting of a Li-6 impurity in a Na condensate at different values for the coupling parameter α at inverse temperature $\beta = 100$ and momentum exchange $k = 1$. In the strong coupling regime the imprint of the relaxed excited state (RES) resonance appears. The inset shows the first three Franck-Condon (FC) peaks at $\alpha = 8$.

function of the exchanged momentum q together with a least square fit to a quadratic dispersion:

$$\omega = \nu + \frac{k^2}{2m^*}, \tag{2.83}$$

where ν and m^* are the fitting parameters (resulting in $\nu = 40.76$ and $m^* = 3.84$). This suggests that the RES can be characterized by a transition frequency ν and an effective mass m^*.

As a consistency test it was checked whether at relatively low temperature the above results satisfy the mass sum rule (2.81) from Ref. [128]. Filling out the expression for the imaginary part of the density-density correlation (2.62) gives the following expression for the f-sum rule (2.81):

$$\frac{\pi}{2m^D\left(\alpha,\vec{k}\right)} - \int_{\varepsilon}^{\omega_c} d\omega\omega \frac{\mathrm{Im}\left[\Sigma\left(\omega,\vec{k}\right)\right]}{\left(\omega^2 - \mathrm{Re}\left[\Sigma\left(\omega,\vec{k}\right)\right]\right)^2 + \left(\mathrm{Im}\left[\Sigma\left(\omega,\vec{k}\right)\right]\right)^2} = \frac{\pi}{2}. \tag{2.84}$$

For numerical reasons a cut-off ω_c had to be introduced which we choose to be: $\omega_c = 500$. A calculation of the left hand side of (2.84) results in the numbers presented in table 2.1 for different values of α and k at $\beta = 100$. These results should be compared with $\pi/2 = 1.5708...$ which gives a fair agreement with small deviations. Deviations were to be expected since we had to introduce a cut-off ω_c in (2.84) and also the choice of ε is somewhat arbitrary, leading to the possibility of double counting a part of the Drude contribution.

We now consider the extended memory function formalism as discussed in section 2.3.2 and give a qualitative analysis of the dependence on the lifetime τ. In Fig. 2.6 the RES peak is presented at different values for τ in the strong coupling regime ($\alpha = 8$). This shows that the inclusion of a lifetime of the order of the polaronic time unit results in a broadening of the RES peak. Naturally a smaller lifetime corresponds to a broader peak. The RES peak can not be distinguished any more if

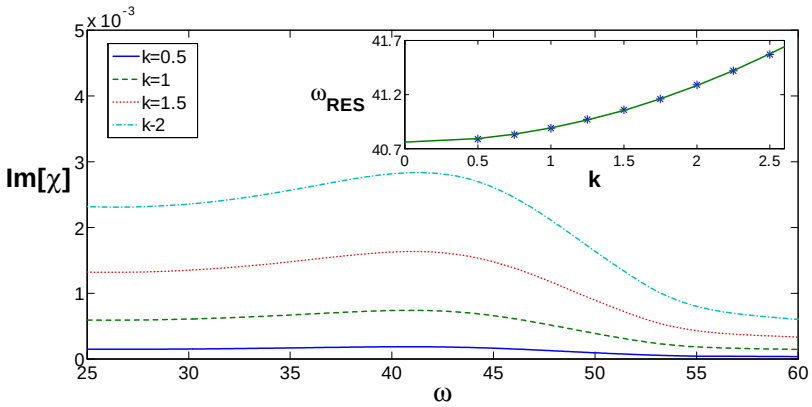

Figure 2.5: The relaxed excited state peak in the Bragg response (2.62) of the polaron system consisting of a Li-6 impurity in a Na condensate in the strong coupling regime ($\alpha = 8$) at inverse temperature $\beta = 100$ for different momentum exchanges k. The inset shows the frequency of the maximum as a function of the exchanged momentum k together with a least square fit to the quadratic dispersion (2.83).

k	$\alpha = 1$	$\alpha = 4$	$\alpha = 8$
1	1.5442	1.6845	1.5532
3	1.5482	1.6419	1.5355
5	1.5506	1.5555	1.4979

Table 2.1: Results of a numerical calculation of the left hand side of expression (2.84) with a cut-off $\omega_c = 500$ introduced for the ω-integral.

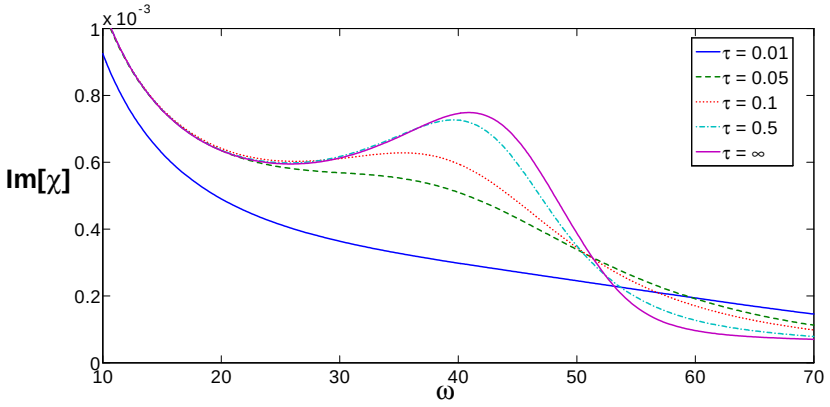

Figure 2.6: The RES peak in the Bragg response (2.62) for the polaron system consisting of a Li-6 impurity in a Na condensate in the strong coupling regime ($\alpha = 8$) at $\beta = 100$ and momentum exchange $k = 1$. Dissipation is considered by considering different lifetimes τ for the eigenstates of the Feynman model system.

the lifetime is of the order of a hundredth of the polaronic time unit. For the present case the Feynman system without the introduction of dissipation is however not in conflict with the Heisenberg uncertainty. This shows that for the present case it might not be necessary to introduce lifetime broadening with the extended memory function formalism.

2.8 Conclusions

We used the Mori-Zwanzig projection operator formalism to derive a formula for the density response function as a function of energy and momentum. This generalizes the existing descriptions of polaron response in that we go beyond the optical absorption, which is retrieved as the limiting case of zero momentum transfer in our formalism. This provides a result that can be used for Bragg spectroscopy but also for other probes of the density response function as for example neutron scattering [139]. This formalism is then applied for the Fröhlich Hamiltonian. For negligible momentum exchange the well-known results from Ref. [60, 127] for the optical absorption are reproduced. We then extend the analysis to Bragg scattering of impurity polarons in a Bose-Einstein condensate. Also the mass sum rule from Ref. [128] is considered.

This is then used to analyze the response of a Li-6 impurity in a Na condensate to Bragg scattering. The resulting Bragg spectra are presented for different momentum exchanges and temperatures in the different polaronic coupling regimes. At weak coupling this results in two distinct peaks. One is revealed as a Drude-like background and corresponds to the scattering of the polaron with thermal Bogoliubov excitations. The other is the Bogoliubov peak which corresponds to the emission of Bogoliubov excitations. The location of the maximum of the Bogoliubov peak follows the Bogoliubov spectrum as a function of the exchanged momentum. In the strong coupling regime a secondary peak emerges which corresponds to a transition to the Relaxed Excited State (RES). A comparison of the RES peaks with a Dia-

grammatic Quantum Monte-Carlo calculation would be highly interesting since a similar comparison for the optical absorption of the solid state polaron led to discrepancies regarding the linewidth and oscillator strength. The use of the mass sum rule from Ref. [128] allowed us to perform a consistency check of our results which resulted in a fair agreement.

The influence of dissipation within the extended memory function formalism was also investigated which was done by introducing a lifetime τ for the eigenstates of the Feynman model system, as was introduced in Ref. [63] for the solid state polaron. This resulted in a broadening of the RES peak as a function of τ.

Chapter 3

Strong coupling formalism*

We now consider the strong coupling formalism which was originally derived with a canonical transformation and a variational impurity wave function [53]. For an impurity in a condensate this treatment is equivalent to solving the Gross-Pitaevskii equation for a small response of the condensate to the impurity which is described with a variational wave function [88]. For the BEC-impurity polaron this resulted in the prediction of a bound state in the self-induced potential at sufficiently large polaronic coupling parameter α (1.34) [25, 82–87]. In this chapter we apply this polaronic strong coupling treatment to examine the lowest relaxed excited states of the BEC-impurity polaron. For these states the corresponding effective mass and the minimal coupling constant required for them to be a solution are calculated.

The strength of this approach is that it allows to derive approximate expressions for the transition energies in a much simpler way than with the full Mori-Zwanzig approach from chapter 2, and with a reasonable accuracy, which improves with increasing coupling. The transition energies obtained here can be used as the spectroscopic fingerprint for the experimental observation of relaxed excited states of impurity atoms in a condensate.

3.1 Strong coupling treatment of the polaron

In this section a summary of the polaronic strong coupling approximation is presented which was introduced by Landau and Pekar for the description of the ground state in Ref. [54]. These results were shown to be accurate in the asymptotic strong coupling limit for a symmetrical, exactly soluble one dimensional polaron model in Ref. [140]. The strong coupling formalism was later extended for the calculation of the energy levels of the lowest relaxed excited state in Refs. [141, 142].

The product Ansatz is assumed which states that the wave function of the system $|\Phi\rangle$ can be written as the product of the wave functions of the impurity $|\psi_I\rangle$ and of the Bogoliubov excitations $|\phi\rangle$: $|\Phi\rangle = |\psi_I\rangle\,|\phi\rangle$. Taking the expectation value of the

*The results of this chapter are published in W. Casteels, T. van Cauteren, J. Tempere and J. T. Devreese - *Strong coupling treatment of the polaronic system consisting of an impurity in a condensate* - Laser Phys. **21**, 1480 (2011).

Fröhlich Hamiltonian (1.17) with respect to $|\Phi\rangle$ gives:

$$\begin{aligned}\left\langle \Phi \left| \widehat{H}_{pol} \right| \Phi \right\rangle &= K + \sum_{\vec{k}} \hbar\omega_{\vec{k}} \left\langle \phi \left| \widehat{\alpha}^{\dagger}_{\vec{k}} \widehat{\alpha}_{\vec{k}} \right| \phi \right\rangle + \sum_{\vec{k}} V_{\vec{k}} \rho_{\vec{k}} \left\langle \phi \left| \widehat{\alpha}_{\vec{k}} + \widehat{\alpha}^{\dagger}_{-\vec{k}} \right| \phi \right\rangle \\ &= K + \sum_{\vec{k}} \hbar\omega_{\vec{k}} \left\langle \phi \left| \left(\widehat{\alpha}^{\dagger}_{\vec{k}} + \frac{V_{\vec{k}} \rho_{\vec{k}}}{\hbar\omega_{\vec{k}}} \right) \left(\widehat{\alpha}_{\vec{k}} + \frac{V^{*}_{\vec{k}} \rho^{*}_{\vec{k}}}{\hbar\omega_{\vec{k}}} \right) \right| \phi \right\rangle \\ &\quad - \sum_{\vec{k}} \frac{\left| V_{\vec{k}} \right|^2 \left| \rho_{\vec{k}} \right|^2}{\hbar\omega_{\vec{k}}}. \end{aligned} \tag{3.1}$$

The result in (3.1) can alternatively be obtained with a canonical transformation, as was originally done in Ref. [53]. Here the K denotes the expectation value of the kinetic energy of the impurity and $\rho_{\vec{k}}$ the expectation value of the Fourier transform of the impurity density:

$$K = \left\langle \psi_I \left| \frac{\widehat{p}^2}{2m_I} \right| \psi_I \right\rangle; \tag{3.2}$$

$$\rho_{\vec{k}} = \left\langle \psi_I \left| e^{i\vec{k}.\widehat{\vec{r}}} \right| \psi_I \right\rangle. \tag{3.3}$$

We now determine the wave function of the Bogoliubov excitations that minimizes the energy (3.1). This means that the wave function $|\phi\rangle$ has to satisfy

$$\left\langle \phi \left| \left(\widehat{\alpha}^{\dagger}_{\vec{k}} + \frac{V_{\vec{k}} \rho_{\vec{k}}}{\hbar\omega_{\vec{k}}} \right) \left(\widehat{\alpha}_{\vec{k}} + \frac{V^{*}_{\vec{k}} \rho^{*}_{\vec{k}}}{\hbar\omega_{\vec{k}}} \right) \right| \phi \right\rangle = 0. \tag{3.4}$$

This results in the following expression for the energy:

$$E = K - \sum_{\vec{k}} \frac{\left| V_{\vec{k}} \right|^2 \left| \rho_{\vec{k}} \right|^2}{\hbar\omega_{\vec{k}}}. \tag{3.5}$$

If a variational wave function is used for the impurity expression (3.5) is strictly speaking an upper bound for the ground state energy. When considering excitations of the impurity's wave function it is assumed that expression (3.5), with appropriate $\rho_{\vec{k}}$, gives a good approximation for the energy of the excited polaron.

3.1.1 Effective mass

The above formalism can be extended to allow for a calculation of the effective mass of the polaron [143–146]. The total momentum operator $\widehat{\vec{\mathcal{P}}}$ of the polaron is given by:

$$\widehat{\vec{\mathcal{P}}} = \widehat{\vec{p}} + \sum_{\vec{k}} \hbar\vec{k} \widehat{\alpha}^{\dagger}_{\vec{k}} \widehat{\alpha}_{\vec{k}}. \tag{3.6}$$

Note that $\widehat{\vec{\mathcal{P}}}$ commutes with the polaron Hamiltonian (1.17) and is thus a constant: $\vec{\mathcal{P}} = \left\langle \widehat{\vec{\mathcal{P}}} \right\rangle$. This is made explicit by introducing a Lagrange multiplier $\vec{v}$ and

minimizing the following expression:

$$\widehat{H}\left(\vec{v}\right)=\widehat{H}_{pol}-\vec{v}.\left(\widehat{\vec{p}}+\sum_{\vec{k}}\hbar\vec{k}\widehat{\alpha}_{\vec{k}}^{\dagger}\widehat{\alpha}_{\vec{k}}-\vec{\mathcal{P}}\right). \tag{3.7}$$

The vector $\vec{v}$ physically corresponds to the average velocity of the polaron. The effective mass of the polaron m^* can then be determined from the relation between the momentum and the average velocity:

$$\vec{\mathcal{P}}=m^*\vec{v}. \tag{3.8}$$

In this case a trial wave function for the system has to be chosen where the impurity has a velocity $\vec{v}$:

$$\left|\Phi'\right\rangle=\exp\left[\frac{im_I\vec{v}.\widehat{\vec{r}}}{\hbar}\right]\left|\psi_I\right\rangle\left|\phi\right\rangle. \tag{3.9}$$

The momentum corresponding to the wave function $|\psi_I\rangle$ is considered zero:

$$\left\langle\psi_I\left|\widehat{\vec{p}}\right|\psi_I\right\rangle=0. \tag{3.10}$$

The following expectation values are needed:

$$\left\langle\Phi\left|\frac{\widehat{\vec{p}}^2}{2m_I}\right|\Phi\right\rangle=\frac{m_Iv^2}{2}+K; \tag{3.11}$$

$$\left\langle\Phi\left|\widehat{\vec{p}}\right|\Phi\right\rangle=m_I\vec{v}; \tag{3.12}$$

$$\left\langle\Phi\left|e^{i\vec{k}.\widehat{\vec{r}}}\right|\Phi\right\rangle=\rho_{\vec{k}}, \tag{3.13}$$

where K and $\rho_{\vec{k}}$ are the same as in (3.2) and (3.3), respectively. Taking the expectation value of $\widehat{H}\left(\vec{v}\right)$ with respect to $|\Phi>$ gives

$$\begin{aligned}E\left(\vec{v}\right) &= \left\langle\Phi\left|\widehat{H}\left(\vec{v}\right)\right|\Phi\right\rangle\\ &= K-\frac{m_Iv^2}{2}+\vec{v}.\vec{\mathcal{P}}-\sum_{\vec{k}}\frac{\left|V_{\vec{k}}\right|^2\left|\rho_{\vec{k}}\right|^2}{\hbar\omega_{\vec{k}}}+\sum_{\vec{k}}\left(\hbar\omega_{\vec{k}}-\hbar\vec{v}.\vec{k}\right)\\ &\quad\times\left\langle\phi\left|\left(\widehat{\alpha}_{\vec{k}}^{\dagger}+\frac{V_{\vec{k}}\rho_{\vec{k}}}{\hbar\omega_{\vec{k}}-\hbar\vec{v}.\vec{k}}\right)\left(\widehat{\alpha}_{\vec{k}}+\frac{V_{\vec{k}}^*\rho_{\vec{k}}^*}{\hbar\omega_{\vec{k}}-\hbar\vec{v}.\vec{k}}\right)\right|\phi\right\rangle.\end{aligned} \tag{3.14}$$

Choosing $|\phi\rangle$ similar to expression (3.4) leads to:

$$E\left(\vec{v}\right)=K-\frac{m_Iv^2}{2}+\vec{v}.\vec{\mathcal{P}}-\sum_{\vec{k}}\frac{\left|V_{\vec{k}}\right|^2\left|\rho_{\vec{k}}\right|^2}{\hbar\omega_{\vec{k}}-\hbar\vec{v}.\vec{k}}. \tag{3.15}$$

We now fix the conservation of the polaron momentum by deriving expression (3.15) with respect to the Lagrange multiplier $\vec{v}$ and setting the resulting expression equal to zero. This results in the following expression:

$$\vec{\mathcal{P}}=m_I\vec{v}+\sum_{\vec{k}}\frac{\left|V_{\vec{k}}\right|^2\left|\rho_{\vec{k}}\right|^2}{\left(\hbar\omega_{\vec{k}}-\hbar\vec{v}.\vec{k}\right)^2}\hbar\vec{k}. \tag{3.16}$$

Performing a Taylor expansion for small $\vec{v}$ gives:

$$\begin{aligned}\sum_{\vec{k}} \frac{\left|V_{\vec{k}}\right|^2 \left|\rho_{\vec{k}}\right|^2}{\left(\hbar\omega_{\overrightarrow{k}} - \hbar\vec{v}.\vec{k}\right)^2}\hbar\vec{k} &= \sum_{\vec{k}} \frac{\left|V_{\vec{k}}\right|^2 \left|\rho_{\vec{k}}\right|^2}{\left(\hbar\omega_{\vec{k}}\right)^2}\hbar\vec{k}\left(1 + 2\frac{\hbar\vec{v}.\vec{k}}{\hbar\omega_{\overrightarrow{k}}} + \mathcal{O}\left(v^2\right)\right) \\ &\approx 2\hbar^2 \sum_{\vec{k}} \frac{\left|V_{\vec{k}}\right|^2 \left|\rho_{\vec{k}}\right|^2}{\left(\hbar\omega_{\overrightarrow{k}}\right)^3}\vec{k}\left(\vec{v}.\vec{k}\right) \qquad (3.17)\end{aligned}$$

Comparing (3.16) for small v with expression (3.8) for the effective mass m^* leads to:

$$m_i^* = m_I + 2\hbar^2 \sum_{\vec{k}} \frac{\left|V_{\vec{k}}\right|^2 \left|\rho_{\vec{k}}\right|^2}{\left(\hbar\omega_{\vec{k}}\right)^3} k_i^2, \qquad (3.18)$$

with $i = x, y, z$. For a general density $\rho_{\vec{k}}$ expression (3.18) is anisotropic. Since there are no preferred directions in the system, the physically realized effective mass corresponds to the lowest value of (3.18) since this value corresponds to the lowest energy.

3.1.2 Variational wave function for the impurity

In the strong coupling approximation the impurity is assumed to be localized within the polaron by the self-induced potential which is approximated as quadratic. The impurity wave function is then chosen to be an eigenstate of the harmonic oscillator:

$$\psi_{n_x,n_y,n_z}(\lambda, \vec{r}) = \prod_{i=x,y,z} \left(2^{n_i} n_i!\right)^{-1/2} \frac{1}{\pi^{1/4}\lambda^{1/2}} H_{n_i}\left(\frac{i}{\lambda}\right) \exp\left(-\frac{r^2}{2\lambda^2}\right), \qquad (3.19)$$

with H_{n_i} the Hermite polynomials, $n_i = 0, 1, 2, ...$ and λ the oscillator length, which is used as a variational parameter. Physically the oscillator length λ can be understood as a measure of the extension of the wave function, a small λ corresponding to a small wave function and thus a highly localized internal state. The corresponding kinetic energy (3.2) for the wave function (3.19) is

$$K^{(n_x,n_y,n_z)}(\lambda) = \frac{1}{2}\left(\frac{3}{2} + n\right)\frac{\hbar^2}{m_I\lambda^2}, \qquad (3.20)$$

with $n = n_x + n_y + n_z$. For the Fourier transform of the density (3.3) we have:

$$\begin{aligned}\rho_{\vec{k}}^{(n_x,n_y,n_z)}(\lambda) &= \left\langle \psi_{n_x,n_y,n_z} \left|\widehat{\rho}_{\vec{k}}\right| \psi_{n_x,n_y,n_z} \right\rangle \\ &= L_{n_x}\left(\frac{k_x^2\lambda^2}{2}\right) L_{n_y}\left(\frac{k_y^2\lambda^2}{2}\right) L_{n_z}\left(\frac{k_z^2\lambda^2}{2}\right) \exp\left[-\frac{k^2\lambda^2}{4}\right], \qquad (3.21)\end{aligned}$$

where $L_n(x)$ are the Laguerre polynomials. Note that the density is a function of the product $\vec{q} = \lambda\vec{k}$, i.e. $\rho_{\vec{k}}(\lambda) = \rho(\vec{q})$.

3.2 Strong coupling approximation applied to an impurity in a condensate

We now substitute the Bogoliubov dispersion (1.15) and the interaction amplitude (1.19) for the polaronic system consisting of an impurity in a condensate in the above derived expressions. If the impurity wave function is assumed to be a harmonic oscillator eigenstate (3.19) the following expression is found for the energy (3.5) (in the polaronic units of table 1.1):

$$E(\lambda) = \frac{1}{2\lambda^2}\left(\frac{3}{2}+n\right) - \frac{\alpha\mu}{2\pi^2}\int d\vec{k}\frac{\rho_k^2(\lambda)}{2+k^2}, \tag{3.22}$$

where α is the polaronic coupling parameter (1.34) and μ is a dimensionless mass factor, defined as:

$$\mu = \frac{(m_I+m_B)^2}{4m_I m_B}. \tag{3.23}$$

From (3.22), it can be seen that in the strong coupling regime the effective coupling parameter is the product $\alpha\mu$. In what follows, we study the system properties as a function of $\alpha\mu$ rather than α. Since the density of the harmonic oscillator eigenfunctions is a function of $\vec{q}=\lambda\vec{k}$ only, (3.22) can be rewritten as:

$$E(\lambda) = \frac{1}{2\lambda^2}\left(\frac{3}{2}+n\right) - \frac{\alpha\mu}{2\pi^2\lambda}\int d\vec{q}\frac{\rho^2(\vec{q})}{2\lambda^2+q^2}. \tag{3.24}$$

Minimization of (3.24) results in the following condition on the variational parameter λ:

$$\frac{1}{\lambda^3}\left(\frac{3}{2}+n\right) = \frac{2\alpha\mu}{\pi^2}\left(\int d\vec{q}\frac{\rho^2(\vec{q})}{\left(2\lambda^2+q^2\right)^2} + \frac{1}{4\lambda^2}\int d\vec{q}\frac{\rho^2(\vec{q})}{2\lambda^2+q^2}\right). \tag{3.25}$$

This equation determines a minimal value for $\alpha\mu$ below which no solution is found, i.e. the requirement to find a solution is:

$$\alpha\mu \geq \min_{\lambda\in\mathcal{R}^+}\left[\frac{\pi^2(n+3/2)}{2\lambda^3\left(\int d\vec{q}\frac{\rho^2(\vec{q})}{\left(2\lambda^2+q^2\right)^2}+\frac{1}{4\lambda^2}\int d\vec{q}\frac{\rho^2(\vec{q})}{2\lambda^2+q^2}\right)}\right]. \tag{3.26}$$

Values of $\alpha\mu$ not satisfying (3.26) would give $\lambda\to\infty$ and thus a completely delocalized impurity meaning that the self-induced potential is too shallow to have this type of wave function as a bound state.

Introducing the Bogoliubov dispersion (1.15) and the interaction amplitude (1.19) in expression (3.18) for the effective mass results in (in polaronic units):

$$m_i^* = 1 + \frac{4\alpha\mu m_B^2\lambda}{\pi^2}\int d\vec{q}\frac{\rho^2(\vec{q})}{\left(2\lambda^2+q^2\right)^2}\frac{q_i^2}{q^2}. \tag{3.27}$$

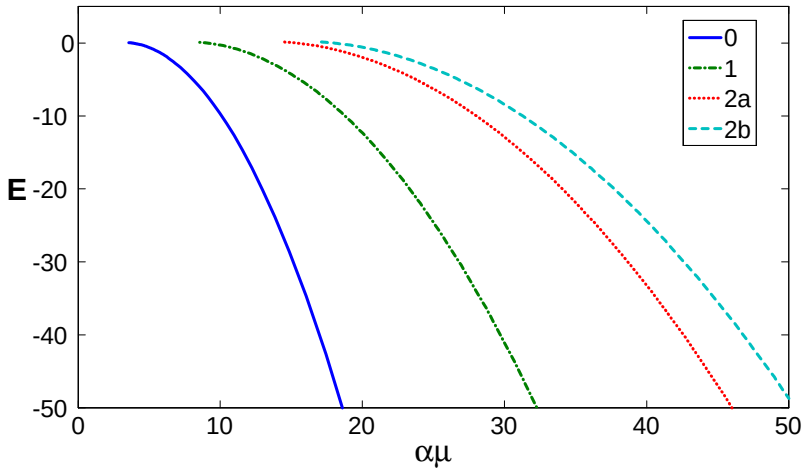

Figure 3.1: The variationally determined energy levels in the self-induced potential as a function of the coupling parameter $\alpha\mu$ for the ground state ("0"), for the first Relaxed Excited State ("1") and for the two types of second relaxed excited states ("2a" and "2b", as discussed in the text).

3.3 Relaxed excited states

If an excited state wave function is considered for $|\psi_I\rangle$, the resulting polaronic state is the relaxed excited state (RES) that we already discussed in chapter 2 and that corresponds to an excitation of the impurity in the self-induced potential adapted to the excited state's wave function. The relaxation of the wave function $|\phi\rangle$ for the Bogoliubov excitations to the impurity wave function can be understood from expression (3.4) which is used to determine $|\phi\rangle$ and depends on the impurity density $\rho_{\vec{k}}$. In this section the numerical solutions for the strong coupling approach are examined for the ground state and the three lowest relaxed excited states. Everything is presented in the polaronic units of table 1.1.

For the ground state, $n = 0$ has to be considered. The first RES corresponds to $n = 1$, i.e. one of the n_i's is taken to be 1. The second RES, corresponding to $n = 2$, can be realized in two distinct ways: either one n_i equals 2 or two n_i's equal 1 which will be indicated as $2a$ and $2b$, respectively.

In Fig. 3.1 the variationally determined energy levels are shown as a function of $\alpha\mu$ for all states discussed above and in Fig. 3.2 the corresponding optimal oscillator length λ of the impurity is presented. Note that the energies of the excited states possess no variational upper bound character. To the left of the curves, the coupling is too weak for the self-induced potential to support these levels. For couplings just large enough for the level to exist the energy (3.5) is positive which means it is metastable and the impurity is expected to be expelled from the condensate. There are, for each state, two special values of $\alpha\mu$: one at which the self-induced potential allows for that state to exist, and one at which the polaron energy (3.5) becomes negative, leading to a stable state. We list these values together with the corresponding optimal value of the variational parameter λ in table 3.1. Since the current formalism is only expected to be valid at strong coupling the physical

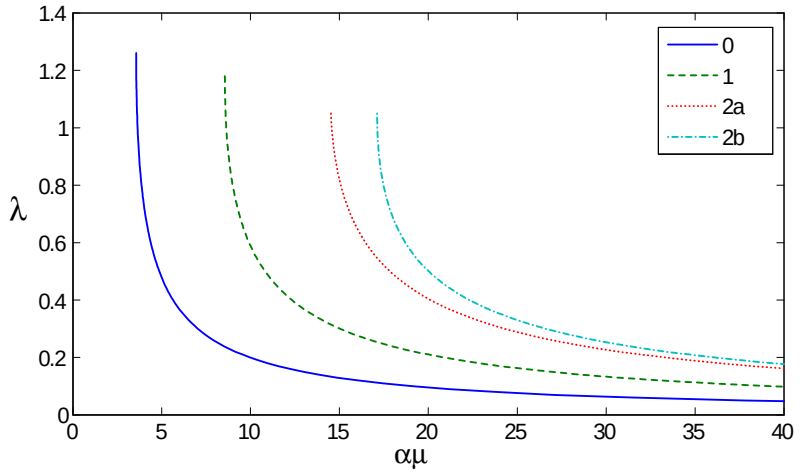

Figure 3.2: The variationally determined harmonic oscillator length of the impurity wave function as a function of $\alpha\mu$ for the ground state ("0") and the three lowest relaxed excited states ("1", "2a" and "2b").

	$(\alpha\mu)_{exist}$	λ	$(\alpha\mu)_{stable}$	λ
ground state	3.56641	1.2668	3.83302	0.8213
first RES	8.55492	1.1850	9.10277	0.7646
second RES (2a)	14.4869	1.1495	15.3764	0.7400
second RES (2b)	17.1152	1.0570	18.0197	0.6852

Table 3.1: The values of $\alpha\mu$ above which the self-induced potential supports the indicated levels, along with the corresponding values of the variational parameter λ (cf. eq. (4.15)). The last two columns give the values of $\alpha\mu$ (and the corresponding λ) above which the indicated levels become stable.

relevance of the values in table 3.1 and of the possible existence of a metastable state is not very clear. From Fig. 3.2 it is clear that an increase of $\alpha\mu$ results in a decrease of λ, corresponding to a stronger self-induced potential and thus to a more localized impurity within the polaron. Furthermore we see that at a given $\alpha\mu$ different oscillator lengths are found for different states which means that a transition to a RES is not only accompanied with the relaxation of the wave function of the BEC but also the impurity's wave function is adapted.

In Fig. 3.3, the behavior of the effective mass m^* (3.27) is presented as a function of $\alpha\mu$ for the states under consideration. The largest effective mass is found for the ground state and it is observed that the effective masses corresponding to the two possibilities for the second RES cross at a coupling parameter $\alpha\mu \approx 28.7$.

In Fig. 3.4 the transition energies are shown for the transition from the ground state to the relaxed excites states under consideration and from the first RES to the two types of the second RES. For larger $\alpha\mu$ more relaxed excited states are expected to exist and as a result there will be more possible transition energies.

In chapter 2 the excitation structure of the polaron system consisting of an impurity in a condensate was considered by calculating the response of the system to Bragg spectroscopy within the Mori-Zwanzig projection operator formalism. The

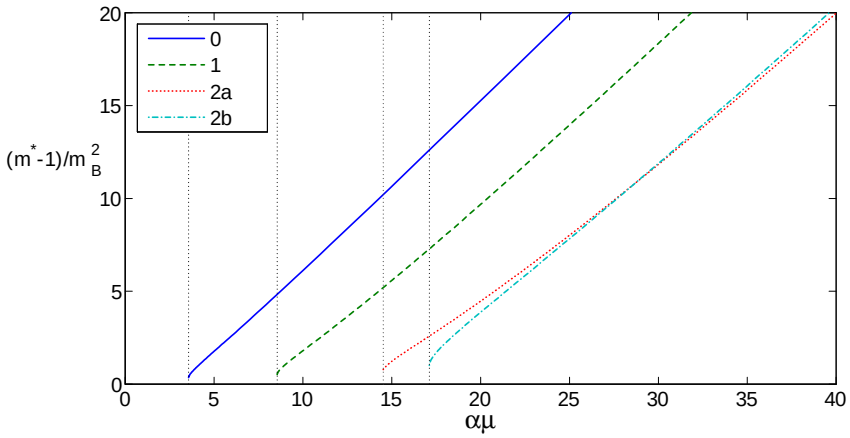

Figure 3.3: This figure shows $(m^* - 1)/m_B^2$ where the effective mass m^* is given by Eq. (3.27) for the ground state ("0") and for the three lowest relaxed excited states ("1", "2a" and "2b"). The values of $(\alpha\mu)$ at which the self-induced potential is deep enough to support these states are also indicated (cf. Table 3.1) by dotted vertical lines.

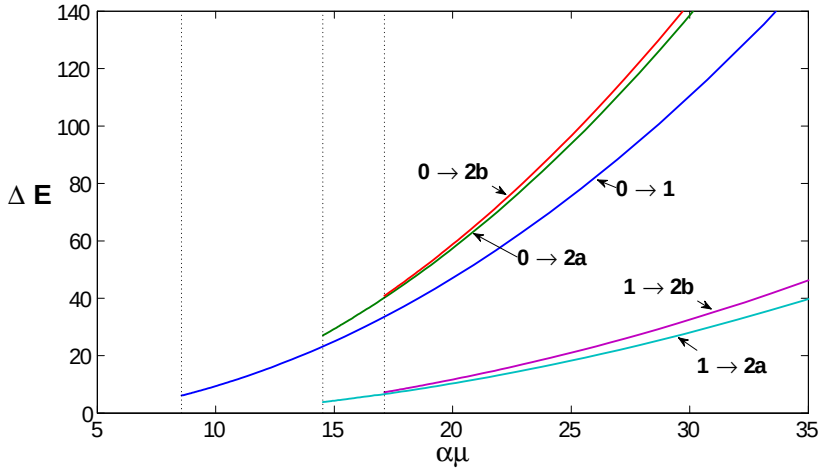

Figure 3.4: Transition energies from the ground state ("0") to the relaxed excited states ("1", "2a" and "2b") and from the first RES ("1") to the two types of the second RES ("2a" and "2b"). The critical coupling parameters $(\alpha\mu)_{exist}$ from table 3.1 for the Relaxed Excited States are also indicated by dotted vertical lines.

system consisting of a Li-6 impurity in a Na condensate was examined which results for the present treatment in $\mu = 1.5209$ for the mass factor (3.23). With this value of μ the present theory is able to describe the strong coupling ground state from $\alpha \gtrapprox 2.5$. This underestimates the critical coupling $\alpha_c \approx 3$ as found with the Feynman variational path integral formalism in Ref. [89]. A numerical calculation of the impurity and condensate ground state wave functions also showed that the strong coupling formalism underestimates the critical coupling value [147]. Fig. 3.3 shows that the self-induced potential becomes deep enough to support a first relaxed excited state at $\alpha \approx 6$. In chapter 2 the transition to the first relaxed excited state is already seen at $\alpha = 4$ and for larger α a larger transition frequency is found, a behavior which is also observed in Fig. 3.4. This shows that the lowest α at which the relaxed excited state appears is slightly smaller in the treatment of chapter 2 as compared to the strong coupling treatment. A comparison of the transition frequency from the ground state to the first relaxed excited state can be made for α larger than 6. At $\alpha = 8$ this results in a difference of about 10% and at $\alpha = 10$ a deviation of about 5% is found. This trend of a better correspondence between the present strong coupling approximation and the all-coupling treatment of chapter 2 at higher coupling parameter is consistent since the strong coupling theory is expected to be more accurate at larger α.

In chapter 2 the effective mass of the lowest relaxed excited state was determined for a Li-6 impurity in a Na condensate as $m^{RES} = 3.84$ at $\alpha = 8$. For the ground state we can use the Feynman variational path integral treatment as in Fig. 1.10 to estimate the ground state effective mass as $m^{GS} = 19.9$ at $\alpha = 8$. These values exhibit the same behavior as in Fig. 3.3 of a larger effective mass of the ground state as compared to the relaxed excited state.

In the present strong coupling calculation the effect of the mass imbalance is contained solely in the factor μ which grows as the masses differ more, leading to a larger $\alpha\mu$. This observation provides an additional tool for facilitating the probing of the strong coupling regime, namely choosing the masses as different as possible: a Li impurity in a Rb condensate will correspond to a more strongly interacting system at the same (Feshbach adapted) scattering lengths than a Li impurity in a Na condensate.

3.4 Conclusions

The polaron strong coupling treatment was applied to investigate the strong coupling regime of the polaronic system consisting of a single impurity in a Bose-Einstein condensate. This showed that at strong coupling the ratio of the impurity and boson masses and the polaronic coupling parameter combine to a single parameter. Within this formalism the critical coupling parameters required for relaxed excited states to appear were deduced, and the effective masses of these states were calculated. For impurity atoms in a condensate, these states can be experimentally most easily probed by laser spectroscopy. The calculation of the transition energies between different relaxed excited states presented here offers a straightforward way to estimate the excitation spectrum. Comparison with the path-integral results for the spectral density obtained within the Mori-Zwanzig framework from chapter 2

shows that the current method quickly becomes very accurate ($<5\%$ for $\alpha \gtrsim 10$) as the coupling strength grows. Furthermore it was shown that the polaronic strong coupling regime is easier to reach when the masses of the bosons and the impurity differ more from each other.

Chapter 4

Bipolarons and the Multi-polaron system

Hitherto we have considered a single impurity in a Bose-Einstein condensate. Introducing multiple impurities unveils a whole range of interesting phenomena. The presence of the Bose-Einstein condensate induces an effective interaction between the impurities [148,149]. If the polaronic coupling is strong enough the BEC-induced interaction can lead to the multi-polaron [86, 88]. The possibility of the formation of a multi-polaron at strong polaronic coupling is also well-known in the solid state context [73,78,150–152]. A special case is the formation of a bound state of two electrons, commonly known as the bipolaron [153,154]. Bipolarons have attracted much attention because of their possible role as an unconventional pairing mechanism for high-temperature superconductivity [65, 66].

In this chapter, we consider a few impurities in a Bose-Einstein condensate and examine the formation of a multi-polaron. We start in section 4.1 by applying the all-coupling Jensen-Feynman variational path integral approach, as developed in Ref. [72] for two electrons in a polar or ionic lattice, to two distinguishable impurity atoms in a Bose-Einstein condensate. This allows us to examine the polaron-bipolaron transition, the bipolaron binding energy and the evolution of the bipolaron radius and its effective mass. In section 4.2 a strong-coupling treatment for multiple impurities in a BEC, based on the Landau-Pekar strong-coupling approach, is considered. This is first applied for two impurities in a condensate to examine the polaron-bipolaron transition and the typical bipolaron properties. Then we apply it to multiple impurities to study the formation of a larger multi-polaron. Finally, in section 4.3, we compare the results of the two presented formalisms for two distinguishable impurities in a BEC and in section 4.4 we conclude.

4.1 All-coupling Jensen-Feynman variational treatment for two impurities in a Bose-Einstein condensate

4.1.1 Formalism

We consider the generic polaronic system of two distinguishable particles interacting with a bosonic bath through the Fröhlich interaction, i.e. any system that can be described by the Hamiltonian (1.21) with $N_I = 2$. The variational all-coupling single polaron treatment, as originally developed by Feynman [55], was extended in Ref. [72] to the case of two polaronic particles. This approach is based on the Jensen-Feynman variational inequality for the free energy $\mathcal{F}$ (1.28):

$$\mathcal{F} \leq \mathcal{F}_0 + \frac{1}{\hbar\beta} \left\langle \mathcal{S} - \mathcal{S}_0 \right\rangle_{\mathcal{S}_0}, \tag{4.1}$$

with $\mathcal{S}$ the action of the polaronic system as described by the Fröhlich Hamiltonian (6.1), $\mathcal{S}_0$ the action of a variational trial system with free energy $\mathcal{F}_0$ and β the inverse temperature T: $\beta = (k_B T)^{-1}$. Eliminating the degrees of freedom of the Bogoliubov excitations leads to an effective polaron action, containing retardation effects:

$$\begin{aligned}\mathcal{S} = & \int_0^{\hbar\beta} d\tau \left[\sum_{i=1}^{N_I} \frac{m_I}{2} \dot{\vec{r}}_i^{\,2}(\tau) + \sum_{i<j} V_{II}\left(\vec{r}_i - \vec{r}_j\right) \right] \\ & - \sum_{j,l=1}^{N_I} \sum_{\vec{k}} \frac{\left|V_{\vec{k}}\right|^2}{\hbar} \int_0^{\hbar\beta} d\tau \int_0^{\hbar\beta} d\sigma G_{\omega_{\vec{k}}}(\tau - \sigma)\, e^{i\vec{k}.[\vec{r}_j(\tau) - \vec{r}_l(\sigma)]},\end{aligned} \tag{4.2}$$

with $G_{\omega_{\vec{k}}}(u)$ the Green's function of the Bogoliubov excitations:

$$G_{\omega_{\vec{k}}}(u) = \frac{\cosh\left[\omega_{\vec{k}}\left(\hbar\beta/2 - |u|\right)\right]}{2\sinh\left(\beta\hbar\omega_{\vec{k}}/2\right)}. \tag{4.3}$$

For a single polaron a variational system was suggested by Feynman that mimics the influence of the interaction with the Bogoliubov excitations on the impurity by a harmonic coupling to a fictitious particle of mass M with oscillator strength κ [55] (see Fig. 1.9). The upper bound for the free energy (4.1) is then minimized as a function of the variational parameters M and κ. In Ref. [72] an extension of this trial system was introduced for the case of two polaronic particles which is schematically presented in Fig. 4.1. As is the case in the Feynman one-polaron trial system the impurities interact quadratically with fictitious particles of mass M with oscillator strength κ. Furtermore, there is a quadratic interaction, with oscillator strength κ', with the fictitious particle of the other impurity. The particles are separated by the vector $\vec{a}$ and they mutually interact quadratically with strength K. For $\kappa' = K = 0$ this reduces to (twice) the Feynman model system. After transforming to the eigenmodes the action of the trial system can be written as:

$$\mathcal{S}_0 = \int_0^{\hbar\beta} d\tau \left[\frac{\mu_0}{2}\dot{\rho}_0^2 + \sum_{j=1}^{3} \left(\frac{\mu_j}{2}\dot{\rho}_j^2 + \frac{1}{2}\mu_j\Omega_j^2\rho_j^2 \right) \right], \tag{4.4}$$

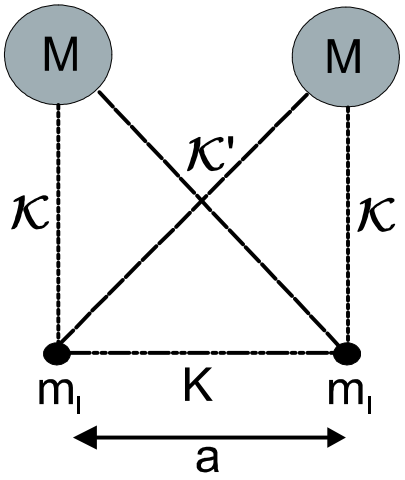

Figure 4.1: Schematical picture of the variational trial system for two polaronic particles, as introduced in Ref. [72]. The black dots represent the impurity atoms of mass m_I and the larger grey dots depict the fictitious particles of mass M. The connecting lines represent harmonic interactions with the corresponding oscillator strengths indicated.

with $\{\vec{\rho}_i\}$ the coordinates of the eigenmodes of the trial system and $\{\Omega_i\}$ the corresponding eigenfrequencies ($\Omega_0 = 0$ corresponds to a translation of the trial system as a whole):

$$\Omega_1^2 = \frac{M + m_I}{M m_I} (\kappa + \kappa'); \tag{4.5}$$

$$\Omega_{2,3}^2 = \frac{1}{2}\left[\frac{M + m_I}{M m_I}(\kappa + \kappa') - \frac{2K}{m_I} \pm \sqrt{\left[\frac{M - m_I}{M m_I}(\kappa + \kappa') - \frac{2K}{m_I}\right]^2 + \frac{4}{m_I M}(\kappa - \kappa')^2}\right]. \tag{4.6}$$

Since all oscillator strengths are positive the eigenfrequencies satisfy the inequalities

$$\Omega_1^2 \geq \Omega_2^2 + \Omega_3^2; \tag{4.7}$$

$$\Omega_2 \geq \nu \geq \Omega_3 \geq 0; \tag{4.8}$$

where we introduced the frequency parameter $\nu = \sqrt{(\kappa + \kappa')/M}$. In expression (4.4) the following mass factors were introduced:

$$\mu_0 = 2(m_I + M); \quad \mu_1 = \frac{2 m_I M}{(m_I + M)}; \quad \mu_2 = 1; \quad \mu_3 = 1. \tag{4.9}$$

The corresponding eigenmodes of the trial system are schematically presented in Fig. 4.2. The action (4.4) shows that the trial system decouples in a free particle and three harmonic oscillators.

After eliminating the degrees of freedom of the two fictitious particles of mass

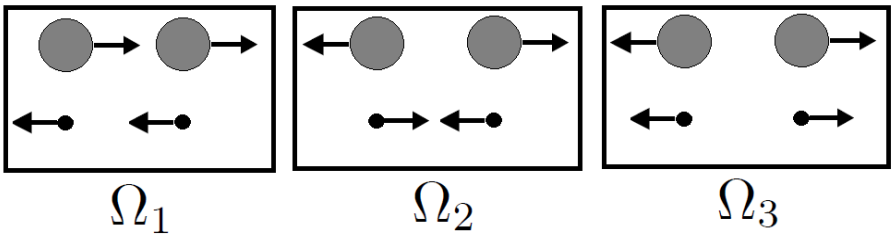

Figure 4.2: Schematic presentation of the eigenmodes corresponding to the eigenfrequencies Ω_1, Ω_2 and Ω_3. The small black dots represent the impurity atoms and the larger grey dots depict the fictitious particles of mass M.

M the effective action of the trial system becomes retarded and can be written as:

$$\begin{aligned}\mathcal{S}_0 = &\int_0^{\hbar\beta} d\tau \left[\sum_{i=1,2} \frac{m_I}{2}\dot{r}_i^2(\tau) - \frac{K}{2}\left(\vec{r}_1 - \vec{r}_2 - \vec{a}\right)^2\right] \\ &+ \frac{\kappa^2 + \kappa'^2}{4M\nu}\int_0^{\hbar\beta} d\tau \int_0^{\hbar\beta} d\sigma G_\nu(\tau-\sigma)\sum_j \left[\vec{r}_j(\tau) - \vec{r}_j(\sigma)\right]^2 \\ &+ \frac{\kappa\kappa'}{M\nu}\int_0^{\hbar\beta} d\tau \int_0^{\hbar\beta} d\sigma G_\nu(\tau-\sigma)\left[\vec{r}_1(\tau) - \vec{r}_2(\sigma) - \vec{a}\right]^2. \end{aligned} \tag{4.10}$$

Applying the Jensen-Feynman inequality in the zero temperature limit then results in an upper bound E for the polaronic contribution to the ground state energy [72]:

$$\begin{aligned}E = &\sum_{j=1}^{3}\frac{3}{2}\hbar\Omega_j - 3\hbar\nu + \sum_{\vec{k}} V_{II}\left(\vec{k}\right) e^{i\vec{k}.\vec{a}} e^{-k^2 D_{12}(0)} \\ &- 2\sum_{\vec{k}} \frac{\left|V_{\vec{k}}\right|^2}{\hbar}\int_0^\infty du e^{-\omega_{\vec{k}}u}\left[e^{-k^2 D_{11}(u)} + e^{i\vec{k}.\vec{a}} e^{-k^2 D_{12}(u)}\right] \\ &- \frac{3}{2}\frac{\Omega_1^2 - \nu^2}{\Omega_1^2}\frac{\hbar\Omega_1}{2} - \frac{3}{2}\frac{\Omega_2^2 - \nu^2}{\Omega_2^2 - \Omega_3^2}\frac{\hbar\Omega_2}{2} - \frac{3}{2}\frac{\nu^2 - \Omega_3^2}{\Omega_2^2 - \Omega_3^2}\frac{\hbar\Omega_3}{2}, \end{aligned} \tag{4.11}$$

where the functions $D_{11}(u)$ and $D_{12}(u)$ are defined as:

$$\begin{aligned}D_{11}(u) = &\frac{\hbar}{2m_I}\left[\frac{\nu^2}{\Omega_1^2}\frac{u}{2} + \frac{\Omega_1^2 - \nu^2}{\Omega_1^2}E(\Omega_1, u)\right. \\ &\left. + \frac{\Omega_2^2 - \nu^2}{\Omega_2^2 - \Omega_3^2}E(\Omega_2, u) + \frac{\nu^2 - \Omega_3^2}{\Omega_2^2 - \Omega_3^2}E(\Omega_3, u)\right]; \end{aligned} \tag{4.12}$$

$$\begin{aligned}D_{12}(u) = &\frac{\hbar}{2m_I}\left[\frac{\nu^2}{\Omega_1^2}\frac{u}{2} + \frac{\Omega_1^2 - \nu^2}{\Omega_1^2}E(\Omega_1, u)\right. \\ &\left. + \frac{\Omega_2^2 - \nu^2}{\Omega_2^2 - \Omega_3^2}F(\Omega_2, u) + \frac{\nu^2 - \Omega_3^2}{\Omega_2^2 - \Omega_3^2}F(\Omega_3, u)\right]; \end{aligned} \tag{4.13}$$

with:

$$E(\Omega, u) = \frac{1 - \exp[-\Omega u]}{2\Omega}; \tag{4.14}$$

$$F(\Omega, u) = \frac{1 + \exp[-\Omega u]}{2\Omega}. \tag{4.15}$$

The next step is to minimize the upper bound E (4.11) as a function of the variational parameters $\{\nu, \Omega_1, \Omega_2, \Omega_3, \vec{a}\}$.

Bipolaron radius

As an estimate for the bipolaron radius R the root mean square of the distance between the impurities is used [72]:

$$\begin{aligned} R &= \sqrt{\left\langle \left[\vec{r}_1(\tau) - \vec{r}_2(\tau)\right]^2 \right\rangle} \\ &= \sqrt{a^2 + 6D_{12}(0)}. \end{aligned} \tag{4.16}$$

whith the function $D_{12}(u)$ as defined in (4.13).

Effective mass of the bipolaron

The effective mass m^* can be derived from the path integral propagation from $\vec{r}_i(0)$ to $\vec{r}_i(T) = \vec{r}_i(0) + \vec{U}T$, for $i = 1, 2$. The ground state energy then behaves as

$$E(U) = E(0) + \frac{m^* U^2}{2}. \tag{4.17}$$

This procedure was implemented by Feynman to derive the effective mass of a single polaron at arbitrary coupling [55]. The same treatment for two particles leads to an expression for the effective mass of the bipolaron:

$$m^* = 2m_I + 2\sum_{\vec{k}} \frac{\left|V_{\vec{k}}\right|^2}{\hbar} \int_0^\infty du e^{-\omega_{\vec{k}} u} \left[e^{-k^2 D_{11}(u)} + e^{i\vec{k}.\vec{a}} e^{-k^2 D_{12}(u)} \right] u^2 k_z^2. \tag{4.18}$$

With the functions $D_{11}(u)$ and $D_{12}(u)$ as defined in (4.12) and (4.13), respectively.

Single polaron limit

The trial system reduces to (twice) the Feynman one-polaron trial system for $K = \kappa' = 0$. For the eigenmodes this corresponds to $\Omega_3 \to 0$ and $\Omega_1 = \Omega_2 = \Omega$. This gives for the functions $D_{11}(u)$ (4.12) and $D_{12}(u)$ (4.13):

$$\lim_{\substack{\Omega_3 \to 0 \\ \Omega_1 = \Omega_2 = \Omega}} D_{11}(u) = \frac{\hbar}{2m_I} \left[\frac{\nu^2}{\Omega^2} u + \frac{\Omega^2 - \nu^2}{\Omega^2} \frac{1 - \exp[-\Omega u]}{\Omega} \right] = D(u); \tag{4.19}$$

$$\lim_{\substack{\Omega_3 \to 0 \\ \Omega_1 = \Omega_2 = \Omega}} D_{12}(u) \to \infty. \tag{4.20}$$

The upper bound for the ground state polaron energy (4.11) becomes in this limit:

$$\lim_{\substack{\Omega_3\to 0\\ \Omega_1=\Omega_2=\Omega}} E = 2\left[\frac{3}{2}\hbar\left(\Omega-\nu\right) - \frac{3}{4}\frac{\Omega^2-\nu^2}{\Omega^2}\hbar\Omega - \sum_{\vec{k}}\frac{\left|V_{\vec{k}}\right|^2}{\hbar}\int_0^\infty du e^{-\omega_{\vec{k}}u}e^{-k^2D(u)}\right]. \tag{4.21}$$

This is (twice) the upper bound for the ground state of a single polaron, as derived by Feynman [55]. The effective mass of the bipolaron becomes in this limit:

$$\lim_{\substack{\Omega_3\to 0\\ \Omega_1=\Omega_2=\Omega}} m^* = 2\left(m_I + \frac{1}{3}\sum_{\vec{k}}\frac{\left|V_{\vec{k}}\right|^2}{\hbar}\int_0^\infty du e^{-\omega_{\vec{k}}u}e^{-k^2D(u)}u^2k^2\right), \tag{4.22}$$

which is (twice) the single polaron effective mass, as derived by Feynman [55].

4.1.2 Two impurities in a Bose-Einstein condensate

We now consider the specific system of two impurity atoms in a Bose-Einstein condensate. Using an s-wave contact pseudo potential within the Born approximation gives for the impurity-impurity interaction:

$$\sum_{\vec{k}} V_{II}\left(\vec{k}\right)e^{i\vec{k}.\vec{a}}e^{-k^2D_{12}(0)} = \frac{\hbar^2a_{II}}{2\sqrt{\pi}m_ID_{12}\left(0\right)^{3/2}}e^{-\frac{a^2}{4D_{12}(0)}}, \tag{4.23}$$

with a_{II} the impurity-impurity scattering length. Introducing the interaction amplitude (1.26) gives for the upper bound for the ground state energy (4.11) (in the polaronic units of table 1.1):

$$\begin{aligned} E = &\sum_{j=1}^{3}\frac{3}{2}\Omega_j - 3\nu + \frac{a_{II}}{2\sqrt{\pi}D_{12}\left(0\right)^{3/2}}e^{-\frac{a^2}{4D_{12}(0)}} \\ &+ \frac{\alpha}{2\pi}\left(\frac{m_B+1}{m_B}\right)^2\int_0^\infty dk\left\{\frac{2m_B}{m_B+1}\right. \\ &\left.-\frac{k^3}{\sqrt{k^2+2}}\int_0^\infty du e^{-\omega_{\vec{k}}u}\left[e^{-k^2D_{11}(u)} + \frac{\sin\left[ak\right]}{ak}e^{-k^2D_{12}(u)}\right]\right\} \\ &- \frac{3}{2}\frac{\Omega_1^2-\nu^2}{\Omega_1^2}\frac{\Omega_1}{2} - \frac{3}{2}\frac{\Omega_2^2-\nu^2}{\Omega_2^2-\Omega_3^2}\frac{\Omega_2}{2} - \frac{3}{2}\frac{\nu^2-\Omega_3^2}{\Omega_2^2-\Omega_3^2}\frac{\Omega_3}{2}, \end{aligned} \tag{4.24}$$

where α is the dimensionless polaronic coupling parameter (1.34). The first term in the k-integrand in the right-hand side of expression (4.24) is a consequence of using the Lippmann-Schwinger equation up to second order for the impurity-boson interaction strength (1.2) in the second term of the total Hamiltonian (1.27) and is needed for convergence. A similar procedure was applied for the single-polaron all-coupling treatment in Ref. [89]. With the interaction amplitude (1.26) the bipolaron effective mass in polaronic units becomes

$$\begin{aligned} m^* &= 2 + \frac{\alpha}{8\pi^2}\left(\frac{1+m_B}{m_B}\right)^2\int d\vec{k}\frac{k}{\sqrt{k^2+2}} \\ &\quad\times\int_0^\infty du e^{-\omega_{\vec{k}}u}\left[e^{-k^2D_{11}(u)} + e^{i\vec{k}.\vec{a}}e^{-k^2D_{12}(u)}\right]u^2k_z^2. \end{aligned} \tag{4.25}$$

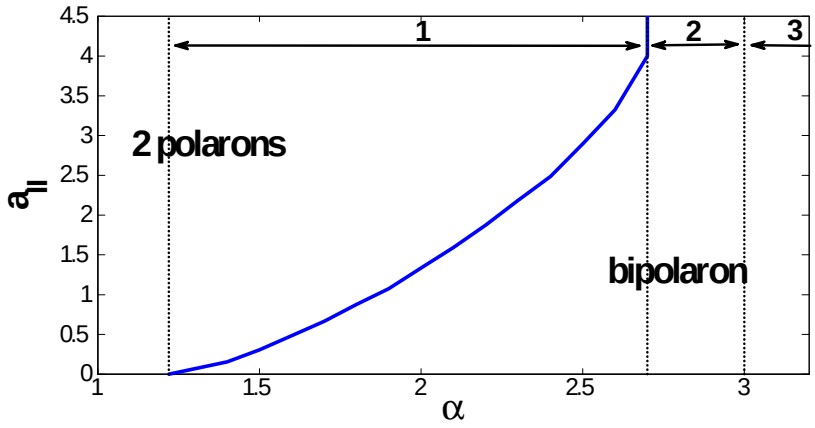

Figure 4.3: The (a_{II}, α) −phase diagram for two Li-6 impurties in a Na condensate with α the coupling parameter and a_{II} the impurity-impurity scattering length. The solid line indicates the polaron-bipolaron transition. The dotted lines at $\alpha = 1.22$, $\alpha = 2.71$ and $\alpha = 3$ indicate the boundaries of the different regions, as discussed in the text.

4.1.3 Results and discussion

For numerical calculations it is favorable to introduce a cutoff K_c for the k-integral in (4.24). Similar to the one-polaron case we use the inverse of the Van der Waals radius of the impurity-boson interaction potential for K_c [89]. We introduce the specific system of a Li-6 impurity in a Na condensate which amounts to $m_B/m_I = 3.8227$ and $\xi K_c = 200$.

Phase diagram

The upper bound for the ground state energy (4.24) was minimized as a function of the variational parameters $\{\vec{a}, \Omega_1, \Omega_2, \Omega_3, \nu\}$ for given values of the coupling parameter α and the impurity-impurity scattering length a_{II}. If the resulting upper bound is lower than twice the upper bound for the one-polaron ground state energy we conclude that it is energetically favorable to form a bipolaron, otherwise the system consists of two separate polarons. This procedure results in the (a_{II}, α)-phase diagram presented in Fig. 4.3 where we have also indicated three regions as a function of α. For $\alpha > 2.71$ the formation of a bipolaron is always energetically favorable, irrespective of a_{II}, and the area with $\alpha \in [2.71, 3]$ is denoted as region 2 (see Fig. 4.3). As discussed in the introduction the Feynman all-coupling singe polaron treatment predicts the transition to the strong coupling regime at $\alpha \approx 3$ [89] and the area with $\alpha > 3$ is denoted as region 3. From Fig. 4.3 it is clear that for $\alpha \in [1.22, 2.71]$ (region 1) the bipolaron is only stable at small values of a_{II}. For $\alpha < 1.22$ a bipolaron is never formed. If the bipolaron is stable the variationally determined vector $\vec{a}$, separating the impurities in the trial system of Fig. 4.1, is always zero in region 1, irrespective of a_{II}, while for $\alpha > 2.71$ it is finite at sufficiently large a_{II} in which case the shape of the bipolaron can be interpreted as a dumbbell.

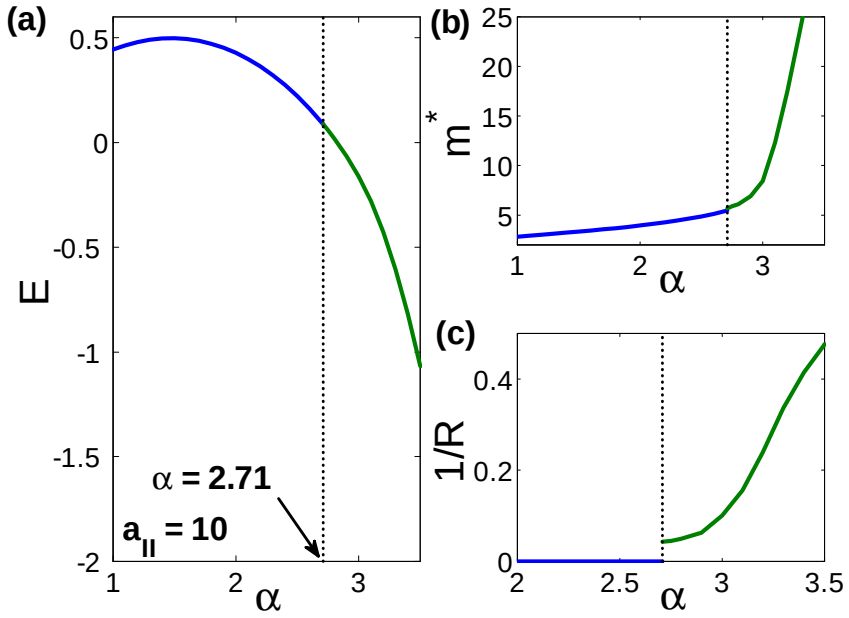

Figure 4.4: The upper bound of the ground state energy (a), the bipolaron effective mass (b) and the inverse of the bipolaron radius (c) are presented as a function of the polaronic coupling parameter α at $a_{II} = 10$ for two Li-6 impurity in a Na condensate. The dotted line at $\alpha = 2.71$ indicates the polaron-bipolaron transition.

Bipolaron mass and radius

In Fig. 4.4 the upper bound (4.24), the polaronic effective mass (4.25) and the inverse bipolaron radius (4.16) are presented as a function of the coupling parameter α at $a_{II} = 10$. For $\alpha < 2.71$ the system consists of two separate polarons while for $\alpha > 2.71$ a bipolaron is formed. For two separate polarons the bipolaron radius is defined as infinity. As a function of α the effective mass exhibits an increasing behavior and for $\alpha > 3$ it increases more rapidly, indicating the transition to the strong coupling regime which is also present for a single polaron [89]. If the bipolaron formation is stable the bipolaron radius decreases as a function of α. This shows that the bipolaron becomes more tightly bound as the coupling is increased.

In Fig. 4.5 the upper bound (4.24), the polaronic effective mass (4.25) and the inverse bipolaron radius (4.16) are presented as a function of the impurity-impurity scattering length a_{II} at $\alpha = 2$ (region 1 in Fig. 4.3). The energy and the effective mass of two polarons are also shown. This reveals that the formation of a bipolaron is only stable for sufficiently small values of a_{II}, with a polaron-bipolaron transition at $a_{II} = 1.3$. From Fig. 4.5 it is clear that in this case the polaron-bipolaron transition is accompanied with a discontinuity in the effective mass. The value $a_{II} = 0.6$ is also indicated in Fig. 4.5 which corresponds to another discontinuity in the effective mass, as well as in the bipolaron radius. For $a_{II} < 0.6$ the bipolaron is relatively small and heavy and the ground state energy and the properties exhibit a strong dependence on a_{II} as compared to the behavior for $a_{II} > 0.6$. This suggests that for $a_{II} < 0.6$ the bipolaron can be considered as a single tightly bound particle, while

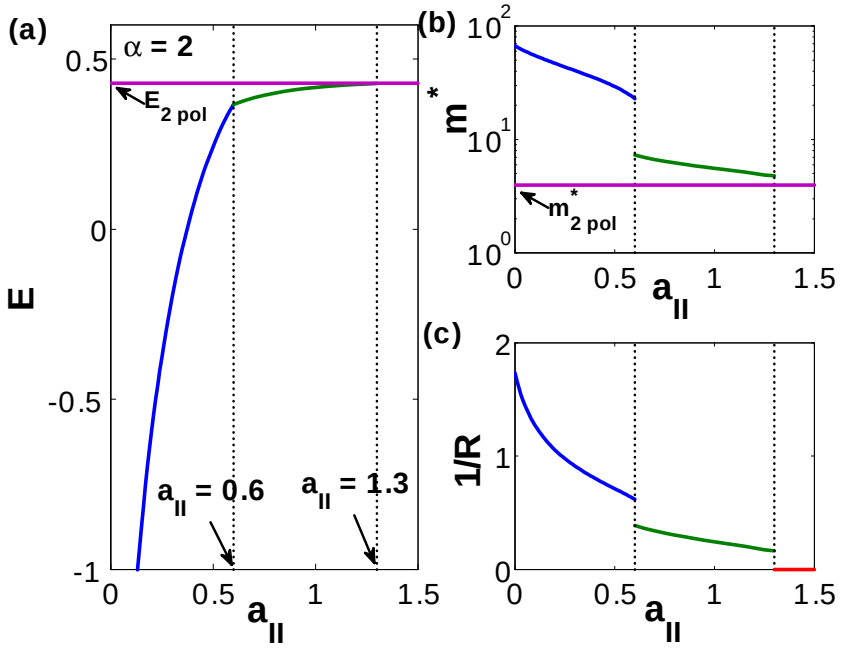

Figure 4.5: The upper bound of the ground state energy (a), the effective mass (b) (note the semi-logarithmic scale) and the inverse of the bipolaron radius (c) are presented as a function of the impurity-impurity scattering length a_{II} at $\alpha = 2$ (region 1 in Fig. 4.3) for two Li-6 impurities in a Na condensate. The polaron-bipolaron transition at $a_{II} = 1.3$ and the transition of the internal bipolaron state (see text) at $a_{II} = 0.6$ are indicated. Also the upper bound for the ground state energy of two separate polarons ($E_{2\text{ pol}}$) and the corresponding effective mass ($m^*_{2\text{ pol}}$) are shown.

for $a_{II} > 0.6$ it consists of a more loosely bound state of two polarons. Increasing a_{II} results in a less tightly bound bipolaron and finally in the formation of two separate polarons.

In Fig. 4.6 the upper bound (4.24), the polaronic effective mass (4.25) and the inverse bipolaron radius (4.16) are presented as a function of the impurity-impurity scattering length a_{II} at $\alpha = 2.85$ (region 2 in Fig. 4.3). The energy of two separate polarons is also indicated which shows that the formation of a bipolaron is always stable, for every value of a_{II}. Also here we find that increasing a_{II} results in a less tightly bound bipolaron. Again we can distinguish two regimes in the a_{II}-dependence of E and m^*, but now without a discontinuity at the transition. At small a_{II} the increase of the ground state energy and the decrease of the effective mass as a function of a_{II} are significantly faster than at higher values of a_{II}, with a transition around $a_{II} \approx 2$. As before, this indicates that at small values of a_{II} the bipolaron can be considered as a single particle while at large values it is more appropriately interpreted as two loosely bound polarons, but now with a continuous transition. Moreover, at small values for aII the variationally determined vector $\vec{a}$, separating the two impurities in the trial system of Fig. 4.1, is zero while for relatively large a_{II} it is finite. This shows that the loosely bound polarons at large a_{II} are spatially separated and the shape can be interpreted as a dumbbell.

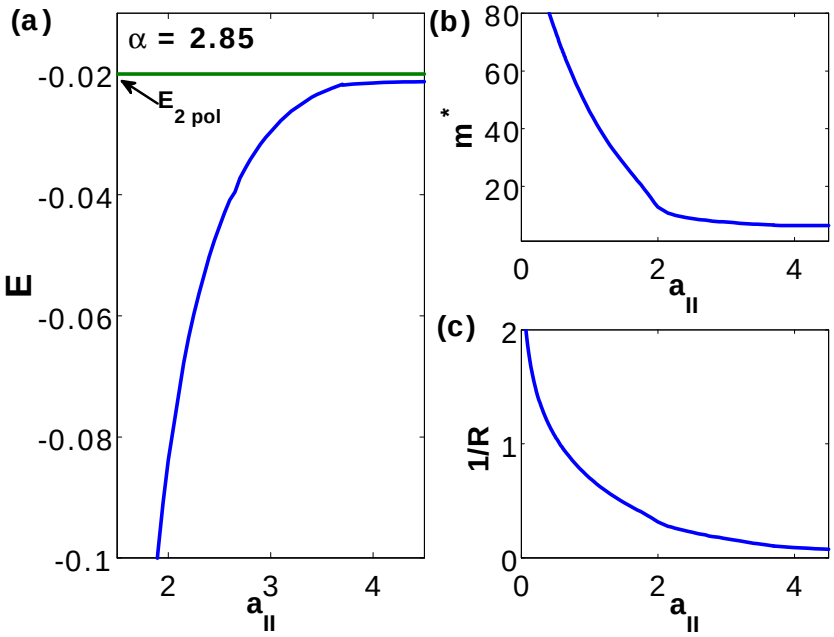

Figure 4.6: The upper bound of the ground state energy (a), the effective mass (b) and the inverse of the bipolaron radius (c) are presented as a function of the impurity-impurity scattering length a_{II} at $\alpha = 2.85$ (region 2 in Fig. 4.3) for two Li-6 impurities in a Na condensate. The upper bound for the ground state energy of two polarons ($E_{2\,\mathrm{pol}}$) is also indicated.

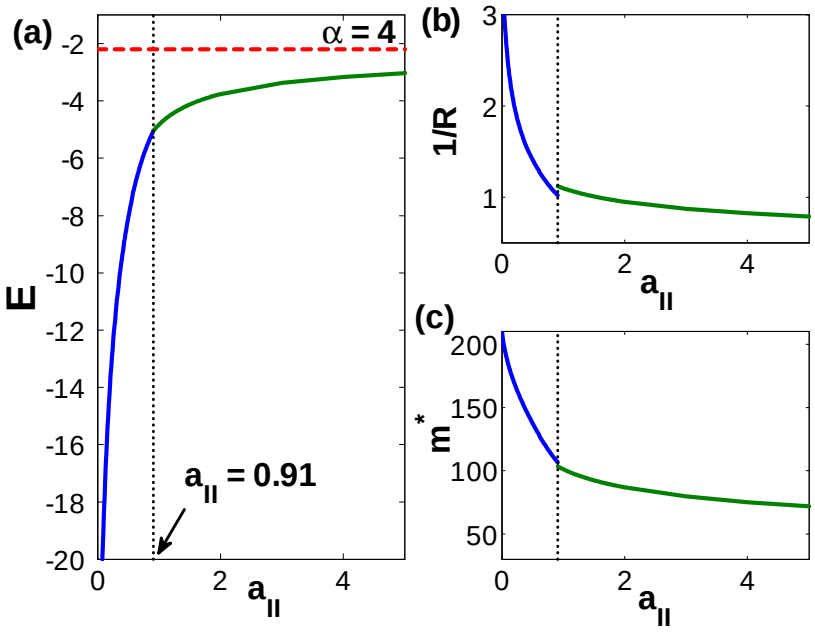

Figure 4.7: The upper bound of the ground state energy (a), the inverse of the bipolaron radius (b) and the effective mass (c) are presented as a function of the impurity-impurity scattering length a_{II} at $\alpha = 4$ (region 3 in Fig. 4.3) for two Li-6 impurities in a Na condensate. The dotted line at $a_{II} = 0.91$ indicates the transition of the internal state of the bipolaron (see text). The dashed line shows the upper bound to the ground state energy in the limit $a_{II} \to \infty$.

Finally, in Fig. 4.7 the upper bound (4.24), the polaronic effective mass (4.25) and the inverse bipolaron radius (4.16) are presented as a function of the impurity-impurity scattering length a_{II} at $\alpha = 4$ (region 3 in Fig. 4.3). The upper bound (4.24) in the limit $a_{II} \to \infty$ is also indicated and is lower than for two separate polarons which shows that formation of a bipolaron is always stable. Also here we observe two regimes as a function of a_{II} with a transition at $a_{II} = 0.91$ which is accompanied with a discontinuity in the effective mass and the bipolaron radius, indicating a transition between a single-particle bipolaron and a more loosely bound state of two polarons. Also in this case the variationally determined vector $\vec{a}$ is zero for the tightly bound bipolaron and non-zero for the loosely bound state of two polarons, resulting in a dumbbell bipolaron.

4.2 Strong coupling formalism for the multi-polaron

We now apply a generalization of the Landau-Pekar strong-coupling treatment for N_I polaronic particles to impurities in a Bose-Einstein condensate to examine the formation of multi-polaron. The formal steps in the derivation are similar to the strong-coupling treatment of a single polaron in chapter 3.

4.2.1 Formalism

For the description of the strong coupling formalism the product Ansatz is used which states that the total wave function ($|\Phi\rangle$) is the product of a part describing the Bogoliubov excitations ($|\phi\rangle$) and a part for the impurities ($\left|\Psi^{(N_I)}\right\rangle$): $|\Phi\rangle = |\phi\rangle \left|\Psi^{(N_I)}\right\rangle$. Taking the expectation value of the Fröhlich Hamiltonian (1.21) with respect to $|\Phi\rangle$ and completing the squares for the Bogoliubov creation and annihilation operators results in:

$$\left\langle \Phi \left| \widehat{H}_{pol}^{(N_I)} \right| \Phi \right\rangle = K + \sum_{\vec{k}\neq 0} \hbar\omega_{\vec{k}} \left\langle \phi \left| \left(\widehat{\alpha}_{\vec{k}}^{\dagger} + \frac{V_{\vec{k}}\rho_{\vec{k}}}{\hbar\omega_{\vec{k}}} \right) \left(\widehat{\alpha}_{\vec{k}} + \frac{V_{\vec{k}}^{*}\rho_{\vec{k}}^{*}}{\hbar\omega_{\vec{k}}} \right) \right| \phi \right\rangle - \sum_{\vec{k}\neq 0} \frac{\left|V_{\vec{k}}\rho_{\vec{k}}\right|^2}{\hbar\omega_{\vec{k}}} + U, \tag{4.26}$$

where K is the kinetic energy, $\rho_{\vec{k}}$ the Fourier transform of the density and U the mutual interaction energy of the impurities:

$$K = \left\langle \Psi^{(N_I)} \left| \sum_{i=1}^{N_I} \frac{\widehat{p_i}^2}{2m_I} \right| \Psi^{(N_I)} \right\rangle; \tag{4.27}$$

$$\rho_{\vec{k}} = \left\langle \Psi^{(N_I)} \left| \sum_{i=1}^{N_I} e^{i\vec{k}.\widehat{\vec{r}}_i} \right| \Psi^{(N_I)} \right\rangle; \tag{4.28}$$

$$U = \left\langle \Psi^{(N_I)} \left| \sum_{i<j}^{N_I} V_{II}\left(\widehat{\vec{r}}_i - \widehat{\vec{r}}_j\right) \right| \Psi^{(N_I)} \right\rangle. \tag{4.29}$$

The expectation value of the Hamiltonian (4.26) is minimal if the wave function of the Bogoliubov excitations is chosen as the vacuum $\left|\phi_g\right\rangle$ for the "displaced operators":

$$\left\langle \phi_g \left| \left(\widehat{\alpha}_{\vec{k}}^{\dagger} + \frac{V_{\vec{k}}\rho_{\vec{k}}}{\hbar\omega_{\vec{k}}} \right) \left(\widehat{\alpha}_{\vec{k}} + \frac{V_{\vec{k}}^{*}\rho_{\vec{k}}^{*}}{\hbar\omega_{\vec{k}}} \right) \right| \phi_g \right\rangle = 0. \tag{4.30}$$

This results in the following expression for the ground state energy:

$$E_0^{(N_I)} = K - \sum_{\vec{k}\neq 0} \frac{\left|V_{\vec{k}}\right|^2 \left|\rho_{\vec{k}}\right|^2}{\hbar\omega_{\vec{k}}} + U. \tag{4.31}$$

This result can alternatively be derived with a canonical transformation, as done by Bogoliubov and Tyablokov for a single polaron [53]. For the impurities we will use a variational wave function, the resulting energy (4.31) is then an upper bound for the ground state energy.

Effective mass

The strong-coupling formalism allows a derivation of the multi-polaron effective mass in a similar way as was done for a single polaron in chapter 3 and for the bipolaron

in Ref. [146]. The total momentum of the polaronic system $\widehat{\vec{\mathcal{P}}}$ is given by

$$\widehat{\vec{\mathcal{P}}} = \widehat{\vec{P}} + \sum_{\vec{k}} \hbar \vec{k} \widehat{\alpha}^{\dagger}_{\vec{k}} \widehat{\alpha}_{\vec{k}}, \tag{4.32}$$

with $\widehat{\vec{P}} = \sum_i^{N_I} \widehat{\vec{p}}_i$. This operator commutes with the Fröhlich Hamiltonian (1.21) and the total momentum is thus a constant of motion: $\left\langle \widehat{\vec{\mathcal{P}}} \right\rangle = \vec{\mathcal{P}}$. We make this explicit by means of a Lagrange multiplier $\vec{v}$ which physically represents the velocity of the system and consider the operator

$$\widehat{H}^{(N_I)}_{pol}(\vec{v}) = \widehat{H}^{(N_I)}_{pol} - \vec{v}.\left(\widehat{\vec{P}} + \sum_{\vec{k}} \hbar \vec{k} \widehat{\alpha}^{\dagger}_{\vec{k}} \widehat{\alpha}_{\vec{k}} - \vec{\mathcal{P}} \right) \tag{4.33}$$

for minimization. The effective mass m^* of the multi-polaron can then be determined from the relation $\vec{\mathcal{P}} = m^* \vec{v}$. The impurity variational wave function $\left|\Psi^{(N_I)}\right\rangle$, with $\left\langle \widehat{\vec{P}} \right\rangle = 0$, has to be adapted to a wave function with finite averaged momentum $\left\langle \widehat{\vec{P}} \right\rangle = N_I m_I \vec{v}$, we use

$$\Psi'^{(N_I)}(\{\vec{r}_i\}) = \exp\left[\frac{i m_I \vec{v}.\sum \vec{r}_i}{\hbar} \right] \Psi^{(N_I)}(\{\vec{r}_i\}). \tag{4.34}$$

Taking the expectation value of $\widehat{H}^{(N_I)}_{pol}(\vec{v})$ with respect to the product wave function $|\phi\rangle \left|\Psi'^{(N_I)}\right\rangle$ and introducing the wave function $\left|\phi_g\right\rangle$ for the Bogoliubov excitations, as in (4.30), results in:

$$E^{(N_I)}(\vec{v}) = K + U - N_I \frac{m_I v^2}{2} + v.\vec{\mathcal{P}} - \sum_{\vec{k}\neq 0} \frac{\left|V_{\vec{k}}\right|^2 \left|\rho_{\vec{k}}\right|^2}{\hbar\omega_{\vec{k}} - \hbar\vec{v}.\vec{k}}, \tag{4.35}$$

with K, $\rho_I\left(\vec{k}\right)$ and U as defined in (4.27), (4.28) and (4.29), respectively. Minimizing expression (4.35) with respect to $\vec{v}$ and performing a Taylor expansion for small $\vec{v}$ gives for the effective mass

$$m^* = N_I m_I + 2\hbar^2 \sum_{\vec{k}\neq 0} \frac{\left|V_{\vec{k}}\right|^2 \left|\rho_{\vec{k}}\right|^2}{\left(\hbar\omega_{\vec{k}}\right)^3} k_z^2, \tag{4.36}$$

with k_z the z-component of $\vec{k}$, which is chosen in the direction of $\vec{v}$.

Variational impurity wave function

For N_I distinguishable particles we consider the following normalized variational wave function:

$$\Psi^{(N_I)}(\{\vec{r}_i\}) = \prod_{i=1}^{N_I} \frac{1}{\left(\pi\lambda^2\right)^{3/4}} \exp\left[-\frac{\left(\vec{r}_i - \vec{a}_i\right)^2}{2\lambda^2} \right], \tag{4.37}$$

which consists of N_I Gaussians with standard deviation λ, centered at $\vec{a}_i$. The corresponding expectation values are

$$K = N_I \frac{3\hbar^2}{4m_I\lambda^2}; \tag{4.38}$$

$$U = \sum_{i<j}^{N_I} \sum_{\vec{k}} V_{II}\left(\vec{k}\right) e^{-\frac{k^2\lambda^2}{2} + i\vec{k}.(\vec{a}_1 - \vec{a}_2)}; \tag{4.39}$$

$$\rho_{\vec{k}} = \exp\left[-\frac{k^2\lambda^2}{4}\right] \sum_{i=1}^{N_I} e^{i\vec{k}.\vec{a}_i}. \tag{4.40}$$

The wave function (4.37) can be extended to the case of identical impurities by using a Slater determinant for fermions or the appropriate symmetrized wave function for bosons.

Single polaron limit

If all the impurities are infinitely separated we expect the multi-polaron to reduce to individual polarons. For the impurity wave function (4.37) this corresponds to the limit $|\vec{a}_i - \vec{a}_j| \to \infty \; \forall i \neq j$. The upper bound for the polaron ground state energy (4.31) becomes in this limit:

$$\lim_{\substack{|\vec{a}_i - \vec{a}_j| \to \infty \\ \forall i \neq j}} E_0^{(N_I)} = N_I \left(\frac{3\hbar^2}{4m_I\lambda^2} - \sum_{\vec{k}\neq 0} \frac{\left|V_{\vec{k}}\right|^2}{\varepsilon_{\vec{k}}} e^{-\frac{k^2\lambda^2}{2}} \right) = N_I E_0^{(1)}. \tag{4.41}$$

This equals N_I times the strong-coupling result for the upper bound for the ground state energy of a single polaron ($E_0^{(1)}$), as expected. The effective mass of the multi-polaron (4.36) becomes in this limit:

$$\lim_{\substack{|\vec{a}_i - \vec{a}_j| \to \infty \\ \forall i \neq j}} m^* = N_I \left(m_I + 2\hbar^2 \sum_{\vec{k}\neq 0} \frac{\left|V_{\vec{k}}\right|^2}{\left(\hbar\omega_{\vec{k}}\right)^3} e^{-\frac{k^2\lambda^2}{2}} k_z^2 \right) = N_I m^*_{pol}. \tag{4.42}$$

This is N_I times the strong-coupling result for the effective mass of a single polaron (m^*_{pol}), again as expected.

4.2.2 Impurities in a Bose-Einstein condensate

We now consider the specific polaronic system consisting of impurities in a BEC. Introducing the Bogoliubov dispersion (1.15), the interaction amplitude (1.26) and the variational wave function (4.37) for N_I distinguishable impurities in the upper bound for the ground state energy (4.31) gives (in the polaronic units of table 1.1):

$$\begin{aligned} E_0^{(N_I)} = & \frac{3N_I}{4\lambda^2} + \frac{2a_{II}}{(2\pi)^{1/2}\lambda^3} \sum_{i<j}^{N_I} \exp\left[-\frac{(\vec{a}_i - \vec{a}_j)^2}{2\lambda^2}\right] \\ & - \frac{2\alpha\mu}{\pi} \int_0^\infty dk k^2 \frac{\exp\left[-\frac{k^2\lambda^2}{2}\right]}{k^2+2} \sum_{i,j}^{N_I} \frac{\sin\left[k\left|\vec{a}_i - \vec{a}_j\right|\right]}{k\left|\vec{a}_i - \vec{a}_j\right|}, \end{aligned} \tag{4.43}$$

where an s-wave contact pseudo potential within the Born approximation was used for the impurity-impurity interaction. We also introduced expression (1.34) for the dimensionless polaronic coupling parameter α and the dimensionless mass factor

$$\mu = \frac{(m_B + m_I)^2}{4 m_B m_I}. \tag{4.44}$$

In the strong coupling regime the mass parameter m_B/m_I and the coupling parameter α combine to a single dimensionless coupling parameter $\alpha\mu$. The effective mass of N_I impurities in a BEC in polaronic units can be written as

$$m^* = N_I m_I + \frac{4\alpha\mu m_B^2}{\pi^2} \int d\vec{k} \frac{\left|\rho_{\vec{k}}\right|^2}{(2+k^2)^2} \frac{k_z^2}{k^2}. \tag{4.45}$$

4.2.3 Results

Bipolaron

First, we examine two impurities in a Bose-Einstein condensate ($N_I = 2$) and the formation of a bipolaron. The bipolaron radius, estimated by the mean square distance between the impurities (4.16), gives for the impurity variational wave function (4.37):

$$R = \sqrt{\left\langle (\vec{r}_1 - \vec{r}_2)^2 \right\rangle} = \sqrt{a^2 + 3\lambda^2}, \tag{4.46}$$

with $a = |\vec{a}_1 - \vec{a}_2|$.

In Fig. 4.8 the phase diagram of two distinguishable impurity atoms in a BEC is presented. With each a_{II} a value $(\alpha\mu)_{exist}$ is associated in such a way that for $\alpha\mu < (\alpha\mu)_{exist}$ the minimization of the right-hand side of expression (4.43) yields no solution at a finite value of λ. If $\alpha\mu > (\alpha\mu)_{exist}$ another value $(\alpha\mu)_{stable}$ can be determined, separating a region with a metastable bipolaron (positive ground state energy) for $\alpha\mu < (\alpha\mu)_{stable}$ from a region with a stable bipolaron (negative ground state energy) for $\alpha\mu > (\alpha\mu)_{stable}$. In the case of a metastable bipolaron the impurities are expected to be expelled from the condensate. However, since the formalism is only expected to be valid at strong coupling, the physical relevance of the metastable bipolaron is not obvious. In the limit $a_{II} \to \infty$ the strong-coupling results for a single polaron from chapter 3 are retrieved: $(\alpha\mu)_{exist} = 3.57$ and $(\alpha\mu)_{stable} = 3.84$. For $\alpha\mu > 3.84$ (region 3) the formation of the bipolaron is always energetically favorable as compared to the formation of two separate polarons, irrespective of a_{II}. For $\alpha\mu \in [3.39, 3.84]$ (region 2) a stable solution only exists if a_{II} is smaller than a critical value which is relatively large and increases rapidly as a function of $\alpha\mu$. For $\alpha\mu \in [1.92, 3.39]$ (region 1) a stable bipolaron also only exists for a_{II} smaller than a critical value, but now this critical value is relatively low and increases much more slowly as a function of $\alpha\mu$, as compared to the behavior in region 2. At weaker coupling ($\alpha\mu < 1.92$) there is never a stable solution. Considering the stable solution, the variationally determined vector $\vec{a}_1 - \vec{a}_2$, which represents the separation between the two Gaussians in the wave function (4.37), is always zero if $\alpha\mu < 3.39$, for $\alpha\mu > 3.39$ it is non-zero at sufficiently large values of a_{II}, resulting in a dumbbell bipolaron.

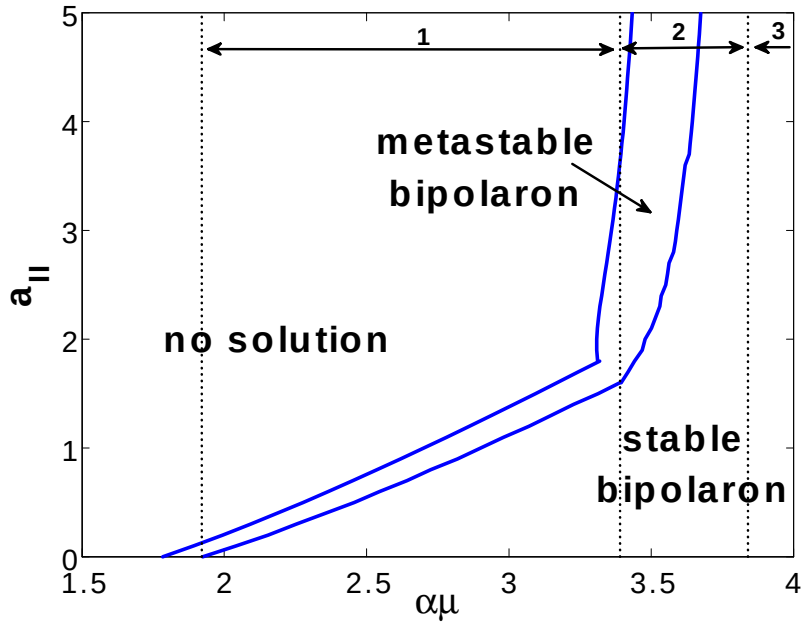

Figure 4.8: The solid lines show the (a_{II}, α)-phase diagram for two distinguishable impurity atoms in a Bose-Einstein condensate as a function of the coupling parameter $\alpha\mu$ and the impurity-impurity scattering length a_{II} as calculated with the strong-coupling formalism. At strong coupling the formation of a bipolaron is stable and at sufficiently weak coupling there is no solution. In between there is a region where the solution results in a positive ground state energy, which means the bipolaron is metastable. The dotted lines at $\alpha\mu = 1.92$, $\alpha v = 3.39$ and $\alpha\mu = 3.84$ indicate the boundaries of the different regions, as discussed in the text.

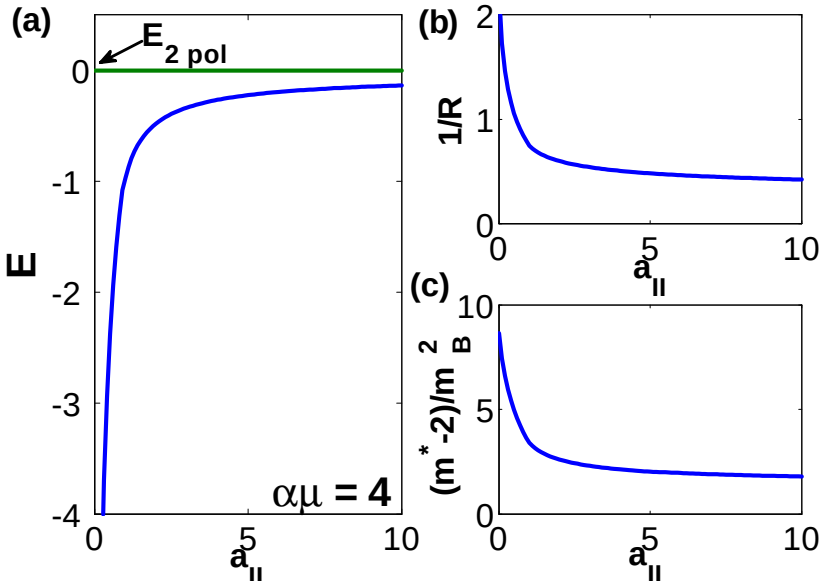

Figure 4.9: The upper bound for the ground state energy (a), the inverse bipolaron radius (b) and the effective mass (c) as a function of the impurity-impurity scattering length a_{II} at $\alpha\mu = 4$ for two distinguishable impurities in a Bose-Einstein condensate. The upper bound for the ground state energy of two polarons ($E_{2\,\mathrm{pol}}$) is also indicated.

In Fig. 4.9 the upper bound for the ground state energy (4.43), the inverse bipolaron radius (4.46) and the effective mass (4.45) are presented as a function of the impurity-impurity scattering length a_{II} for two distinguishable impurities in a BEC at $\alpha\mu = 4$. The upper bound for the ground state energy of two single polarons is also indicated which shows that the formation of a bipolaron is energetically favorable for all finite values of a_{II}. From Fig. 4.9 we see that for increasing a_{II} the bipolaron binding energy decreases, the radius increases and the effective mass decreases, showing that the bipolaron becomes less tightly bound. In the limit $a_{II} \to \infty$ the bipolaron effective mass becomes twice the effective mass of a single polaron. Considering the a_{II}-dependence of the properties reveals two regimes with a transtition at $a_{II} = 0.85$. For $a_{II} < 0.85$ there is a relatively strong dependence of the properties on a_{II} as compared to the behavior for $a_{II} > 0.85$. Furthermore, the variationally determined vector $\vec{a}_1 - \vec{a}_2$, representing the distance between the two centers of the Gaussians in the wave function (4.37), is only non-zero for $a_{II} > 0.85$. This is consistent with our earlier interpretation, in that for $a_{II} < 0.85$ the bipolaron is tightly bound while for $a_{II} > 0.85$ it is a more loosely bound dumbbell bipolaron.

A similar analysis can be made for identical impurities by anti-symmetrizing the wave function (4.37) for fermions or symmetrizing it for bosons. In the case of two identical bosons the same qualitative results are retrieved as we find for distinguishable impurities. For identical fermions the symmetry of the wave function results in a vanishing expectation value of the s-wave contact pseudo potential (4.39) which implies that at ultra low temperatures identical fermions behave as non-

interacting particles. The only remaining parameter is the coupling parameter $\alpha\mu$ and we find $(\alpha\mu)_{exist} = 3.09$ as a minimum for a solution to exist and $(\alpha\mu)_{stable} = 3.31$ as a minimum to find a stable solution. Furthermore, if a solution exists, it is always energetically favorable to form a bipolaron as compared to two separate polarons.

Multi-polaron

We now examine the multi-polaron by minimizing the upper bound for the ground state energy (4.43) for $N_I = 1, 2, ..., 8$ distinguishable impurities. In Ref. [88] a similar procedure was presented, but the expectation values of the positions of the impurities was considered equal which corresponds to the variational wave function (4.37) with $\vec{a}_i = \vec{a}_j \ \forall i, j$.

In Fig. 4.10 (a) the resulting $(a_{II}, \alpha\mu)$-phase diagram is presented for $N_I = 1, 2, ..., 8$ distinguishable impurities in a Bose-Einstein condensate as a function of the polaronic coupling $\alpha\mu$ and the impurity-impurity scattering length a_{II}. Similar to before for the bipolaron, we find for each a_{II} a minimum coupling value $(\alpha\mu)_{exist}$ for a solution of the minimization of (4.43) to exist at finite λ and another minimum value $(\alpha\mu)_{stable}$ ($(\alpha\mu)_{stable} > (\alpha\mu)_{exist}$) to find a stable solution. In the limit $a_{II} \to \infty$ the one-polaron strong-coupling results are found for any number of impurities: $(\alpha\mu)_{exist} = 3.57$ and $(\alpha\mu)_{stable} = 3.84$. In Fig. 4.10 (a) only $(\alpha\mu)_{stable}$ is presented for clarity. This shows that if the number of impurities N_I is increased $(\alpha\mu)_{stable}$ decreases, resulting in a larger stability region. This behavior of a smaller critical coupling value for the formation of a larger multi-polaron was also reported in Ref. [88].

The $(a_{II}, \alpha\mu)$-phase diagram in Fig. 4.10 (a) for a specific number N_I of impurities is qualitatively the same as for the bipolaron in Fig. 4.8. This means the same qualitative regions can be distinguished as a function of $\alpha\mu$ we did for the bipolaron in Fig. 4.8 and we present a general analysis, valid for every value of N_I .In region 3 the formation of the multi-polaron is always energetically favored as compared to N_I separate polarons. Furthermore, the variationally determined locations of the impurities $\vec{a}_i$ coincide at sufficiently small a_{II}, indicating that the multi-polaron behaves as a tightly bound single particle, while at relatively large a_{II} we find $\vec{a}_i \neq \vec{a}_j \ \forall i \neq j$, indicating a bound droplet of N_I polarons (cfr. the dumbbell bipolaron). In region 2 the minimization of the right-hand side of (4.43) yields no stable solution if a_{II} is larger than a critical value which is relatively large and increases rapidly as a function of $\alpha\mu$. In region 1 there is also no stable solution for a_{II} above a critical value which is now relatively low and increases slowly as a function of $\alpha\mu$. In this regime the behavior of the critical a_{II} as a function of $\alpha\mu$ resembles a straight line and it was shown in Ref. [88] that in the limit $N_I \to \infty$ this line is well-approximated by the boundary for phase separation [155–158]:

$$\frac{a_{II}}{\xi} = \alpha\mu. \tag{4.47}$$

For $\alpha\mu \ll 1$ there is never a solution.

In Fig. 4.10 (b) the upper bound for the multi-polaron ground state energy per impurity is presented as a function of the impurity-impurity scattering length a_{II} at $\alpha\mu = 4$. For $a_{II} \to \infty$ all curves tend to the single-polaron result. At finite a_{II}

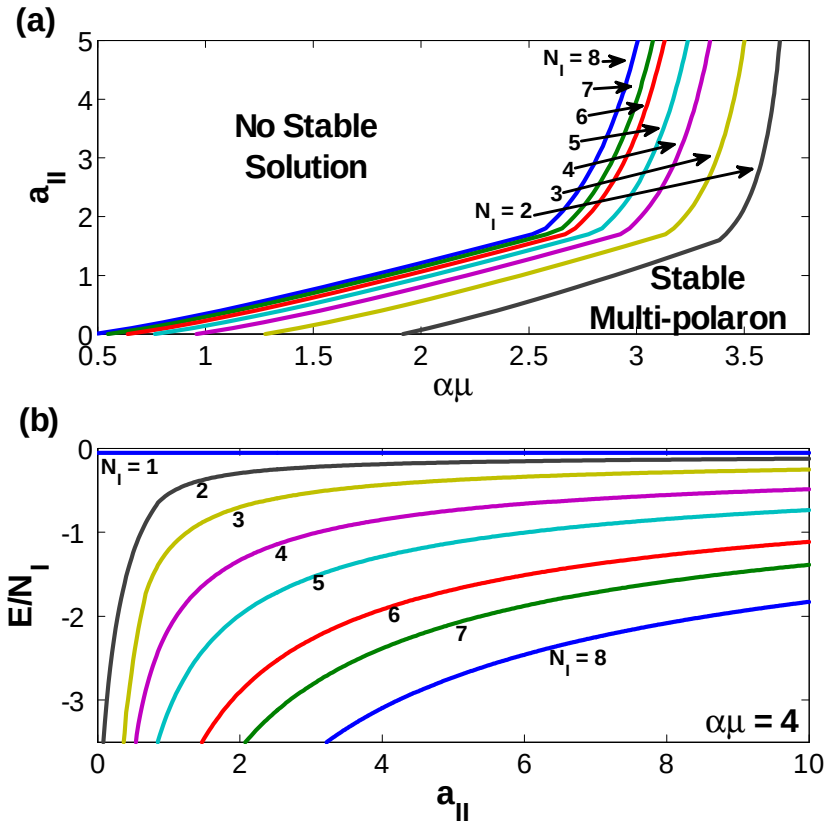

Figure 4.10: In (a) the $(a_{II}, \alpha\mu)$-phase diagram for N_I distinguishable impurities in a Bose-Eintein condensate with respect to the formation of a stable multi-polaron is presented with $\alpha\mu$ the coupling parameter and a_{II} the impurity-impurity scattering length. In (b) the upper bound for the multi-polaron ground state energy per impurity is presented as a function of the impurity-impurity scattering length a_{II} for distinguishable impurities at $\alpha\mu = 4$.

the ground state energy per particle decreases as N_I is increased, showing that it is energetically favorable for the impurities to cluster or to form a multi-polaron.

For positive impurity-boson scattering length there is a depletion of the condensate in the vicinity of the multi-polaron. This can be detrimental for the polaronic description since the Bogoliubov approximation breaks down at large depletion. This possible restriction is only expected to be important if the multi-polaron is in the single-particle regime at relatively small a_{II}. In the case of a bound state of separate single-polarons the mean distance between the impurities is typically of the order of the healing length which shows that the depletion is spread out over a large volume and the Bogoliubov approximation is not endangered. These considerations result in a maximum for the number of impurities in a single-particle multi-polaron which for typical experimental parameters is of the order of 1 [88].

4.3 Comparison of the bipolaron results from the two formalisms

The results of the strong-coupling formalism of section 4.2, applied to the specific system of two distinguishable Li-6 impurities in a Na condensate ($m_B/m_I = 3.82$ and $\mu = 1.52$) can be compared to the results of the path integral treatment of Sec. 4.1, in the case of the bipolaron. The phase diagrams in Figs. 4.3 and 4.8 exhibit a similar qualitative behavior. In both cases there is no formation of a bipolaron if the polaronic coupling is to weak and at slightly stronger coupling (region 1) the bipolaron is only formed at relatively small a_{II}. In region 2 the all-coupling approach from section 4.1 predicts always formation of the bipolaron while according to the strong-coupling approach there is no bipolaron formation at relatively large values of a_{II}. In region 3 both formalisms agree on the prediction that the bipolaron is always formed, irrespective of a_{II}. Quantitatively the strong-coupling formalism underestimates the critical coupling parameter for bipolaron formation, as compared to the all-coupling approach. Note that the strong-coupling approach also underestimates the critical coupling value for the transition to the strong coupling regime, as compared to a numerical study [147].

Considering the a_{II}-dependence of the properties both formalisms reveal two distinct regimes. The behavior at relatively small a_{II} corresponds to a tightly bound bipolaron that behaves as a single-particle while at relatively large a_{II} it is better interpreted as a loosely bound dumbbell bipolaron. The all-coupling approach predicts a possible discontinuity in the polaronic properties at this transition which diminishes as the coupling is increased and ultimately, well in the strong-coupling regime, vanishes, as also predicted by the strong-coupling treatment.

4.4 Conclusions

The Jensen-Feynman all-coupling polaron treatment was applied for two distinguishable impurities in a condensate. This showed that if the polaronic coupling is strong enough a bipolaron is formed. We also calculated the bipolaron effective mass and the bipolaron radius. Considering the dependence of the polaronic properties on the impurity-impurity scattering length a_{II} results in the determination of two regimes as a function of a_{II}, a tightly bound bipolaron that behaves as a single particle at relatively small a_{II} and a more loosely bound dumbbell bipolaron at sufficiently large a_{II}. If the coupling is sufficiently strong or weak this transition is found to be accompanied by a discontinuity in the properties of the bipolaron which becomes less pronounced as the coupling is increased towards the strong-coupling regime.

We also applied a Landau-Pekar-type strong-coupling treatment to impurities in a Bose-Einstein condensate. For two distinguishable impurities in a BEC at strong coupling this leads to similar results as found by the all-coupling treatment. This strong-coupling treatment was then extended to identical impurities. For identical bosons this results in the same qualitative results as for distinguishable impurities. For identical fermions the mutual s-wave interaction vanishes and above a critical

coupling strength the formation of a bipolaron is always energetically favored as compared to two separate polarons.

The strong-coupling treatment was then applied for multiple impurities in a BEC to consider the formation of a multi-polaron. We find that the multi-polaron becomes stable at weaker coupling as the number of impurities is increased, in accordance with the result of Ref. [88]. Furthermore, the ground state energy per particle decreases as N_I is increased which shows that clustering is energetically favorable in the strong coupling regime.

Chapter 5

Polaron in reduced dimensions*

As discussed in the introduction, optical lattices can be used to modify the geometry of a system in the context of ultracold gases which allows a reduction of the dimensionality. For deep optical lattices these systems can be described by a low-dimensional theory with effective interatomic interactions that depend on the confinement length. This dependence of the interaction strength on the confinement length can exhibit confinement-induced resonances, thus allowing an additional experimental handle on the system as the confinement strength is externally tunable.

In the context of the solid state polaron the study of reduced dimensions revealed the existence of polaronic scaling relations predicting an enhancement of the strong coupling regime in lower dimensions [67–69]. These scaling relations are applicable for polaronic systems with an interaction amplitude $V_{\vec{k}}$ that is a homogeneous function which is not the case for the BEC-impurity polaron.

In this chapter we expand the calculations of the ground state and response properties of an impurity atom in a condensate in 3D to the case of reduced dimensions. We start by showing that also in lower dimensions the Hamiltonian of an impurity in a condensate can be mapped onto the Fröhlich Hamiltonian. Then, the Jensen-Feynman variational principle is applied to calculate an upper bound for the free energy. Also the effective mass and the radius of the polaron are estimated. Subsequently, the treatment of chapter 2 for the polaronic response to Bragg spectroscopy is applied to reduced dimensions.

5.1 Impurity in a condensate in d dimensions

Strictly speaking it is not possible to have long-range order in reduced dimensions and thus no Bose-Einstein condensation [159, 160]. However, for all practical situations the system only occupies a finite volume for which true long-range order is not required. In Refs. [161] and [162] it is shown that in one and two dimensions, respectively, at temperatures well below a critical temperature T_c a trapped Bose gas is characterized by the presence of a true condensate while just below T_c this is a quasicondensate. A quasicondensate exhibits phase coherence over a radius R_ϕ

*The results of this chapter are published in W. Casteels, J. Tempere and J. T. Devreese - *Polaronic properties of an impurity in a Bose-Einstein condensate in reduced dimensions* - Phys. Rev. A **86**, 043614 (2012).

that is smaller than the size of the system but greatly exceeds the healing length ξ. Since the radius of the polaron R_{pol} is typically of the order of ξ (see later) we have $R_{pol} \ll R_\phi$. This shows that the polaronic features are also present for an impurity in a quasicondensate. In the following we no longer make the distinction and use the name condensate for both situations.

We again assume that the bosons form a condensate by applying the Bogoliubov approximation, as outlined in section 1.1.3. Using contact-interactions for the interparticle interactions and following the same steps as in section 1.3 shows that the Hamiltonian of the system of an impurity in a condensate in d dimensions also maps onto the Fröhlich Hamiltonian (1.17) with the Bogoliubov dispersion (1.15) and the interaction amplitude (1.26). If the dimensionality is kept general the healing length can be defined as $\xi = \hbar/\sqrt{2m_B N_0 g_{BB}}$. The main difference to the three dimensional case is that all vectors are d-dimensional and that the interaction amplitudes g_{BB} and g_{IB} depend on the strength of the confinement.

5.2 Polaronic ground state properties in d dimensions

In this section we summarize the main results of the Feynman all-coupling description of a polaron with special emphasis on the dependency on the dimension (see for example Ref. [29] for more details). This is then applied to the polaronic system consisting of an impurity in a condensate.

5.2.1 Jensen-Feynman variational principle

Introducing the model system from Ref. [55] (and schematically presented in Fig. 1.9) to the Jensen-Feynman inequality (1.28) in d dimensions leads to [67]:

$$\begin{aligned}\mathcal{F} \leq & \frac{d}{\beta}\left\{\ln\left[2\sinh\left(\frac{\beta\hbar\Omega}{2}\right)\right] - \ln\left[2\sinh\left(\frac{\beta\hbar\Omega}{2\sqrt{1+M/m}}\right)\right]\right\} \\ & - \frac{1}{\beta}\ln\left[V\left(\frac{m+M}{2\pi\hbar^2\beta}\right)^{d/2}\right] - \frac{d}{2\beta}\frac{M}{m+M}\left[\frac{\hbar\beta\Omega}{2}\coth\left[\frac{\hbar\beta\Omega}{2}\right] - 1\right] \\ & - \sum_{\vec{k}}\frac{\left|V_{\vec{k}}\right|^2}{\hbar}\int_0^{\hbar\beta/2} du\mathcal{G}\left(\vec{k},u\right)\mathcal{M}_{M,\Omega}\left(\vec{k},u\right), \end{aligned} \tag{5.1}$$

with V the volume and $\mathcal{G}\left(\vec{k},u\right)$ the Green's function of the Bogoliubov excitations:

$$\mathcal{G}\left(\vec{k},u\right) = \frac{\cosh\left[\omega_{\vec{k}}\left(u-\hbar\beta/2\right)\right]}{\sinh\left[\hbar\beta\omega_{\vec{k}}/2\right]}; \tag{5.2}$$

and $\mathcal{M}_{M,\Omega}\left(\vec{k},u\right)$ the memory function:

$$\begin{aligned}\mathcal{M}_{M,\Omega}\left(\vec{k},u\right) &= \exp\left(-\frac{\hbar k^2}{2\left(m+M\right)}\left\{u-\frac{u^2}{\hbar\beta}\right.\right.\\ &\left.\left.-\frac{M}{m}\frac{\cosh\left[\Omega\hbar\beta/2\right]-\cosh\left[\Omega\left(\hbar\beta/2-u\right)\right]}{\Omega\sinh\left(\hbar\beta\Omega/2\right)}\right\}\right). \qquad (5.3)\end{aligned}$$

We also introduced the eigenfrequency Ω of the model system: $\Omega = W\sqrt{1+M/m_I}$. The parameters Ω and M are then determined variationally by minimizing the right-hand side of the inequality (5.1). This treatment also allows an estimation of the radius of the polaron as the root mean square of the reduced coordinate $\vec{r}$ of the model system [163]:

$$\sqrt{\langle r^2\rangle} = \sqrt{d\frac{\hbar}{2\Omega}\frac{m_I+M}{Mm_I}\coth\left(\frac{\beta\hbar\Omega}{2}\right)}. \qquad (5.4)$$

In [55] Feynman also presented a calculation of the polaronic effective mass m^* at zero temperature:

$$m^* = m_I + \frac{1}{d}\sum_{\vec{k}} k^2\frac{\left|V_{\vec{k}}\right|^2}{\hbar}\int_0^\infty du e^{-\omega_{\vec{k}}u}\mathcal{F}_{M,\Omega}\left(\vec{k},u\right)u^2, \qquad (5.5)$$

with:

$$\begin{aligned}\mathcal{F}_{M,\Omega}\left(\vec{k},u\right) &= \lim_{\beta\to\infty}\mathcal{M}_{M,\Omega}\left(\vec{k},u\right)\\ &= \exp\left\{-\frac{\hbar k^2}{2\left(m+M\right)\Omega}\left[\Omega u+\frac{M}{m}\left(1-e^{-\Omega u}\right)\right]\right\}. \qquad (5.6)\end{aligned}$$

We consider a temperature dependent effective mass by using Eq. (5.5) with temperature dependent variational parameters M and Ω.

5.2.2 Polaron consisting of an impurity in a condensate

We now introduce the Bogoliubov spectrum (1.15) and the interaction amplitude (1.26) for the description of an impurity in a condensate. This allows us to write the Jensen-Feynman inequality (5.1) as (in the polaronic units from table 1.1):

$$\begin{aligned}\mathcal{F} \leq\ & \frac{d}{\beta}\left\{\ln\left[2\sinh\left(\frac{\beta\Omega}{2}\right)\right]-\ln\left[2\sinh\left(\frac{\beta\Omega}{2\sqrt{1+M}}\right)\right]\right\}\\ &-\frac{1}{\beta}\ln\left[V\left(\frac{1+M}{2\pi\beta}\right)^{d/2}\right]-\frac{d}{2\beta}\frac{M}{1+M}\left[\frac{\beta\Omega}{2}\coth\left[\frac{\beta\Omega}{2}\right]-1\right]\\ &-\frac{\alpha^{(d)}}{4\pi}\left(\frac{m_B+1}{m_B}\right)^2\int_0^\infty dk\frac{k^d}{\sqrt{k^2+2}}\int_0^{\beta/2}du\mathcal{G}\left(k,u\right)\mathcal{M}_{M,\Omega}\left(k,u\right), \qquad (5.7)\end{aligned}$$

where we introduced the dimensionless coupling parameter $\alpha^{(d)}$ as follows:

$$\alpha^{(d)} = 4\pi \frac{2\pi^{d/2}}{\Gamma\left(\frac{d}{2}\right)} N_0 g_{IB}^2 \left(\frac{m_I \xi^2}{\hbar^2}\right)^2 \frac{V}{(2\pi\xi)^d} \left(\frac{m_B}{m_B + m_I}\right)^2, \tag{5.8}$$

with $\Gamma(x)$ the gamma function. The prefactor was chosen to be in agreement with expression (1.34) for $\alpha^{(3)}$. Note that the coupling parameter depends on the impurity-boson interaction amplitude g_{IB} and also implicit on the boson-boson interaction amplitude g_{BB} through the dependency on the healing length ξ. As discussed before the interatomic interaction amplitudes, and thus also the coupling parameter, can be externally tuned through a Feshbach resonance or in reduced dimensions also with a confinement induced resonance.

Renormalization of the impurity-boson contact interaction in 2 dimensions

For $d = 2$ the k-integral in (5.7) contains an ultraviolet divergence. This is also the case in 3 dimensions [89] and can be resolved by renormalizing the impurity-boson contact interaction. Since the term containing this divergence in (5.7) is proportional to g_{IB}^2 it is sufficient to consider the Lippmann-Schwinger equation up to second order for the impurity-boson scattering matrix $T_{IB}(E)$ (1.2):

$$T_{IB}(E) = g_{IB} - g_{IB}^2 \sum_{\vec{k}} \frac{1}{\frac{\hbar^2 k^2}{2m_r} - E}, \tag{5.9}$$

with E the kinetic scattering energy and m_r the reduced mass ($m_r^{-1} = m_I^{-1} + m_B^{-1}$). Note that, opposed to the three dimensional case, we can not take the low energy limit $E \to 0$ in 2 dimensions since this results in an infrared divergence. We now consider the second term of the total Hamiltonian (1.27) and use the Lippmann-Schwinger equation up to second order (5.9) for the impurity-boson interaction strength g_{IB}:

$$N_0 g_{IB} = N_0 T_{IB}^{2D}(E) + N_0 g_{IB}^2 \sum_{\vec{k}} \frac{1}{\frac{\hbar^2 k^2}{2m_r} - E}. \tag{5.10}$$

Adding the second term of (5.10) to the upper bound for the free energy (5.7) lifts the ultraviolet divergence. For $d = 2$ this term can be written as:

$$N_0 g_{IB}^2 \sum_{\vec{k}} \frac{1}{\frac{\hbar^2 k^2}{2m_r} - E} = \frac{\alpha^{(2)}}{2\pi} \frac{\hbar^2}{m_I \xi^2} \frac{m_B + m_I}{m_B} \int_0^\infty \frac{k}{k^2 - 2m_r E/\hbar^2} dk, \tag{5.11}$$

which clearly shows the infrared divergence in the low energy limit $E \to 0$. For numerical considerations we introduce a cutoff K_c for the k-integral. This enables us to calculate the integral in (5.11) as

$$\begin{aligned} \frac{\alpha^{(2)}}{2\pi} \frac{\hbar^2}{m_I \xi^2} \frac{m_B + m_I}{m_B} \int_0^{K_c} \frac{k}{k^2 - 2m_r \xi^2 E/\hbar^2} dk &= \frac{\alpha^{(2)}}{4\pi} \frac{\hbar^2}{m_I \xi^2} \frac{m_B + m_I}{m_B} \ln\left(\frac{\frac{\hbar^2 K_c^2}{2m_r} - E}{E}\right) \\ &\approx \frac{\alpha^{(2)}}{4\pi} \frac{\hbar^2}{m_I \xi^2} \frac{m_B + m_I}{m_B} \ln\left(\frac{\hbar^2 K_c^2}{2m_r E}\right), \end{aligned} \tag{5.12}$$

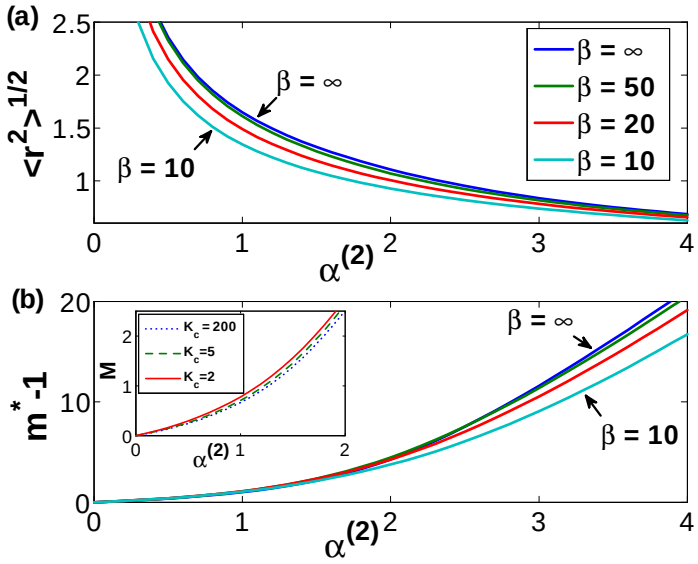

Figure 5.1: The groundstate properties of the polaron consisting of a Li-6 impurity in a Na condensate in 2 dimensions. In (a) the radius of the polaron (5.4) is presented and in (b) the effective mass (5.5) as a function of the polaronic coupling parameter $\alpha^{(2)}$ at different temperatures ($\beta = (k_B T)^{-1}$) and with a cutoff $K_c = 200$. The inset shows the variational parameter M for different values of the cutoff K_c at $\beta = 50$.

where in the second step we used that the kinetic scattering energy E is much smaller than the cutoff energy $\hbar^2 K_c^2/(2m_r)$. Equation (5.12) shows that the value of E is not important since it only results in an energy shift and therefore has no influence on the physical properties of the system.

5.2.3 Results

The presented treatment is now applied to the system of a Li-6 impurity in a Na condensate ($m_B/m_I = 3.82207$) in low dimensions. All results are presented in the polaronic units of table 1.1.

In Fig. 5.1 the polaronic ground state properties in 2 dimensions are presented as a function of the coupling parameter $\alpha^{(2)}$. In (a) the polaron radius is shown and in (b) the effective mass of the polaron at different temperatures. The observed behavior is analogous to the three-dimensional case in Fig. 1.10 and suggests that for growing $\alpha^{(2)}$ the self-induced potential becomes stronger, leading to a bound state at high enough $\alpha^{(2)}$. However, as compared to the three-dimensional case, the transition is much smoother with a transition region between $\alpha^{(2)} \approx 1$ and $\alpha^{(2)} \approx 3$. This behavior is in agreement with the mean-field results of Refs. [82, 147], where also a smooth transition to the strong coupling regime was found for $d = 2$. For the cutoff K_c the inverse of the Van der Waals radius for sodium is used which results in $K_c = 200$. To check whether this cutoff is large enough we have plotted the variational mass parameter M in the inset of Fig. 5.1(b) at different values of K_c which reveals already a reasonable convergence at $K_c \approx 5$.

In Fig. 5.2 the results for the 1-dimensional case are presented. In (a) the

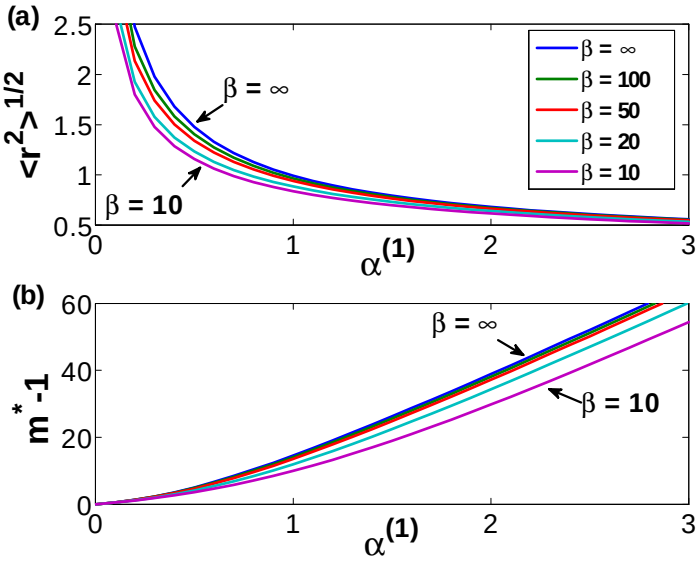

Figure 5.2: The polaronic ground state properties of a Li-6 impurity in a Na condensate in 1 dimension. The radius (a) and the effective mass (b) are presented as a function of the polaronic coupling parameter $\alpha^{(1)}$ at different temperatures ($\beta = (k_B T)^{-1}$).

polaron radius is plotted and (b) shows the effective mass of the polaron at different temperatures. For growing $\alpha^{(1)}$ the characteristics of the appearance of a bound state in the self-induced potential are again observed. The characteristics of the weak coupling regime are however not present and the transition region is between $\alpha^{(1)} = 0$ and $\alpha^{(1)} \approx 1$. This is again in agreement with the mean-field results of Refs. [82, 147] for $d = 1$.

A comparison of Figs. 5.2 and 5.1 shows that the polaronic effective mass increases as the dimension is reduced, suggesting a more pronounced polaronic effect as the dimension is lowered.

5.3 Response to Bragg scattering in d dimensions

As discussed in chapter 2 the response of a system to Bragg spectroscopy is proportional to the imaginary part of the density response function $\chi\left(\omega, \vec{k}\right)$ (2.3). Note that the derivation in chapter 2 does not depend on the dimension of the system and we can use expression (2.62) also for reduced dimensions (where the polaronic units of table 1.1 are used):

$$\mathrm{Im}\left[\chi\left(\vec{k},\omega\right)\right] = -k^2 \frac{\mathrm{Im}\left[\Sigma\left(\omega,\vec{k}\right)\right]}{\left(\omega^2 - \mathrm{Re}\left[\Sigma\left(\omega,\vec{k}\right)\right]\right)^2 + \left(\mathrm{Im}\left[\Sigma\left(\omega,\vec{k}\right)\right]\right)^2}, \tag{5.13}$$

with $\Sigma\left(\omega,\vec{k}\right)$ the memory function (2.43). For the numerical calculations the representation for the self energy as derived in section 2.3.4 is used. We also use the

mass rule from from Ref. [128] and discussed in section 2.6 as a consistency check.

5.3.1 Results

Here, we present the Bragg response for a Li-6 impurity in a Na condensate ($m_B/m_I = 3.82207$) in reduced dimensions. All results are presented in the polaronic units of table 1.1.

In Fig. 5.3 the Bragg response (5.13) is presented at different temperatures and for a momentum exchange $k = 1$ in 1 and 2 dimensions at weak polaronic coupling ($\alpha^{(1)} = 0.01$ and $\alpha^{(2)} = 0.1$). In both cases the Drude-like background at small ω and the Bogoliubov peak are observed. Qualitatively this is the same behavior as we found for the three-dimensional case in Fig. 2.2. Quantitatively we observe that the amplitude of the Bogoliubov emission peak increases as the dimension is reduced.

In 1D another sharp peak is observed, as can be seen in Fig. 5.3, at $\omega = \omega_k$ (with ω_k the Bogoliubov dispersion (1.15) and k the exchanged momentum) which broadens as the temperature is increased and dominates the Bogoliubov emission peak at relatively high temperatures. This extra peak in 1D is associated with the weak coupling regime since at intermediate coupling the sharp structure disappears and the peak merges with the Bogoliubov emission peak. As shown in section 2.5.1 our response treatment reduces to the Gurevich-Lang-Firsov results at weak coupling and the sharp peak is also present in this formalism in 1D. The location indicates that it corresponds to the process where both the exchanged energy $\hbar\omega$ and momentum $\hbar\vec{k}$ are transferred to a Bogoliubov excitation, as schematically presented in Fig. 5.4. The width of the peak is inversely proportional to the lifetime of the formed Bogoliubov excitation, showing that this lifetime is infinite at temperature zero and decreases if the temperature is increased due to incoherent scattering with thermal excitations. Whether this extra peak is experimentally observable is questionable since it is only visible at relatively high temperatures where in reduced dimensions thermal phase fluctuations can become important and destroy the polaronic features.

Fig. 5.5 presents the Bragg response for different momentum exchange k at a temperature $\beta = 100$ (where the sharp peak at the Bogoliubov dispersion in 1D is too narrow to perceive). The insets show the location of the maximum of the Bogoliubov emission peak as a function of the exchanged momentum together with a least square fit to the Bogoliubov spectrum (1.15) which results in a good agreement. The optimal fitting parameter is determined as $m_B = 4.3159$ (4.2216) in 1D (2D). This is analogous to the behavior in 3D in Fig. 2.3.

In Figs. 5.6 and 5.7 we have zoomed in on the tail of the Bogoliubov emission peak for different values of the coupling parameter in 1 and 2 dimensions, respectively. At larger values for the polaronic coupling parameter $\alpha^{(d)}$ a secondary peak emerges which corresponds to a transition to the relaxed excited state (RES), similar to the three dimensional case as discussed in section 2.7. In the inset the location of this secondary peak is plotted as a function of the exchanged momentum together with a least square fit to the following quadratically spectrum:

$$\omega(k) = \omega + \frac{\hbar^2 k^2}{2m}, \tag{5.14}$$

which shows a good agreement at small k. This suggests that, as for the three

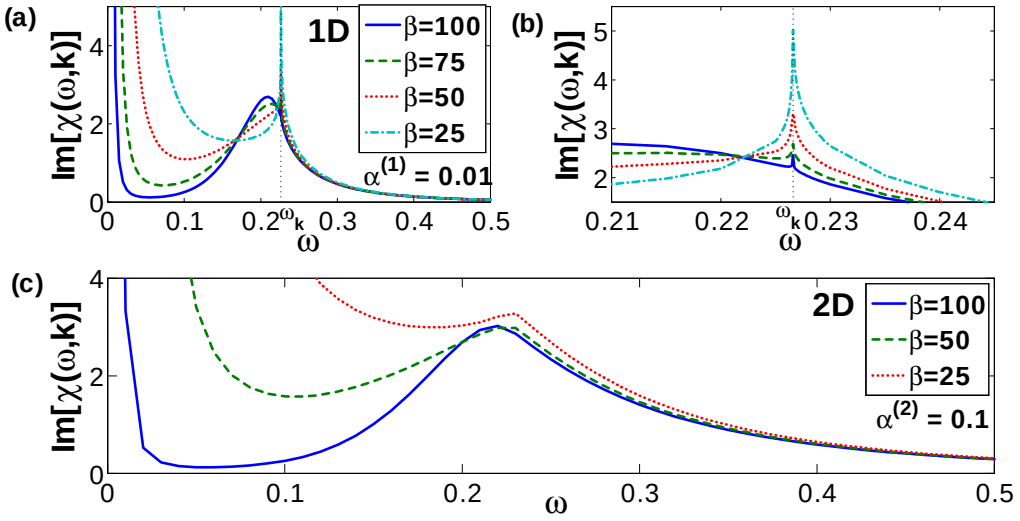

Figure 5.3: The Bragg response (5.13) is presented as a function of ω at weak polaronic coupling, momentum exchange $k = 1$ and at different temperatures ($\beta = (k_B T)^{-1}$) in 1D (a) and 2D (c). In both cases the Drude-like background and the Bogoliubov peak are observed. In 1D another sharp peak is present at $\omega = \omega_k$, with ω_k the Bogoliubov dispersion (1.15). In (b) we have zoomed in on this sharp peak in 1D.

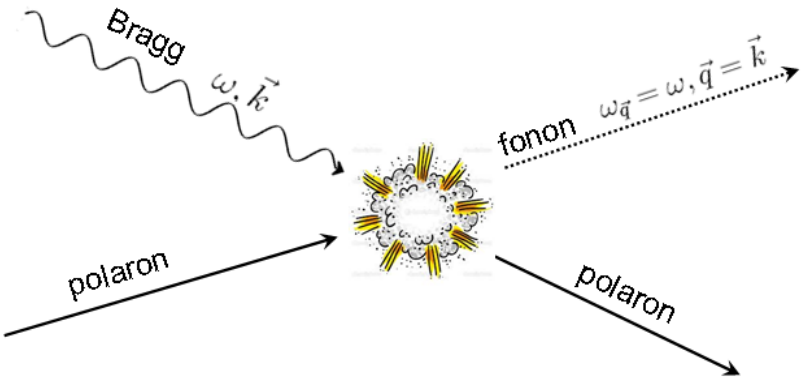

Figure 5.4: Schematical presentation of the event that corresponds to the narrow peak in the Bragg response at $\omega = \omega_{\vec{k}}$ in 1D in Fig. 5.3. Both the momentum $\hbar\vec{k}$ and the energy $\hbar\omega$ that are introduced by the Bragg pulse are transferred to a Bogoliubov excitation with momentum $\hbar\vec{q} = \hbar\vec{k}$ and energy $\hbar\omega_{\vec{q}} = \hbar\omega$. The final state of the polaron is the same as the initial state.

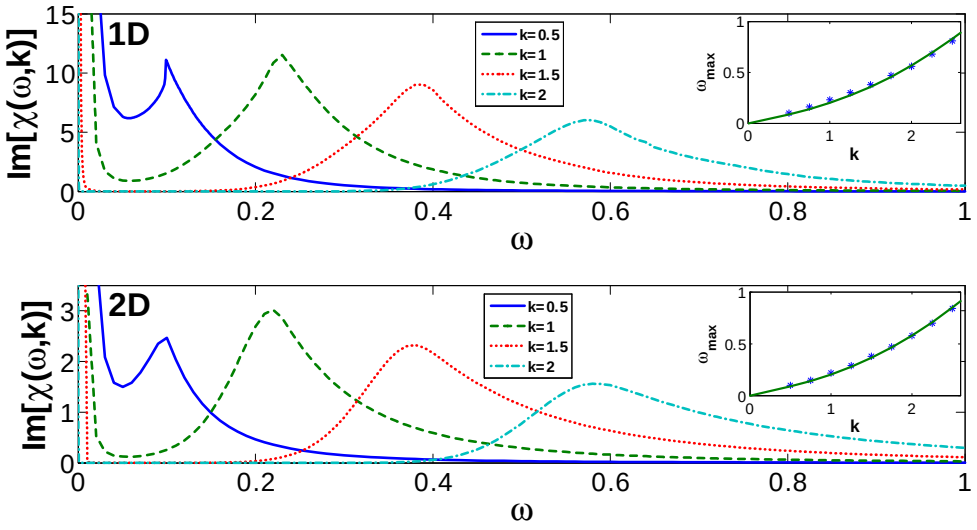

Figure 5.5: The Bragg response at weak polaronic coupling ($\alpha^{(d)} = 0.1$) for different exchanged momenta k in 1 and 2 dimensions and at a temperature $\beta = 100$. The inset shows the location of the maximum of the peak as a function of the exchanged momentum (markers) together with a least square fit to the Bogoliubov spectrum (1.15) (full line), this results in $m_B = 4.3159$ (4.2216) for the fitting parameter in 1D (2D).

	$\alpha^{(1)} = 0.1$	$\alpha^{(1)} = 3$
$k = 1$	1.5440	1.5547
$k = 3$	1.5544	1.5743

Table 5.1: Here we show the sum of the two terms at the left hand side of the mass sum rule (2.84) in 1 dimension at $\beta = 100$ and at different values for $\alpha^{(1)}$ and k.

dimensional case, the state corresponding to the secondary peak can be characterized by a transition frequency ω and an effective mass m.

Finally, we have checked whether the spectra satisfy the mass sum rule (2.81) from Ref. [128]. We calculated the sum of the two terms on the left hand side of expression (2.84) which is presented in table 5.1 for $d = 1$ and in table 5.2 for $d = 2$ at $\beta = 100$ and at different values for α and k. These values should be compared to $\pi/2 = 1.5708$ which results in a fair agreement with small deviations which are to be expected since numerically we had to introduce a cutoff for the ω-integral in (2.81) and the choice of the parameter ε in (2.81) is somewhat arbitrary resulting in a double counting of part of the weight of the Drude peak.

5.4 Conclusions

We calculated the polaronic ground state properties of an impurity in a Bose-Einstein condensate and the response of this system to Bragg spectroscopy in reduced dimensions. For this purpose we introduced a polaronic coupling parameter $\alpha^{(d)}$ (5.8)

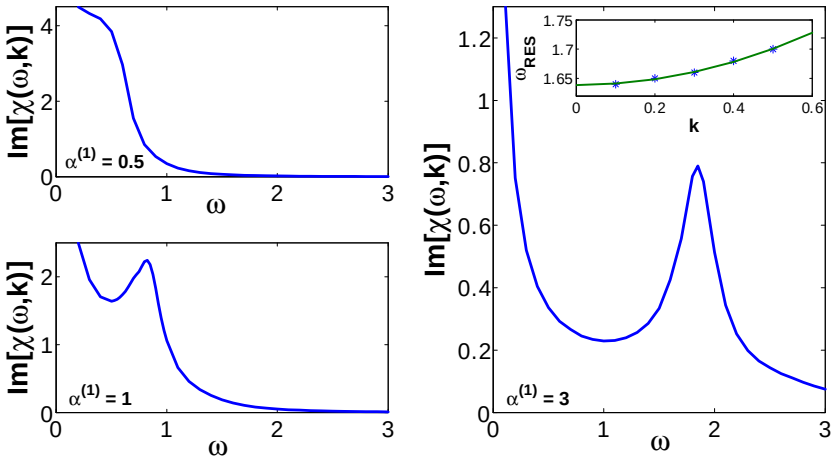

Figure 5.6: Here we zoomed in on the tail of the Bogoliubov peak for momentum exchange $k = 1$ and temperature $\beta = 100$ in 1 dimension. This shows that at larger values for $\alpha^{(1)}$ a secondary peak emerges. The inset shows the location of the maximum of this secondary peak at $\alpha^{(1)} = 3$ as a function of the exchanged momentum (markers) together with a least square fit to a quadratic spectrum (5.14) (solid line), this results in $\omega = 1.6386$ and $m = 2.0107$ for the fitting parameters.

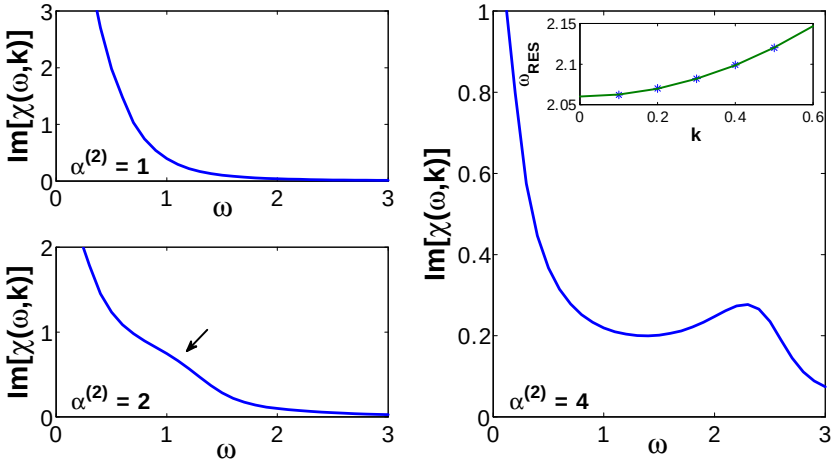

Figure 5.7: Here we zoomed in on the tail of the Bogoliubov peak for momentum exchange $k = 1$ and temperature $\beta = 100$ in 2 dimensions. Also here a secondary peak emerges at larger values for $\alpha^{(2)}$. The inset shows the location of the maximum of this secondary peak at $\alpha^{(2)} = 4$ as a function of the exchanged momentum (markers) together with a least square fit to a quadratic spectrum (5.14) (solid line), this results in $\omega = 2.0601$ and $m = 2.0755$ for the fitting parameters.

	$\alpha^{(2)} = 1$	$\alpha^{(2)} = 4$
$k = 1$	1.5678	1.5734
$k = 3$	1.5669	1.5800

Table 5.2: Here we show the sum of the two terms at the left hand side of the mass sum rule (2.84) in 2 dimensions at $\beta = 100$ and at different values for $\alpha^{(2)}$ and k.

which depends on the dimension. For increasing $\alpha^{(d)}$ the ground state properties suggest that the self-induced potential accommodates a bound state, resulting in a large effective mass and a small polaron radius. As compared to the three-dimensional case the transition to the strong coupling regime is smoother in reduced dimension and for $d = 1$ the characteristics of the weak coupling regime are absent. As the dimension is reduced the characteristics of the polaronic strong coupling regime are already observed at lower polaronic coupling. Furthermore, lowering the dimension is accompanied with a larger effective mass which suggests a more pronounced polaronic effect for low-dimensions.

The Bragg response of the system revealed a peak corresponding to the emission of Bogoliubov excitations, the Drude-like background and the emergence of a secondary peak in the strong coupling regime, analogous to the three dimensional case of chapter 2. The amplitude of these polaronic features grows as the dimensionality is reduced. This is good news since it indicates that lowering the dimension can facilitate an experimental detection of strong-coupling polaronic features. In 1D another sharp peak is observed at weak polaronic coupling that corresponds to the full transition of the exchanged energy and momentum to a Bogoliubov excitation.

Another advantage of considering reduced dimensions is the possibility of using confinement-induced resonances which permits a tuning of the polaronic coupling parameter independent from the magnetic-field induced Feshbach resonance.

Chapter 6

Many-polaron description in the polaronic weak coupling regime *

In this chapter we apply the weak coupling many-polaron formalism to the case of many impurities in a condensate. The main motivation is that there are presently many experiments with ultracold binary mixtures, of which the two species can either be different hyperfine states of the same atom [164, 165] or different atoms [166]. Without the use of a Feshbach resonance these systems are typically in the polaronic weak-coupling regime. Nowadays Feshbach resonances in these mixtures have become a well established experimental tool [95, 99, 104].

In section 1.3 it was shown that if the Bogoliubov approximation is valid the Hamiltonian of N_I impurities in a Bose-Einstein condensate can be mapped onto the Fröhlich N_I-polaron Hamiltonian $\widehat{H}_{pol}^{(N_I)}$, given by:

$$\begin{aligned}\widehat{H}_{pol}^{(N_I)} &= \sum_{i}^{N_I} \frac{\widehat{\vec{p}}_i^{\,2}}{2m_I} + \sum_{\vec{k}} \hbar\omega_{\vec{k}} \widehat{\alpha}_{\vec{k}}^{\dagger} \widehat{\alpha}_{\vec{k}} + \sum_{\vec{k}} \sum_{i}^{N_I} \left(V_{\vec{k}} \widehat{\alpha}_{\vec{k}} e^{i\vec{k}.\widehat{\vec{r}}_i} + V_{\vec{k}}^{\dagger} \widehat{\alpha}_{\vec{k}}^{\dagger} e^{-i\vec{k}.\widehat{\vec{r}}_i} \right) \\ &\quad + \frac{1}{2} \sum_{i \neq j}^{N_I} U\left(\widehat{\vec{r}}_i - \widehat{\vec{r}}_j\right). \end{aligned} \tag{6.1}$$

The first term represents the kinetic energy of the impurities with mass m_I and position (momentum) operators $\widehat{\vec{r}}_i$ ($\widehat{\vec{p}}_i$), the second term gives the energy of the Bogoliubov excitations with dispersion $\omega_{\vec{k}}$ (1.15) and creation (annihilation) operator $\widehat{a}_{\vec{k}}^{\dagger}$ ($\widehat{a}_{\vec{k}}$), the third term is the interaction between the impurities and the Bogoliubov excitations with interaction amplitude $V_{\vec{k}}$ (1.26) and the fourth term represents the mutual interaction between the impurities, with $U(\vec{r})$ the interaction potential.

The weak and intermediate coupling theory for the Fröhlich polaron of Lee, Low and Pines [52] was extended by Lemmens, Brosens and Devreese [75] to the case of an interacting polaron gas. Similarly, the optical absorption theory of Devreese,

*The theoretical derivation presented in this chapter and the application to fermionic impurities is published in W. Casteels, J. Tempere and J. T. Devreese - *Many-polaron description of impurities in a Bose-Einstein condensate in the weak-coupling regime* - Phys. Rev. A **84**, 063612 (2011). The application to bosonic impurities in a condensate is published in W. Casteels, J. Tempere and J. T. Devreese - *Weak coupling many-polaron description of ultracold bosonic impurities in a condensate* - The European physical journal Special topics **217**, 163 (2013).

Goovaerts and De Sitter [61] was extended to the case of interacting polarons in Ref. [76]. In these extensions, the effect of the interactions between the polarons is taken into account through the structure factor of the electron gas. The goal of this chapter is to apply a similar generalization to extend the polaronic theory of a single impurity in a condensate to the case of a dilute gas of interacting impurities.

We start by summarizing the main results of Refs. [75, 76] on the weak coupling treatment of the Fröhlich solid state N-polaron system together with an indication of what changes if one considers impurities in a BEC. It turns out that also in this case the interaction between the impurities is incorporated in the formalism through the structure factor of the impurities. Furthermore both the inertial and spectral effective masses are considered. This allows for an investigation of the ground state properties and of the response of the system to Bragg spectroscopy.

We then examine different possibilities for the impurities by considering different structure factors. We start with the structure factor of an ideal fermionic gas. This corresponds to the experimental system of spin-polarized fermionic impurities. Then the structure factor of an ultracold dilute gas of bosons is introduced which corresponds to weakly interacting bosonic impurities.

6.1 Weak coupling treatment of the many-polaron gas

6.1.1 Ground state properties of the many-polaron gas

The weak coupling variational method, as introduced in Ref. [52] by Lee, Low and Pines for the description of a single polaron, was generalized in Ref. [75] to the case of a many-polaron system. With this purpose the following variational wave function was introduced:

$$|\Psi_{LDB}>=\widehat{U}\,|0\rangle\,|\psi\rangle\,, \tag{6.2}$$

with $|0\rangle$ the vacuum wave function for the bosonic excitations, $|\psi\rangle$ the wave function of the impurities and $\widehat{U}$ a canonical transformation of the form:

$$\widehat{U}=\exp\left\{\sum_{i}^{N}\sum_{\vec{k}}\left[f_{\vec{k}}\widehat{\alpha}_{\vec{k}}e^{i\vec{k}.\widehat{\vec{r}}_i}-f_{\vec{k}}^{*}\widehat{\alpha}_{\vec{k}}^{\dagger}e^{-i\vec{k}.\widehat{\vec{r}}_i}\right]\right\}, \tag{6.3}$$

where $f_{\vec{k}}$ are variational functions. This gives for the reduced Hamiltonian:

$$\begin{aligned}\widehat{H}_{red}&=\left\langle 0\left|U^{-1}\widehat{H}_{pol}^{(N)}U\right|0\right\rangle\\&=\sum_{i}^{N}\frac{\vec{p}_i^{\,2}}{2m_I}+\frac{1}{2}\sum_{i\neq j}V\left(\widehat{\vec{r}}_i-\widehat{\vec{r}}_j\right)-N\sum_{\vec{k}}\left[V_{\vec{k}}f_{\vec{k}}^{*}+V_{\vec{k}}^{\dagger}f_{\vec{k}}\right]\\&+N\sum_{\vec{k}}\left(\hbar\omega_{\vec{k}}+\frac{\hbar^2k^2}{2m_I}\right)\left|f_{\vec{k}}\right|^2,\end{aligned} \tag{6.4}$$

with $V(\vec{r})$ the total interaction between two impurities separated by $\vec{r}$:

$$V(\vec{r}) = U(\vec{r}) - 2\sum_{\vec{k}} \left[V_{\vec{k}} f_{\vec{k}}^{*} + V_{\vec{k}}^{\dagger} f_{\vec{k}} - \hbar\omega_{\vec{k}} \left| f_{\vec{k}} \right|^2 \right] e^{i\vec{k}.\vec{r}}, \tag{6.5}$$

where the first term is the direct interaction and the second gives the induced interaction. Taking the expectation value with respect to the impurity wave function $|\psi\rangle$ gives

$$\begin{aligned} E &= \left\langle \psi \left| \widehat{H}_{red} \right| \psi \right\rangle \\ &= N\varepsilon_{kin} + \frac{1}{2} N \sum_{\vec{k}} v\left(\vec{k}\right) \left(S\left(\vec{k}\right) - 1 \right) + N \sum_{\vec{k}} \left(\hbar\omega_{\vec{k}} S\left(\vec{k}\right) + \frac{\hbar^2 k^2}{2m_I} \right) \left| f_{\vec{k}} \right|^2 \\ &- N \sum_{\vec{k}} \left[V_{\vec{k}} f_{\vec{k}}^{*} + V_{\vec{k}}^{\dagger} f_{\vec{k}} \right] S\left(\vec{k}\right), \end{aligned} \tag{6.6}$$

where $N\varepsilon_{kin}$ is the kinetic energy:

$$N\varepsilon_{kin} = \left\langle \psi \left| \sum_{i}^{N} \frac{\widehat{p}_i^2}{2m_I} \right| \psi \right\rangle; \tag{6.7}$$

and $S\left(\vec{k}\right)$ the static structure factor of the impurities:

$$S\left(\vec{k}\right) = 1 + \frac{1}{N} \left\langle \psi \left| \sum_{i \neq j}^{N} e^{i\vec{k}.(\vec{r}_i - \vec{r}_j)} \right| \psi \right\rangle. \tag{6.8}$$

Minimizing the energy (6.6) with respect to the variational parameters $f_{\vec{k}}$ gives:

$$f_{\vec{k}} = \frac{V_{\vec{k}}}{\hbar\omega_{\vec{k}} + \frac{\hbar^2 k^2}{2m_I S\left(\vec{k}\right)}}. \tag{6.9}$$

Introducing this in the energy (6.6) gives the following upper bound for the energy:

$$\frac{E}{N} \leq \varepsilon_{kin} + \frac{1}{2} \sum_{\vec{k}} v\left(\vec{k}\right) \left[S\left(\vec{k}\right) - 1 \right] - \sum_{\vec{k}} \frac{S^2\left(\vec{k}\right) \left| V_{\vec{k}} \right|^2}{\hbar\omega_{\vec{k}} S\left(\vec{k}\right) + \frac{\hbar^2 k^2}{2m_I}}. \tag{6.10}$$

Inertial effective mass

Another important property of the polaronic system is the effective mass of the polarons which was calculated within the one-polaron weak coupling formalism in Ref. [52]. The generalization of this derivation to many polarons allows a determination of this effective mass which is related to the many-polaron system as a whole and shall be called the inertial effective mass $m^{(in)}$ in the following. The total momentum of the system is:

$$\widehat{\vec{\mathcal{P}}} = \sum_{i} \widehat{\vec{p}}_i + \sum_{\vec{k}} \hbar\vec{k} \widehat{\alpha}_{\vec{k}}^{\dagger} \widehat{\alpha}_{\vec{k}}. \tag{6.11}$$

Note that $\widehat{\vec{\mathcal{P}}}$ commutes with the Hamiltonian (6.1) and thus is a conserved quantity. This conserved quantity can be explicitly introduced in the minimization process by means of a Lagrange multiplier $\vec{v}$, which corresponds to the velocity of the polaron (analogous as in section 3.1.1):

$$\widehat{H}_{pol}^{N}\left(\vec{v}\right)=\widehat{H}_{pol}^{N}-\vec{v}.\left(\sum_{i}\widehat{\vec{p}}_{i}+\sum_{\vec{k}}\hbar\vec{k}\widehat{\alpha}_{\vec{k}}^{\dagger}\widehat{\alpha}_{\vec{k}}-\vec{\mathcal{P}}\right). \tag{6.12}$$

We will consider the expectation value of (6.12) with respect to the adapted LDB wave function $\left|\Psi_{LDB}^{(\vec{v})}\right\rangle$ which corresponds to (6.2) but now the impurities have a velocity $\vec{v}$:

$$\left|\Psi_{LDB}^{(\vec{v})}\right\rangle=\exp\left[-im_{I}\sum_{i}\frac{\vec{v}.\vec{r}_{i}}{\hbar}\right]\left|\Psi_{LDB}\right\rangle. \tag{6.13}$$

Taking the expectation value of (6.12) with respect to $\left|\Psi_{LDB}^{(\vec{v})}\right\rangle$ gives:

$$\begin{aligned}\left\langle\Psi_{LDB}^{(\vec{v})}\left|\widehat{H}\left(\vec{v}\right)\right|\Psi_{LDB}^{(\vec{v})}\right\rangle=&N\varepsilon_{kin}-N\frac{m_{I}v^{2}}{2}+\vec{v}.\vec{\mathcal{P}}+\frac{1}{2}N\sum_{i\neq j}v\left(\vec{k}\right)\left[S\left(\vec{k}\right)-1\right]\\&-N\sum_{\vec{k}}\left[V_{\vec{k}}f_{\vec{k}}^{*}+V_{\vec{k}}^{\dagger}f_{\vec{k}}\right]S\left(\vec{k}\right)\\&+N\sum_{\vec{k}}\left[\left|f_{\vec{k}}\right|^{2}\left(\hbar\omega_{\vec{k}}S\left(\vec{k}\right)+\frac{\hbar^{2}k^{2}}{2m_{I}}-\hbar\vec{v}.\vec{k}\right)\left|f_{\vec{k}}\right|^{2}\right].\end{aligned} \tag{6.14}$$

Minimization of (6.14) with respect to $\left\{f_{\vec{k}}\right\}$ gives:

$$f_{\vec{k}}=\frac{V_{\vec{k}}S\left(\vec{k}\right)}{\hbar\omega_{\vec{k}}S\left(\vec{k}\right)+\frac{\hbar^{2}k^{2}}{2m_{I}}-\hbar\vec{v}.\vec{k}}. \tag{6.15}$$

Minimization with respect to $\vec{v}$ gives:

$$\vec{\mathcal{P}}=Nm_{I}\vec{v}+N\sum_{\vec{k}}\hbar\vec{k}\frac{\left|V_{\vec{k}}S\left(\vec{k}\right)\right|^{2}}{\left(\hbar\omega_{\vec{k}}S\left(\vec{k}\right)+\frac{\hbar^{2}k^{2}}{2m_{I}}-\hbar\vec{v}.\vec{k}\right)^{2}}, \tag{6.16}$$

if we consider the velocity $\vec{v}$ to be small we can write:

$$\vec{\mathcal{P}}=Nm_{I}\vec{v}+\frac{2}{3}\hbar^{2}N\sum_{\vec{k}}\frac{\left|V_{\vec{k}}\right|^{2}S^{2}\left(k\right)}{\left(\hbar\omega_{\vec{k}}S\left(k\right)+\frac{\hbar^{2}k^{2}}{2m_{I}}\right)^{3}}k^{2}\vec{v}, \tag{6.17}$$

where isotropy of the system was assumed. We can now identify the inertial effective mass $m^{(in)}$ through the expression $\vec{\mathcal{P}}=Nm^{(in)}\vec{v}$, this results in:

$$m^{(in)}=m_{I}+\frac{2}{3}\hbar^{2}\sum_{\vec{k}}\frac{\left|V_{\vec{k}}\right|^{2}S^{2}\left(k\right)}{\left(\hbar\omega_{\vec{k}}S\left(k\right)+\frac{\hbar^{2}k^{2}}{2m_{I}}\right)^{3}}k^{2}. \tag{6.18}$$

Note that the inertial effective mass (6.18) is a property of the polaron system as a whole. This is important for an experiment where the behavior of all the impurities together is studied. For example when one studies the collective oscillation of the impurities in a harmonic trap the resulting effective oscillation frequency and amplitude depends on this inertial effective mass. This dependence has been exploited to determine the effective mass of a single impurity in a BEC in a one dimensional setup from a measurement of the oscillation amplitude [103]. A similar technique was also used to experimentally determine the effective mass of Fermi polarons in Ref. [117].

Note that for the ground state properties the presence of multiple impurities is completely described through the static structure factor $S\left(\vec{k}\right)$ of the impurities. In the limit of vanishing density the static structure factor becomes 1 and the expressions for the energy and the effective mass of a single polaron from Ref. [52] are retrieved.

6.1.2 Bragg response of the many-polaron gas

In Ref. [76] the optical absorption of the N-polaron gas consisting of electrons interacting with phonons was calculated within the weak coupling formalism. The polaronic system consisting of impurities in a BEC can not be probed with optical absorption but instead an appropriate experimental technique is Bragg spectroscopy as shown in chapter 2. This means that a finite momentum exchange has to be taken into account which is negligible in the case of the optical absorption calculation. Furthermore it is the density-density correlation function (2.3) that determines the response instead of the current-current correlation which is needed for the optical absorption. These two are however closely related since the application of two partial integrations transforms equation (2.3) into a correlation function of the time derivative of the density $\dot{\rho}_{\vec{k}}$ after which one can use the Fourier transform of the continuity equation ($\dot{\rho}_{\vec{k}} = i\vec{k}.\vec{j}_{\vec{k}}$) to obtain a current-current correlation function:

$$\chi\left(\omega, \vec{k}\right) = -\frac{i}{\hbar\omega^2}\int_0^\infty dt e^{i\omega t}\left\langle\left[\vec{k}.\widehat{j}_{\vec{k}}\left(t\right), \vec{k}.\widehat{j}_{\vec{k}}^{\dagger}\right]\right\rangle. \tag{6.19}$$

Two more partial integrations give:

$$\chi\left(\omega, \vec{k}\right) = \frac{i}{\hbar\omega^4}\int_0^\infty de^{i\omega t}\left\langle\left[\vec{k}.\widehat{\dot{j}}_{\vec{k}}\left(t\right), \vec{k}.\widehat{\dot{j}}_{\vec{k}}^{\dagger}\right]\right\rangle. \tag{6.20}$$

The time derivative of the current can be calculated through the Heisenberg equation of motion:

$$\begin{aligned}\widehat{\dot{j}}_{\vec{k}} &= \frac{i}{\hbar}\left[\widehat{H}, \widehat{j}_{\vec{k}}\right] \\ &= -\frac{i}{m}\sum_{\vec{q}} V_{\vec{q}}\left(\widehat{\alpha}_{\vec{q}} + \widehat{\alpha}_{-\vec{q}}^{\dagger}\right)\vec{q}\widehat{\rho}_{\vec{k}+\vec{q}}.\end{aligned} \tag{6.21}$$

This allows us to write the density-density correlation (6.20) as:

$$\chi\left(\omega,\vec{k}\right) = \frac{i}{\hbar\omega^4}\frac{1}{m^2}\sum_{\vec{q},\vec{q}'}\left(\vec{k}.\vec{q}\right)\left(\vec{k}.\vec{q}'\right)\int_0^\infty dt e^{i\omega t} \times\left\langle\left[e^{i\widehat{H}t/\hbar}V_{\vec{q}}\left(\widehat{\alpha}_{\vec{q}}+\widehat{\alpha}^\dagger_{-\vec{q}}\right)\widehat{\rho}_{\vec{k}+\vec{q}}e^{-i\widehat{H}t/\hbar},V^\dagger_{\vec{q}'}\left(\widehat{\alpha}^\dagger_{\vec{q}'}+\widehat{\alpha}_{-\vec{q}'}\right)\widehat{\rho}^\dagger_{\vec{k}+\vec{q}'}\right]\right\rangle. \tag{6.22}$$

We now calculate the expectation value with respect to the LDB wave function (6.2), for this we need the following expectation value:

$$\begin{aligned}\mathcal{J}\left(\vec{q},\vec{q}'\right) &= \left\langle\Psi_{LDB}\left|\left[e^{i\widehat{H}t/\hbar}V_{\vec{q}}\left(\widehat{\alpha}_{\vec{q}}+\widehat{\alpha}^\dagger_{-\vec{q}}\right)\widehat{\rho}_{\vec{k}+\vec{q}}e^{-i\widehat{H}t/\hbar},V^\dagger_{\vec{q}'}\left(\widehat{\alpha}^\dagger_{\vec{q}'}+\widehat{\alpha}_{-\vec{q}'}\right)\widehat{\rho}^\dagger_{\vec{k}+\vec{q}'}\right]\right|\Psi_{LDB}\right\rangle \\ &= \left\langle\psi\left|\left\langle 0\left|\left[e^{i\widehat{H'}t/\hbar}\widehat{U}^{-1}V_{\vec{q}}\left(\widehat{\alpha}_{\vec{q}}+\widehat{\alpha}^\dagger_{-\vec{q}}\right)\widehat{\rho}_{\vec{k}+\vec{q}}\widehat{U}e^{-i\widehat{H'}t/\hbar},\right.\right.\right.\right. \\ &\left.\left.\left.\left.\widehat{U}^{-1}V^\dagger_{\vec{q}'}\left(\widehat{\alpha}^\dagger_{\vec{q}'}+\widehat{\alpha}_{-\vec{q}'}\right)\widehat{\rho}^\dagger_{\vec{k}+\vec{q}'}\widehat{U}\right]\right|0\right\rangle\right|\psi\right\rangle. \end{aligned} \tag{6.23}$$

With $\widehat{H'}=U^{-1}HU$ the transformed Hamiltonian. Transforming the creation and annihilation operators gives:

$$\widehat{U}^{-1}V_{\vec{q}}\left(\widehat{\alpha}_{\vec{q}}+\widehat{\alpha}^\dagger_{-\vec{q}}\right)\widehat{\rho}_{\vec{k}+\vec{q}}\widehat{U} = V_{\vec{q}}\left(\widehat{\alpha}_{\vec{q}}-f^*_{\vec{k}}\widehat{\rho}_{\vec{k}}+\widehat{\alpha}^\dagger_{-\vec{q}}-f_{-\vec{k}}\widehat{\rho}_{\vec{k}}\right)\widehat{\rho}_{\vec{k}+\vec{q}}. \tag{6.24}$$

Maintaining only terms of the order $|V_{\vec{q}}|^2$ (the variational parameters $f_{\vec{k}}$ are of the order $V_{\vec{k}}$) gives:

$$\begin{aligned}\mathcal{J}\left(\vec{q},\vec{q}'\right) &= \delta_{\vec{q},\vec{q}'}\left|V_{\vec{q}}\right|^2\left\langle\psi\left|\left\langle 0\left|e^{i\widehat{H'}t/\hbar}\left(\widehat{\alpha}_{\vec{q}}+\widehat{\alpha}^\dagger_{-\vec{q}}\right)\widehat{\rho}_{\vec{k}+\vec{q}}e^{-i\widehat{H'}t/\hbar}\left(\widehat{\alpha}^\dagger_{\vec{q}}+\widehat{\alpha}_{-\vec{q}}\right)\widehat{\rho}^\dagger_{\vec{k}+\vec{q}}\right.\right.\right. \\ &\left.\left.\left.-\left(\widehat{\alpha}^\dagger_{\vec{q}}+\widehat{\alpha}_{-\vec{q}}\right)\widehat{\rho}^\dagger_{\vec{k}+\vec{q}}e^{i\widehat{H'}t/\hbar}\left(\widehat{\alpha}_{\vec{q}}+\widehat{\alpha}^\dagger_{-\vec{q}}\right)\widehat{\rho}_{\vec{k}+\vec{q}}e^{-i\widehat{H'}t/\hbar}\right|0\right\rangle\right|\psi\right\rangle \\ &= \delta_{\vec{q},\vec{q}'}\left|V_{\vec{q}}\right|^2\left\langle\psi\left|\left\langle 0\left|\widehat{\alpha}_{\vec{q}}(t)\,\widehat{\rho}_{\vec{k}+\vec{q}}(t)\,\widehat{\alpha}^\dagger_{\vec{q}}\widehat{\rho}^\dagger_{\vec{k}+\vec{q}}-\widehat{\alpha}_{-\vec{q}}\widehat{\rho}^\dagger_{\vec{k}+\vec{q}}\widehat{\alpha}^\dagger_{-\vec{q}}(t)\,\widehat{\rho}_{\vec{k}+\vec{q}}(t)\right|0\right\rangle\right|\psi\right\rangle. \end{aligned} \tag{6.25}$$

Introducing this in (6.22) gives:

$$\chi\left(\omega,\vec{k}\right) = -\frac{1}{\hbar\omega^4}\frac{2}{m^2}\sum_{\vec{q}}\left|V_{\vec{q}}\right|^2\left(\vec{k}.\vec{q}\right)^2\int_0^\infty dt e^{i\omega t}\,\mathrm{Im}\,\mathcal{K}\left(\vec{k},\vec{q}\right), \tag{6.26}$$

with:

$$\begin{aligned}\mathcal{K}\left(\overrightarrow{q},\overrightarrow{k}\right) &= \left\langle\psi\left|\left\langle 0\left|\widehat{\alpha}_{\vec{q}}(t)\,\widehat{\rho}_{\vec{k}+\vec{q}}(t)\,\widehat{\alpha}^\dagger_{\vec{q}}\widehat{\rho}^\dagger_{\vec{k}+\vec{q}}\right|0\right\rangle\right|\psi\right\rangle \\ &= e^{-i\omega_{\overrightarrow{q}}t}\left\langle\psi\left|\widehat{\rho}_{\vec{k}+\vec{q}}(t)\,\widehat{\rho}^\dagger_{\vec{k}+\vec{q}}\right|\psi\right\rangle, \end{aligned} \tag{6.27}$$

where the inversion symmetry of the system was used: $\chi\left(\omega,\vec{k}\right)=\chi\left(\omega,-\vec{k}\right)$. Taking the imaginary part of (6.26) leads to

$$\mathrm{Im}\,\chi\left(\omega,\vec{k}\right) = \frac{1}{\omega^4}\frac{\pi}{m_I^2}\sum_{\vec{q}}\left(\vec{k}.\vec{q}\right)^2\left|V_{\vec{q}}\right|^2 S\left(\vec{q}+\vec{k},\omega-\omega_{\vec{q}}\right), \tag{6.28}$$

which is proportional to the Bragg response (2.1). In (6.28) $S\left(\vec{k},\omega\right)$ is the dynamic structure factor of the impurities:

$$S\left(\vec{k},\omega\right) = \frac{1}{2\pi\hbar}\int_{-\infty}^{\infty}dt e^{i\omega t}\left\langle\psi\left|\widehat{\rho}_{\vec{k}}(t)\,\widehat{\rho}^\dagger_{\vec{k}}\right|\psi\right\rangle. \tag{6.29}$$

Spectral effective mass

The response also allows a determination of an effective mass which we shall call the spectral effective mass and denote by $m^{(spec)}$. This is done with the mass sum rule from Ref. [128] (discussed in section 2.6) which was generalized for the many-polaron system in Ref. [77]:

$$\frac{N\pi}{2m^{(spec)}} + \int_{0^+}^{\infty} d\omega\ \omega \lim_{\vec{k}\to 0} \frac{\mathrm{Im}\left[\chi\left(\vec{k},\omega\right)\right]}{k^2} = \frac{N\pi}{2m_I}, \tag{6.30}$$

which is valid at zero temperature. The origin of this sum rule is a δ-peak at $\omega = 0$ in the response, the spectral weight of this δ-peak in the $\vec{k} \to 0$ limit equals the first term in (6.30) as discussed in section 2.6. From (6.30) we find the following expression for the spectral effective mass:

$$m^{(spec)} = \frac{m_I}{1 - \frac{2m_I}{N\pi}\int_0^{\infty} d\omega\omega \lim_{\vec{k}\to 0} \frac{\mathrm{Im}\left[\chi\left(\vec{k},\omega\right)\right]}{k^2}}. \tag{6.31}$$

It is important to note that the spectral effective mass is a single particle property and is thus not the same as the inertial effective mass of expression (6.36). Only in the limit of one polaron the two masses coincide as in this limit we have:

$$S\left(\vec{k}\right) = 1; \tag{6.32}$$

$$S\left(\vec{k},\omega\right) = \delta\left(\hbar\omega - \frac{\hbar^2 k^2}{2m_I}\right). \tag{6.33}$$

In this limit equations (6.18) and (6.31) coincide and become the Lee-Low-Pines expression for the effective mass [52]. The polaronic spectral effective mass has been experimentally determined for the Fröhlich solid state polaron by measuring the spectral weight of the Drude peak in an optical study of Nb-doped $SrTiO_3$ [135,136].

Note that in this formalism the influence of multiple impurities on the polaronic response is solely determined by the dynamic structure factor of the impurities.

6.2 Spin-polarized fermionic impurities

In this section we apply the results of the previous section to the case of a spin-polarized gas of fermionic impurities. Because of the Pauli exclusion principle the s-wave scattering length is zero which results in essentially no interactions between the impurities at low temperature. This means the impurities can be described as an ideal fermionic gas for which the static and dynamic structure factors are known. All results in this section are presented for Li-6 impurities in a Na condensate and in the polaronic units of table 1.1.

As discussed in the introduction the Bogoliubov approximation has to be valid to be able to map the system of impurities in a condensate onto the Fröhlich polaron. In the case of multiple impurities also the stability of the mixture against phase separation is important since in the latter case we can not use the polaronic

description. At zero temperature it was shown in Refs. [148, 149] that for identical fermionic impurities the mixture will be stable if the following inequality is satisfied:

$$n^{1/3} \leq \frac{(6\pi)^{2/3}}{12\pi} \frac{m_B m_I}{(m_B + m_I)^2} \frac{a_{BB}}{a_{IB}^2}, \tag{6.34}$$

with n the density of the fermionic impurities.

6.2.1 Ground state properties

The static structure factor of an ideal fermionic gas at zero temperature is given by [167]:

$$S\left(\vec{k}\right) = \begin{cases} \frac{3}{2}\frac{k}{2k_F} - \frac{1}{2}\left(\frac{k}{2k_F}\right)^3 & \text{if } k < 2k_F \\ 1 & \text{if } k \geq 2k_F \end{cases}, \tag{6.35}$$

where k_F is the Fermi wave vector which, for a non-degenerate spin polarized gas, is given by $k_F = (6\pi^2 n)^{1/3}$, with n the impurity density. Introducing the kinetic energy ε_{kin} of an ideal fermionic gas together with the Bogoliubov dispersion (1.15) and the interaction amplitude (1.26) in the expression for the ground state energy (6.10) leads to:

$$\begin{aligned} \frac{E}{N} &= \frac{3}{10}k_F^2 - \frac{\alpha}{2\pi}\left(\frac{m_B+1}{m_B}\right)^2 \\ &\quad \times \int_0^\infty dk k^2 \left[\frac{m_B S^2\left(\vec{k}\right)}{k\sqrt{k^2+2}S\left(\vec{k}\right) + m_B k^2}\left(\frac{k^2}{k^2+2}\right)^{1/2} - \frac{m_B}{m_B+1}\right], \end{aligned} \tag{6.36}$$

with α the polaronic coupling parameter (1.34). The first term represents the kinetic energy of the impurities and the second is the polaronic contribution, the interaction energy vanishes since we are describing an ideal gas. Note that in the polaronic contribution an additional term is included which is needed to obtain a converging expression. This term is a consequence of using the Lippmann-Schwinger equation up to second order (1.2) for the boson-impurity interaction strength in the second term of the total Hamiltonian (1.27). In the $n \to \infty$ limit the polaronic contribution becomes:

$$\lim_{n\to\infty} \frac{E_{pol}}{N} = -\frac{\alpha}{2\pi}\left(\frac{m_B+1}{m_B}\right)^2 k_F \int_0^2 dk \left[k^2 \frac{m_B S\left(\vec{k}k_F\right)}{k^2 S\left(\vec{k}k_F\right) + m_B k^2} - \frac{m_B}{m_B+1}\right], \tag{6.37}$$

which grows linearly with k_F as the number of particles is increased. Since the kinetic energy of the Fermi gas grows as k_F^2, the relative contribution of the polaronic energy with respect to the kinetic energy decreases. In the limit of large densities, the kinetic energy dominates the polaronic effect.

Introducing the Bogoliubov dispersion (1.15) and the interaction amplitude (1.26) in the expression for the polaron inertial effective mass (6.18) results in:

$$m^{(in)} = 1 + \frac{4\alpha}{3\pi}\left(\frac{m_B+1}{m_B}\right)^2 \int_0^\infty dk \frac{1}{\sqrt{2+k^2}} \frac{k^2 S^2\left(\vec{k}\right)}{\left(\frac{1}{m_B}\sqrt{k^2+2}S\left(\vec{k}\right) + k\right)^3}. \tag{6.38}$$

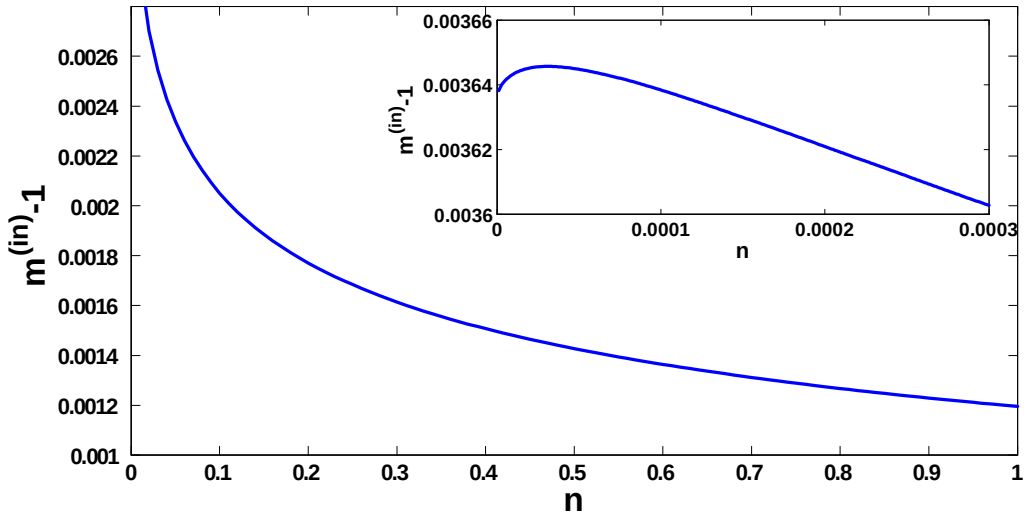

Figure 6.1: The inertial effective mass of the polarons (3.27) as a function of the density for Li-6 impurities in a Na condensate at $\alpha = 0.01$. The inset shows the behavior at small densities. In the limit $n \to 0$ the effective mass of a single polaron is retrieved and for $n \to \infty$ the effective mass becomes the bare impurity mass.

This expression is shown in Fig. 6.1 as a function of the impurity density. In the limit $n \to 0$ the one-polaron result is retrieved, which was already anticipated using formula (6.18). In the $n \to \infty$ limit we find for the inertial effective mass:

$$\lim_{n\to\infty} m_I^* = 1 + \lim_{n\to\infty} \left(\frac{m_B+1}{m_B}\right)^2 \frac{4}{3}\frac{\alpha}{\pi}\frac{1}{k_F}\int_0^2 dk \frac{kS^2\left(\vec{k}k_F\right)}{\left(m_B^{-1}kS\left(\vec{k}k_F\right)+k\right)^3} \quad (6.39)$$

$$= 1, \quad (6.40)$$

i.e. it becomes equal to the bare impurity mass which again shows that the polaron effect vanishes at large impurity density. The reason is that the mean distance between the impurities reduces as the density increases and at a certain point the polarons start to overlap. As this overlap becomes greater the separate polarons become less distinct and the polaronic effects diminish. For the solid state polaron the same qualitative behavior as in Fig. 6.1 was found for the effective mass if the electrons are described as a free gas [77, 168].

6.2.2 Response to Bragg spectroscopy

For the response the dynamic structure factor is needed, which for an ideal fermionic gas at temperature zero is given by [134]:

$$S\left(\vec{q},\omega\right) = \frac{1}{4\pi^2 q}\theta\left(\omega\right)\begin{cases} \omega & \text{if } \frac{k_F^2}{2} > \frac{1}{2q^2}\left(\omega+\frac{q^2}{2}\right)^2 \\ \frac{k_F^2}{2} - \frac{1}{2q^2}\left(\omega-\frac{q^2}{2}\right)^2 & \text{if } \frac{k_F^2}{2} < \frac{1}{2q^2}\left(\omega+\frac{q^2}{2}\right)^2, \\ 0 & \text{if } \frac{k_F^2}{2} < \frac{1}{2q^2}\left(\omega-\frac{q^2}{2}\right)^2 \end{cases} \quad (6.41)$$

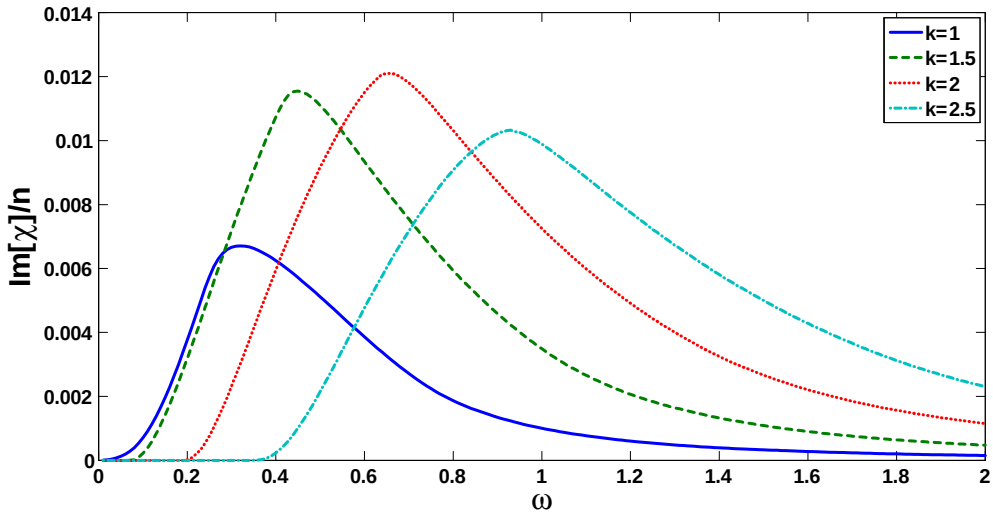

Figure 6.2: The Bragg response (6.42) of the polaronic system consisting of polarized Li-6 impurities in a Na condensate as a function of ω for different values of the exchanged momentum k. The impurity density is taken $n = 0.01$ and the polaronic coupling parameter is $\alpha = 0.01$.

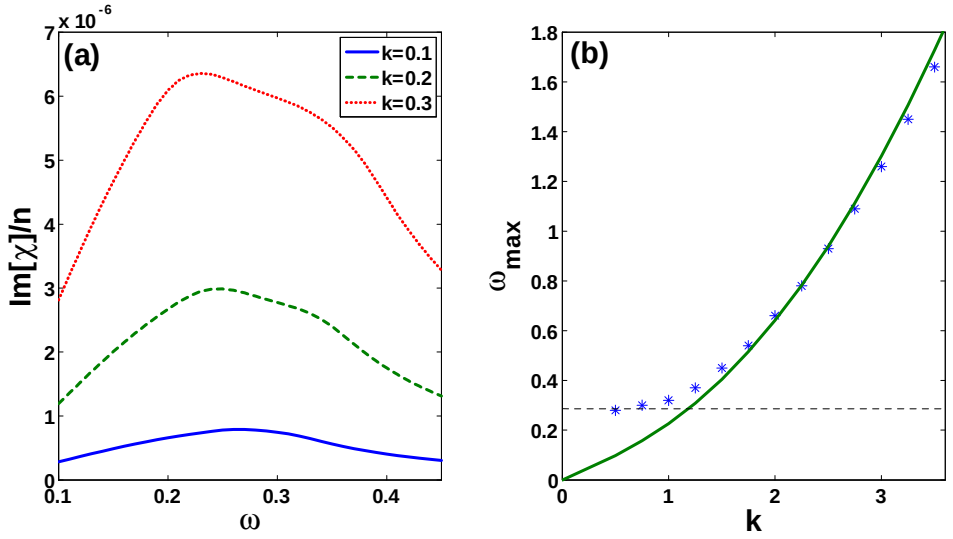

Figure 6.3: In (a) the Bragg response (6.42) is shown of the polaronic system consisting of polarized lithium-6 impurities in a sodium condensate as a function of ω for different values of the exchanged momentum k at relatively small k, revealing the shoulder structure of the peak. In (b) the position of the maximum of the peak in the Bragg response is presented (markers) together with the Bogoliubov spectrum (1.15) (full line) and the Fermi frequency ω_F (dotted line). In both plots the impurity density is $n = 0.01$ and the polaronic coupling parameter is $\alpha = 0.01$.

with $\theta(\omega)$ the Heaviside step function. Introducing the Bogoliubov dispersion (1.15) and the interaction amplitude (1.26) in the expression for the imaginary part of the density response function (6.28) leads to

$$\mathrm{Im}\,\chi\left(\omega,\vec{k}\right)=\frac{\alpha}{16\pi\omega^4}\left(\frac{m_B+1}{m_B}\right)^2\sum_{\vec{q}}\left(\vec{k}.\vec{q}\right)^2\frac{q^3}{\sqrt{q^2+2}}S\left(\vec{k}+\vec{q},\omega-\omega_{\vec{q}}\right). \quad (6.42)$$

In Fig. 6.2 the Bragg response (6.42) is shown as a function of ω for various momentum exchanges. A peak is seen that represents the emission of Bogoliubov excitations and that is shifted to higher frequencies for larger momentum exchange. This behavior is to be expected since more energy is needed to create a Bogoliubov excitation with a higher momentum.

In Fig. 6.3 (a) we have zoomed in on the peak for small values of the momentum exchange k which reveals a shoulder structure. This behavior was also observed in the context of the optical absorption of solid state polarons in Refs. [76, 168]. It is a consequence of the Pauli exclusion principle which provides a constraint on the number of fermions that can participate in the Bragg scattering process and it was shown in Ref. [168] that a maximal allowed participation is reached for $\omega=\omega_{\vec{k}}+\omega_F$ (with $\omega_F=\hbar k_F^2/(2m_I)$, the Fermi frequency). This phenomenon provides a redistribution of the weight of the main peak towards this value which explains the shoulder structure in Fig. 6.3 (a). At larger values of the exchanged momentum k the effect diminishes. In Fig. 6.3 (b) the location of the maximum of the peak is plotted as a function of k together with the Bogoliubov dispersion (1.15) which indeed is a better fit at larger k. At smaller k there is a deviation towards the Fermi frequency, as expected from this Pauli blocking mechanism.

In Fig. 6.4 the peak in the Bragg response is presented for different impurity densities. Note that for higher densities the spectral weight of the Bogoliubov peak diminishes. This is not in contradiction with the f-sum rule: the spectral weight of the $\omega=0$ delta peak in the spectrum compensates the change in the spectral weight of the Bogoliubov peak, in accordance with the mass sum rule (6.30) from Ref. [128]. For $\vec{k}\to 0$ the weight of this δ-function is related to the spectral effective mass such that an attenuation of the Bogoliubov peak corresponds to a decrease of the spectral effective mass. The spectral effective mass deduced with the sum rule (6.30) is presented in Fig. 6.5 as a function of the impurity density. Note that the spectral effective mass behaves only qualitatively the same as the inertial effective mass from Fig. 6.1 and only in the limits $n\to 0$ and $n\to\infty$ the same result is retrieved.

We would like to emphasize that the different definitions of the effective mass result in another behavior and can in general not be compared. This also means that for an experiment it is important to know which effective mass is of importance for the specific setup.

6.3 Bosonic impurities

We now apply the weak coupling many-polaron formalism for ultracold bosonic impurities in a Bose-Einstein condensate. Experimentally these mixtures can consist

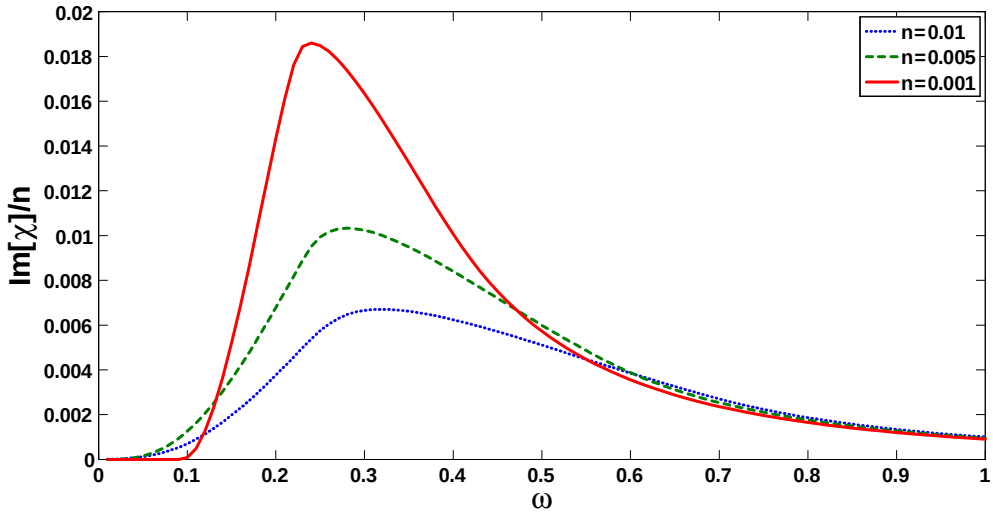

Figure 6.4: The Bragg response (6.42) of the polaronic system consisting of polarized Li-6 impurities in a Na condensate as a function of ω for different impurity densities n. The exchanged momentum is taken $k = 1$ and the polaronic coupling parameter is $\alpha = 0.01$.

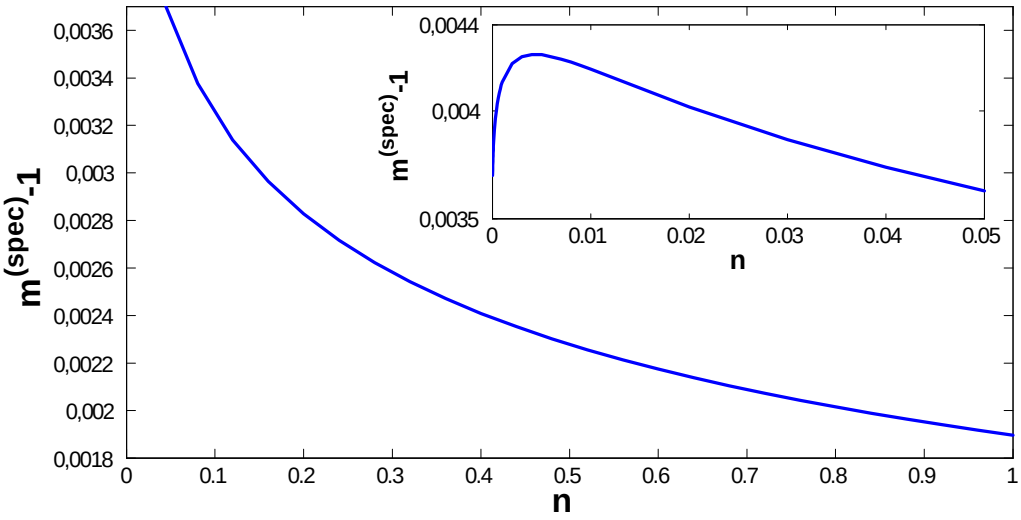

Figure 6.5: The spectral effective mass of the polarons as a function of the impurity density for Li-6 impurities in a Na condensate at $\alpha = 0.01$ as determined by the sum rule (6.30).

of different hyperfine states of the same atom or of different species. The static and dynamic structure factors of ultracold bosons, as derived in Ref. [169], are employed to calculate the ground state properties and the response of the system to Bragg spectroscopy. Both the inertial and spectral effective masses are considered and compared. Since the system has to be stable with respect to phase separation the following criterion has to be satisfied [157]:

$$g_{IB}^2 < g_{II} g_{BB}.$$

6.3.1 Structure factors

In Ref. [169] the static and dynamic structure factors were derived for an ultracold dilute bosonic gas. In the case of a homogeneous gas the static structure factor is given by:

$$S\left(\vec{k}\right) = \frac{\hbar^2 k^2}{2m_I \varepsilon_{\vec{k}}^I}, \tag{6.43}$$

with $\varepsilon_{\vec{k}}^I$ the Bogoliubov dispersion of the bosonic impurity condensate:

$$\varepsilon_{\vec{k}}^I = \frac{\hbar^2 k}{2m_I}\sqrt{k^2 + 16\pi n_I a_{II}}, \tag{6.44}$$

where n_I is the impurity density and a_{II} the impurity-impurity scattering length. The first two terms in (6.36) give the ground state energy of a homogeneous condensate. The corresponding dynamic structure factor is given by:

$$S\left(\vec{q}, E\right) = N_I \frac{q^2}{2m_I \varepsilon_{\vec{q}}^I} \delta\left(E - \varepsilon_{\vec{q}}^I\right). \tag{6.45}$$

6.3.2 Results and discussion

From the above equations it is clear that the parameters that express the many-body nature of the impurities, namely the density n and the scattering length a_{II}, combine to a single parameter which is the product $n_I a_{II}$ of the two. Here we examine the polaronic properties as a function of $n_I a_{II}$ and of the mass ratio m_B/m_I. As usual all results are presented in the polaronic units of table 1.1.

In the limit of vanishing impurity density or non-interacting impurities, i.e. $n_I a_{II} \to 0$, all derived expressions reduce to the Lee-Low-Pines results for a single polaron in the weak coupling regime [89]. In the opposite limit of many impurities or strong mutual interaction between the impurities ($n_I a_{II} \to \infty$) both inertial and spectral effective mass (see Fig. 6.6) converge to the bare mass of the impurity which indicates that the polaronic features vanish in this limit. From Fig. 6.6 it is clear that the two definitions for the effective mass only coincide in the two previously considered limits.

Fig. 6.6 (c) shows the Bragg response (6.28) as a function of ω at different values of the parameter $n_I a_{II}$, revealing the peak that corresponds to the emission of Bogoliubov excitations. As the parameter $n_I a_{II}$ is increased the response per particle decreases which is consistent with the previous observation of diminishing polaronic

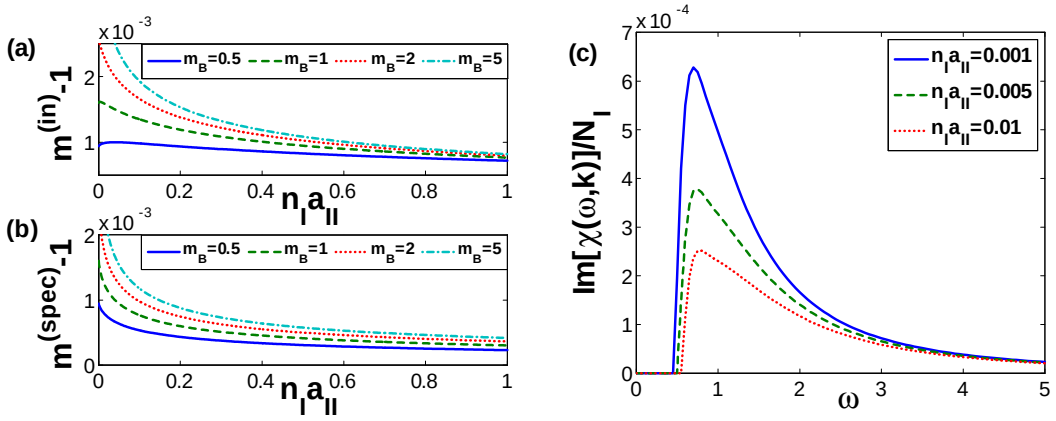

Figure 6.6: The inertial (a) and spectral (b) effective masses of ultracold bosonic impurities in a Bose-Einstein condensate as a function of $n_I a_{II}$ at different values of m_B and with $\alpha = 0.01$. In (c) the response of multiple bosonic impurities to Bragg scattering is shown as a function of the transferred energy at different values of $n_I a_{II}$ and at $\alpha = 0.01$ and $k = 1$.

effects for increasing $n_I a_{II}$. This is similar to the cases of fermionic impurities (see Fig. 6.4) and electrons in a polar lattice [75, 76] where the polaronic features also diminish in the limit of high density.

In Fig. 6.7 the imaginary part of the density response function (6.28) is presented as a function of ω, at different values for the exchanged momentum k. It is clear that the peak consists of two contributions which at relatively small k results in a shoulder structure. At relatively high k the shoulder disappears and the maximum of the peak shifts according to the Bogoliubov dispersion (1.15) (see Fig. 6.7 (d)). At low k the dominating contribution to the peak has a maximum with a location that is independent of k and is determined by the recoil of the impurities.

6.4 Conclusions

The weak coupling many-polaron formalism which has been developed in the context of solid state polarons in Refs. [75] and [76] was applied to the polaronic system consisting of impurity atoms in a Bose-Einstein condensate. The properties of the ground state and the response to Bragg spectroscopy were examined. A derivation was presented of the inertial effective mass, which is related to the ground state of the many-polaron system as a whole, and of the spectral effective mass, which is deduced from the dynamic response. It turns out that the ground state properties are determined by the static structure factor of the impurities while the response is governed by the dynamic structure factor, as in the case of the solid state polarons.

This generalization of the many-polaron formalism was then applied to the case of spin-polarized fermionic impurities which can be described as an ideal gas for which the structure factors are known. The numerical calculations were done for Li-6 impurities in a Na condensate. Both the ground state properties and the Bragg response indicate that in the limit of high impurity density the polaron effect disappears, which is also the case for solid state polarons. In the Bragg response a

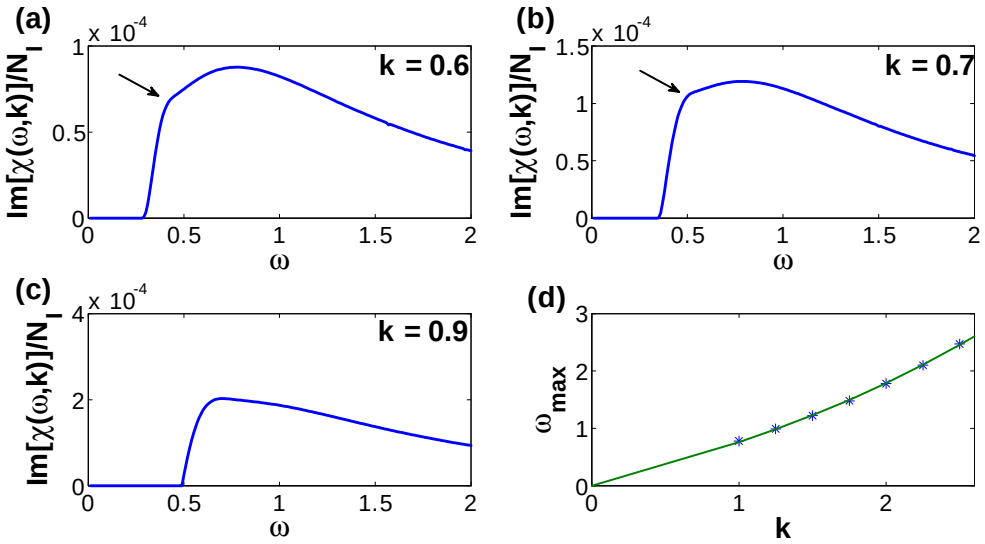

Figure 6.7: In (a), (b) and (c) the response of multiple bosonic impurities to Bragg scattering is presented as a function of ω at $n_I a_{II} = 0.01$, $m_B = 1$ and $\alpha = 0.01$ and at different momentum exchange k. In (a) and (b) the shoulder feature is indicated. In (d) the location of the maximum is presented (markers) at relatively high k as a function of k together with a least square fit to the Bogoliubov dispersion (1.15) with fitting parameters $m_B = 1.8374$ and $\xi = 0.5430$.

peak was observed that corresponds to the emission of Bogoliubov excitations. The behavior of this peak as a function of the exchanged momentum exhibits a shoulder structure which is a manifestation of the Pauli exclusion principle. At large impurity density the spectral weight shifts to the δ-peak at $\omega = 0$ and in the limit $n \to \infty$ all the spectral weight is in this peak which means there is no polaronic effect. It was also shown that the two considered definitions for the effective mass exhibit a different quantitative behavior.

Then we applied the weak-coupling many-polaron formalism to the case of dilute ultracold bosonic impurities. It was shown that the relevant parameter to describe the many-body effects is the product $n_I a_{II}$. Similar to the case of fermionic impurities the inertial and spectral effective masses only coincide in the limits $n_I a_{II} \to 0$ and $n_I a_{II} \to \infty$. The response of the system to Bragg spectroscopy revealed a peak corresponding to the emission of Bogoliubov excitations which consists of two contributions. One is dominant at low momentum exchange k and is determined by the recoil of the impurities. The other contribution dominates at high k and corresponds to the transfer of both momentum and energy to a Bogoliubov excitation.

Chapter 7

Polaron consisting of an ion in a condensate*

Motivated by the experimental realization of trapping a single ion in a condensate [100, 101] and the development of optical traps for ions [170] this chapter is devoted to the description of the polaronic ground state properties of a charged impurity in a condensate. Furthermore, because of the greater range of the ion-atom interaction, the effective polaronic coupling parameter is expected to be larger, as compared to a neutral impurity, which can facilitate an experimental probing of the polaronic strong coupling regime. However, this also leads to a stronger depletion of the condensate around the impurity and a good correspondence between the Fröhlich Hamiltonian and the cold atom system is only possible when the Bogoliubov approximation is valid which assumes a small depletion.

First, a pseudo potential is introduced to describe the ion-boson interaction. This is needed because the greater range of the interaction excludes the use of a contact potential. A short range cutoff is introduced which will influence the results and is an experimentally unknown parameter. Then the Landau-Pekar strong coupling treatment is applied which allows an estimation of an upper bound for the polaronic coupling strength for the Bogoliubov approximation to be applicable. The all-coupling path integral approach is then applied to estimate the values of the critical coupling constant for the transition to the strong coupling regime. The results of these two approaches allows us to identify a regime where ions in condensates can model strong-coupling polarons. We also consider the effect of the ion trap strength.

7.1 Atom-ion pseudo potential

A main problem in the description of the ion-atom interaction is how to model the behavior at small distances [171–173]. One possibility is to fix the phase of the relative wave function at small distances [174, 175]. Another approach is to use a hard sphere potential [176] at small r. Here, we use a short-range cutoff characterized

*The results from this chapter, applied to a Ba^+ ion in a Rb condensate (which corresponds to the experimental system of Ref. [101]), are published in W. Casteels, J. Tempere and J. T. Devreese - *Polaronic Properties of an Ion in a Bose-Einstein Condensate in the Strong-Coupling Limit* - J. Low Temp. Phys. **162** 266 (2011).

by a parameter b and write the ion-atom potential as:

$$V(r) = -\frac{C_4}{(r^2+b^2)^2}. \tag{7.1}$$

The long range behavior of this potential is characterized by the Van der Waals parameter C_4, while at small length scales it is the parameter b that determines the potential. The reason we choose this particular potential is the expression of the Fourier transform, which is convenient to work with:

$$V(\vec{k}) = -\frac{\pi^2 C_4 e^{-kb}}{b}. \tag{7.2}$$

7.1.1 Scattering length

In this section we calculate the scattering length associated with the potential (7.1). The scattering length is experimentally measurable and contains information about the parameter b. We start with the Schrödinger equation for two particles interacting at low energy through a spherical symmetric potential (see for example Ref. [177]):

$$\frac{\hbar^2}{2m_r}\frac{\mathrm{d}^2 u}{\mathrm{d}r^2} - V(r)u = 0, \tag{7.3}$$

where m_r is the reduced mass and $u(r) = rR(r)$, with $R(r)$ the radial part of the wave function and r the distance between the two particles. For $r \to \infty$ the potential $V(r)$ is negligible and the Schrödinger equation is solved as:

$$u(r) = c(r-a) \tag{7.4}$$

which is the definition of the scattering length a. By solving (7.3) for arbitrary r we can determine a by looking at the behavior for $r \to \infty$. Inserting the potential (7.1) in the Schrödinger equation (7.3) gives:

$$\frac{\mathrm{d}^2 u}{\mathrm{d}r^2} + \frac{R^2}{(r^2+b^2)^2}u = 0, \tag{7.5}$$

with R the characteristic length of the potential: $R = \sqrt{2m_r C_4/\hbar^2}$. The general solution of this differential equation is:

$$\begin{aligned} u(r) &= \frac{C_1}{b}\exp\left[\frac{i\sqrt{R^2+b^2}\arctan(\frac{r}{b})}{b}\right]\sqrt{b^2+r^2} \\ &\quad + \frac{C_2}{b}\exp\left[-\frac{i\sqrt{R^2+b^2}\arctan(\frac{r}{b})}{b}\right]\sqrt{b^2+r^2}, \end{aligned} \tag{7.6}$$

where C_1 and C_2 are two constants. Applying the boundary condition $u(0) = 0$ gives $C_1 = -C_2 = C$ and thus:

$$u(r) = \frac{2iC}{b}\sqrt{b^2+r^2}\sin\left(\frac{\sqrt{R^2+b^2}\arctan(\frac{r}{b})}{b}\right). \tag{7.7}$$

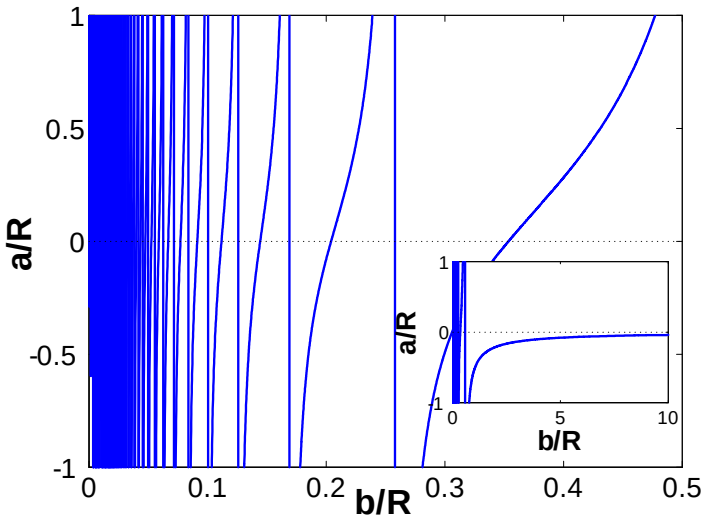

Figure 7.1: The scattering length a (7.9) as a function of the parameter b. The inset shows the behavior at larger values for b.

For the scattering length we need the $r \to \infty$ dependence:

$$\lim_{r\to\infty} u(r) \approx \frac{2iC}{b}\left[\sin\left(\frac{\sqrt{R^2+b^2}\pi}{2b}\right) r - \cos\left(\frac{\sqrt{R^2+b^2}\pi}{2b}\right)\frac{\sqrt{R^2+b^2}}{2}\right]. \tag{7.8}$$

Comparing this with (7.4) gives for the scattering length:

$$a = \cot\left(\frac{\sqrt{R^2+b^2}\pi}{2b}\right)\frac{\sqrt{R^2+b^2}}{2}. \tag{7.9}$$

This relation is presented in Fig. 7.1 which shows that the parameter b is not uniquely determined by the scattering length. It also depends on the number of bound states the potential (7.1) accommodates. Each time a bound state enters the potential the scattering length diverges, which explains the behavior in Fig. 7.1. From Fig. 7.1 it is clear that with the experimentally given values for R and a correspond multiple possible values for b but it is typically smaller than R.

7.2 The Fröhlich Hamiltonian

We can use the Hamiltonian (1.22) for an ion in a gas of bosons by taking $N_I = 1$ and using expression (7.1) for V_{IB}. Assuming the bosons form a condensate by applying the Bogoliubov shift leads in the same way as discussed in section 1.3 to the Hamiltonian (1.27). This maps onto the polaron Hamiltonian describing the ion interacting with the Bogoliubov excitations of the condensate through the polaronic interaction with amplitude

$$V_{\vec{k}} = -\frac{\pi^2 C_4 e^{-kb}}{b}\sqrt{N_0}\left(\frac{(\xi k)^2}{(\xi k)^2+2}\right)^{1/4}, \tag{7.10}$$

with ξ the healing length of the condensate and N_0 the number of bosons in the condensate.

In deriving the Fröhlich polaron Hamiltonian the Bogoliubov approximation is used which states that a macroscopic number of the bosons are in the one particle ground state. Care has to be taken whether this approximation is still applicable in the vicinity of the ion because of the relatively strong ion-atom interaction. We will derive a condition that has to be satisfied in order to map the system onto the Fröhlich polaron.

7.3 Strong coupling limit

7.3.1 Ground state properties

Here we apply the Landau-Pekar strong coupling treatment from chapter 3 for the ground state properties of to the polaronic system consisting of an ion in a condensate. Introducing the Bogoliubov dispersion (1.15) and the interaction amplitude (7.10) into the upper bound (3.5) for the polaronic energy of the ground state results in (from now on the polaronic units of table 1.1 are used):

$$E_0 \leq \frac{3}{4\lambda^2} - \frac{\pi}{8}\alpha\mu \int_0^\infty dk k^2 \frac{e^{-2kb}\exp(-\frac{\lambda^2 k^2}{2})}{k^2+2}, \tag{7.11}$$

with λ a variational parameter that corresponds to the width of the impurity wave function. We also introduced the dimensionless mass factor μ (3.23) and defined the dimensionless polaronic coupling strength as follows:

$$\alpha = \frac{R^4}{a_{BB} b^2 \xi}, \tag{7.12}$$

with a_{BB} the boson-boson scattering length. In Fig. 7.2 the upper bound for the polaronic energy is presented as a function of $\alpha\mu$ for different values of the parameter b, together with the variationally determined λ. This shows a decreasing dependence on $\alpha\mu$ which becomes stronger as b is reduced. With every value of b corresponds a critical coupling value $(\alpha\mu)_c$ below which Eq. (7.11) has no minimum at finite λ. This value, $(\alpha\mu)_c$, is also presented in Fig. 7.2 as a function of b. This indicates that at low $\alpha\mu$ the self-induced potential is not strong enough to localize the ion wave function. To investigate the polaronic effects for intermediate and weak coupling, the Feynman all-coupling approach is required.

The polaronic coupling parameter (7.12) is experimentally tunable by means of a Feshbach resonance for a_{BB} or by the dependence of the healing length ξ on the condensate density. Let us make an estimate for the order of magnitude of the non-interfered coupling parameter (7.12). The characteristic length R of the ion-boson potential is typically of the order of the healing length and the scattering length a_{BB} and the parameter b are typically an order of magnitude smaller, this gives

$$\alpha \sim 100.$$

The masses of the ion and the bosons are typically of the same order which gives $\mu \sim 1$.

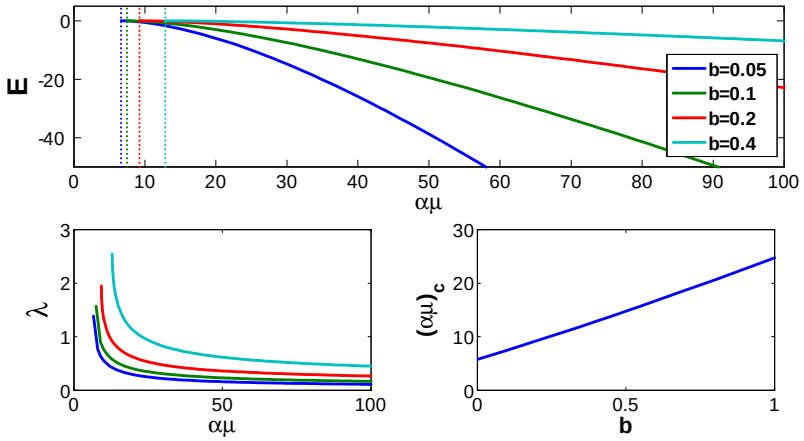

Figure 7.2: The upper bound for the polaronic energy E (7.11) and the variationally determined parameter λ as a function of $\alpha\mu$ at different values of b (in units of ξ). The minimum value of $\alpha\mu$ below which Eq. (7.11) has no minimum $(\alpha\mu)_c$ is also presented as a function of b (in units of ξ).

7.3.2 Condensate density depletion

As mentioned before the Bogoliubov approximation has to be valid in order to be able to map the BEC-ion system to the Fröhlich Hamiltonian which means the depletion may not be too large. As a quantification of the depletion we use the parameter $\Delta\rho$, defined as:

$$\Delta\rho = \lim_{r\to 0} \frac{n_0 - \rho_B\left(\vec{r}\right)}{n_0}. \tag{7.13}$$

Within the strong coupling formalism the lowest order correction to the homogeneous boson density is [25]

$$n_0 - \rho_B\left(\vec{r}\right) = \sqrt{N_0}\sum_{\vec{k}} e^{i\vec{k}.\vec{r}} \sqrt{\frac{E_{\vec{k}}}{\hbar\omega_{\vec{k}}} \frac{V_{\vec{k}}\rho_{\vec{k}}}{\left(\hbar\omega_{\vec{k}}\right)^2}}.$$

For an ion in a condensate we thus find

$$\Delta\rho = \frac{R^2}{b}\left(1+m_B\right) 2\int_0^\infty dk e^{-kb} \frac{k^2}{k^2+2} \exp\left(-\frac{k^2\lambda^2}{4}\right). \tag{7.14}$$

For the Bogoliubov approximation to be applicable the condition $\Delta\rho \ll 1$ has to be satisfied. From (7.14) it is clear that $\Delta\rho$ depends on the parameters R, b, m_B and α (through the dependence on the variational parameter λ). To get an estimation of the order of magnitude of (7.14) we insert $R = 1$ and $m_B = 1$ as typical values. Using these values the value of $\alpha\mu$ that corresponds to $\Delta\rho = 1$ is presented in Fig. 7.3 as a function of b. This can be interpreted as a maximum value for $\alpha\mu$ for which the Bogoliubov approximation can be justified. For $\alpha\mu$ larger than this value the depletion is too large and the polaronic description fails. The polaronic system of a (charged) impurity dressed by a cloud of Bogoliubov excitations then evolves into the formation of a mesoscopic molecular ion as the bosons bind to the ion [178]. If

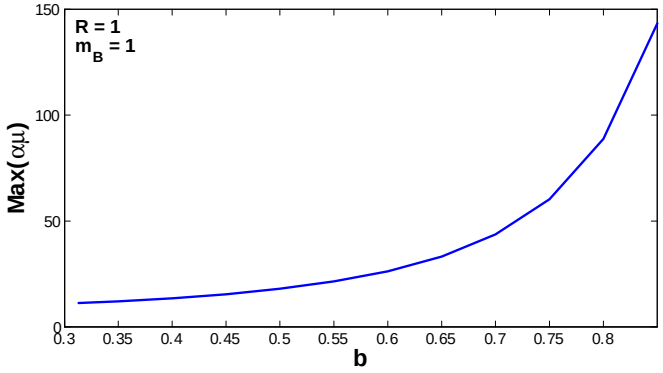

Figure 7.3: The value of $\alpha\mu$ that corresponds with $\Delta\rho = 1$ as a function of b for $R = 1$ and $m_B = 1$.

the dimensionality is reduced, the effects of strong coupling are exhibited at lower values of α (see chapter 5) which should also hold for the depletion, consistent with results for an ion in a Tonks-Girardeau gas [175].

Another factor that can alter the polaron effect is the strength of the ion trap. Ion traps usually lead to a very tight confinement of the ion as compared to the Bose condensate. This property is useful when ions are applied to locally probe the properties of a quantum gas [179]. But when the ion trap confinement length is shorter than the polaron size (well estimated by the variational parameter λ) the transition from strong to weak coupling regimes can be masked. To avoid this, it is necessary that the self-induced potential is not dominated by the externally applied trap. This is realized when the confinement length r_0 of the ion trap is large compared to λ. If this is not the case, the present formalism is still applicable, but λ is no longer a variational parameter, rather it should be fixed to $\lambda = r_0$. In a Paul trap, an additional difficulty appears: the micromotion of the ion, driven by the rf trapping fields, leads to atom losses from the condensate and heating [100]. This difficulty should be overcome by (recently demonstrated) optical trapping of ions [170].

7.4 Feynman variational path integral treatment

In this section the Feynman all-coupling polaronic treatment is applied for an ion in a condensate. We introduce the Bogoliubov dispersion (1.15) and the interaction amplitude (7.10) to the Jensen-Feynman inequality (5.1) in 3D. This results in an upper bound for the polaronic free energy which is then minimized as a function of the variational parameters M and Ω. In this formalism the bosonic mass m_B and the coupling parameter α can not be combined into a single parameter. In Fig. 7.4 the resulting upper bound for the polaronic energy is presented as a function of $\alpha\mu$ for different values of m_B at temperature zero. Also the variational mass parameter M, which is related to the effective mass as $m^* \approx m_I + M$ [163], and the root mean square of the reduced coordinate of the model system $\sqrt{\langle r^2 \rangle}$ (5.4), which estimates the polaronic size [163], are presented as a function of $\alpha\mu$. This shows a

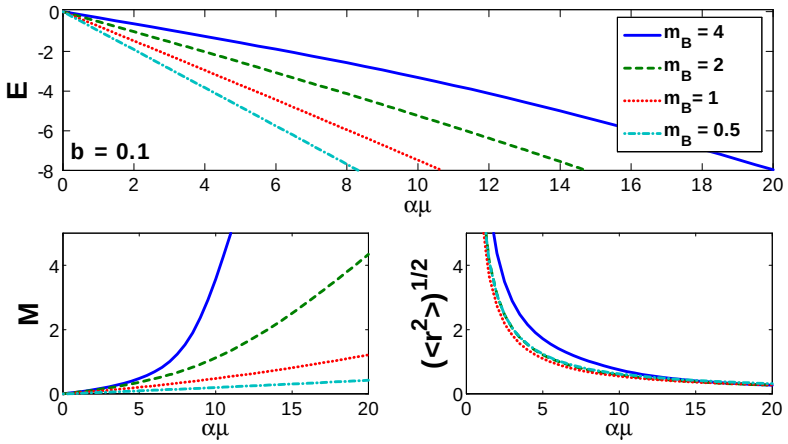

Figure 7.4: The upper bound for the polaronic energy E, the mass parameter M and $\sqrt{\langle r^2 \rangle}$ are shown for an ion in a Bose-Einstein condensate as a function of $\alpha\mu$ for different values of m_B at temperature zero.

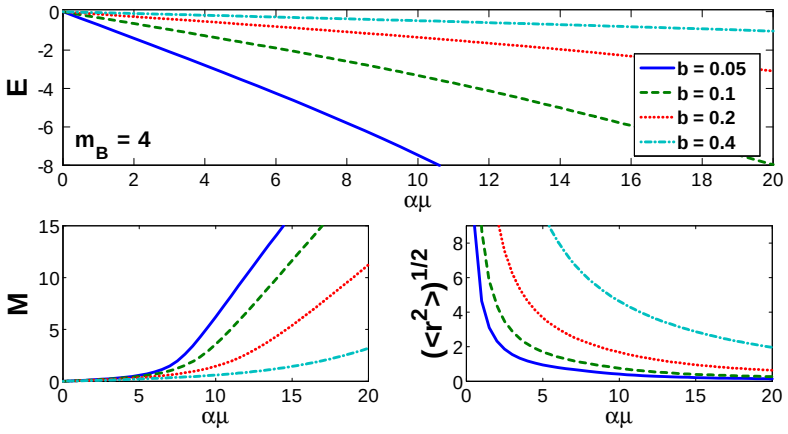

Figure 7.5: The upper bound for the polaronic energy E, the mass parameter M and $\sqrt{\langle r^2 \rangle}$ are presented for an ion in a condensate as a function of $\alpha\mu$ for different values of the parameter b at temperature zero.

decreasing behavior of the energy at the small $\alpha\mu$ values below the critical $(\alpha\mu)_c$ that were inaccessible with the Landau-Pekar strong-coupling treatment outlined in the previous section. The energy remains negative (indicating that the polaronic effect leads to a reduction in energy at all coupling), which is different from the result obtained for a neutral impurity, but similar to the result for the solid state polaron. The behavior of M as a function of $\alpha\mu$ shows the same characteristics as for a neutral impurity in Fig. 1.10. Comparing the behavior of $\sqrt{\langle r^2 \rangle}$ the same asymptotic behavior is retrieved at weak and strong coupling, but the lump at intermediate coupling in Fig. 1.10 is not present for a charged impurity. This behavior signals a transition from a quasi-free polaron at small $\alpha\mu$ to the strong-coupling regime at large $\alpha\mu$ where we expect that the internal wave function of the ion is localized by the self-induced potential. Furthermore we observe that the transition becomes less abrupt as the bosonic mass parameter m_B decreases.

In Fig. 7.5 the upper bound for the polaronic energy E is presented, together with M and $\sqrt{\langle r^2 \rangle}$, as a function of $\alpha\mu$ for different values of b at $m_B = 4$ and temperature zero. Also here a stronger dependence of the energy on the coupling parameter $\alpha\mu$ is found as b decreases, similar to the strong-coupling behavior in Fig. 7.2. Focusing on the mass parameter shows that the critical value $(\alpha\mu)_c$ grows as b increases which is again similar to the behavior in Fig. 7.2. Furthermore, the transition becomes less abrupt as b increases.

In Fig. 7.6 the upper bound for the polaronic free energy is presented, together with M and $\sqrt{\langle r^2 \rangle}$, as a function of $\alpha\mu$ for different values of the temperature. This temperature dependence is similar to the behavior in Fig. 1.10 for a neutral impurity.

These results show that the path-integral treatment predicts for the critical polaronic coupling strength $(\alpha\mu)_c \sim 10$.

7.5 Conclusions

In this chapter the possibility of studying strong-coupling polaronic effects using an ion in a condensate was investigated. The advantage of using ions over neutral impurities is that the ion–atom interaction leads to stronger coupling. The disadvantage of using ions is that the depletion of the condensate may be too strong, so that the Bogoliubov approximation breaks down and the mapping of the Hamiltonian to the Fröhlich Hamiltonian becomes invalid. A short range cutoff had to be introduced for the ion-boson interaction. This cut-off cannot be uniquely fixed by a measurement of the s-wave scattering length, and this excludes at the moment a quantitative analysis of the system.

Using a variational wave function, valid at strong coupling, the depletion was calculated which resulted in an upper bound for the polaronic coupling strength for the Bogoliubov approximation to be valid. Using the all-coupling path-integral treatment with a variational model system, the onset of the sought-after strong coupling regime is estimated at $(\alpha\mu)_c \sim 10$. An estimate for a typical value of the coupling parameter resulted in $\alpha\mu \sim 100$. This is well within the strong coupling regime but also in the range where the depletion can destroy the polaron. A possible solution is to tune the coupling parameter to a smaller coupling constant or to go

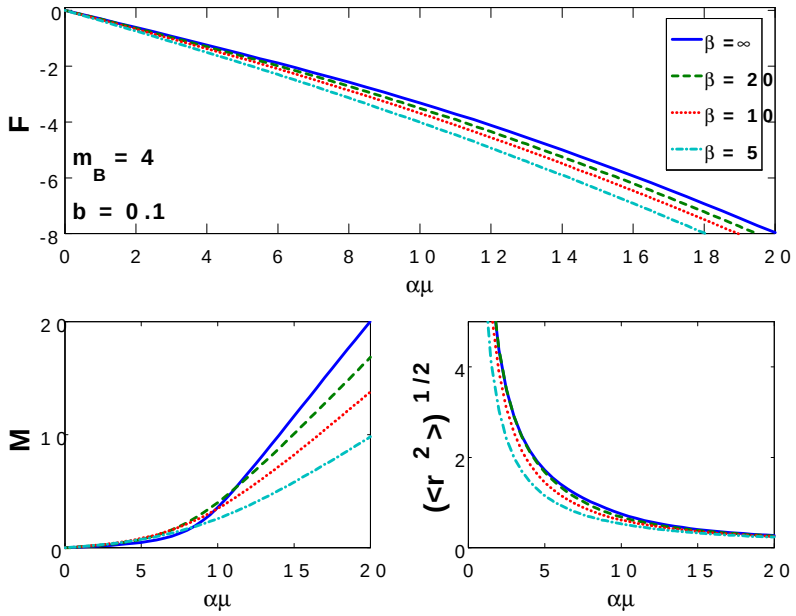

Figure 7.6: The upper bound for the polaronic free energy F, the mass parameter M and $\sqrt{\langle r^2 \rangle}$ are presented for an ion in a condensate as a function of $\alpha\mu$ for different values of the temperature T ($\beta = (k_B T)^{-1}$).

to reduced dimensions.

Chapter 8

Closing

8.1 Final conclusions

In this thesis we have studied polaron physics from the perspective of an impurity in a Bose-Einstein condensate. The impurity is dressed with bogoliubov excitations of the condensate, and can be treated as a quasiparticle, the BEC-impurity polaron. This is more than just a quantum-gas analogy of the solid state polaron consisting of an electron together with its lattice deformation. The great potential of quantum gases lies in the possibility to fine tune experimental parameters such as the interaction strength and the dimensionality. This allows to study the polaron problem in regimes and under conditions that have been inaccessible before. Several aspects were treated in this thesis, in particular (i) response properties, (ii) many-body effects for the interacting polaron gas, (iii) effects of reduced dimensionality. The techniques that had been developed for solid state polarons had to be extended, for example in the case of the response properties, the probes can also exchange momentum in the impurity-BEC case (in contrast to the optical absorption studied for solid state polarons). In that sense, I have not only explored a new environment for polarons, but also contributed to the further developments of the theoretical techniques for the study of polaron physics in other fields.

In chapter 2 the dynamic response properties of the impurity-BEC polaron are examined. Since the considered impurity is neutral an extension of the usual optical absorption description is derived which is applicable for Bragg spectroscopy and incorporates a finite momentum exchange to the system. The optical absorption results are retrieved in the limiting case of vanishing momentum exchange. It is shown that the Bragg spectra exhibit the typical polaronic dynamical response features such as the Drude background and the Bogoliubov peak which corresponds to the emission of Bogoliubov excitations. At strong coupling a secondary peak emerges which is associated with a transition to the relaxed excited state (RES). The RES corresponds to an excitation of the impurity in the self-induced potential, which has relaxed to the excited impurity wave function. Because of the complex nature of this response formalism a simplified description of the polaronic excitation structure at strong coupling is presented in chapter 3. This allows a quick estimation of the location of the excitations in the spectrum which can be handy for a potential

experimenter.

The ground state properties of multiple impurities in a Bose-Einstein condensate are considered in chapter 4. For two impurities a generalization of the Feynman all-coupling variational theory is applied which shows that at strong coupling the impurities form a bound state, commonly known as a bipolaron. A strong-coupling treatment is also presented and the results of the two formalisms are compared which results in a qualitative agreement in general and a quantitative agreement at strong coupling. The strong-coupling treatment is then extended to an arbitrary number of impurities which results in the prediction of the formation of a multi-polaron at strong coupling.

In chapter 5 the effects of reducing the dimension are studied. This shows that the polaronic effects grow as the dimension is lowered which suggests that a potential experimental detection could be facilitated by reducing the dimension. Furthermore, the polaronic coupling parameter becomes a function of the confinement strength which results in an extra experimental tool to probe the different coupling regimes.

In chapter 6 multiple impurities are considered at weak coupling. This is experimentally relevant since the first experiments are expected to be in the weak coupling regime. The effective mass of the polarons and the response to Bragg spectroscopy are studied. These properties exhibit features that are a consequence of the many-body nature of the impurities. It appears that there are different possible definitions for the effective mass of the polarons which only coincide in the limits of a single impurity and of an infinite density of impurities. In the latter case, all the polaron related effects disappear as the average distance between impurities becomes much smaller than the polaron size.

Finally, chapter 7 deals with an ion instead of a neutral impurity in a BEC. The resulting interaction between the ion and the condensate atoms is relatively strong which excludes the use of a contact interaction and a pseudopotential is introduced with a cutoff at small distances. It is shown that the Hamiltonian of this system can also be mapped onto the Fröhlich polaron Hamiltonian, provided the Bogoliubov approximation is valid. However, the exact value of this cutoff is unknown which excludes a quantitative study of the system. Furthermore, because of the strong ion-atom interaction there will be a relatively strong depletion of the condensate around the ion which can jeopardize the Bogoliubov approximation. A qualitative study of the system is presented which shows that there is a range of the parameters that allows the observation of polaronic effects.

8.2 Scientific contributions

8.2.1 Publications

- W. Casteels, J. Tempere and J. T. Devreese - *Polaronic Properties of an Ion in a Bose-Einstein Condensate in the Strong-Coupling Limit* - J. Low Temp. Phys. **162** 266 (2011).

- W. Casteels, J. Tempere and J. T. Devreese - *Response of the polaron system consisting of an impurity in a Bose-Einstein condensate to Bragg spectroscopy*

- Phys. Rev. A **83**, 033631 (2011).

- W. Casteels, T. Van Cauteren, J, Tempere and J. T. Devreese - *Strong coupling treatment of the polaronic system consisting of an impurity in a condensate* - Laser Phys. **21**, 1480 (2011).

- W. Casteels, J. Tempere and J. T. Devreese - *Many-polaron description of impurities in a Bose-Einstein condensate in the weak-coupling regime* - Phys. Rev. A **84**, 063612 (2011).

- W. Casteels, J. Tempere and J. T. Devreese - *Polaronic properties of an impurity in a Bose-Einstein condensate in reduced dimensions* - Phys. Rev. A **86**, 043614 (2012).

- W. Casteels, J. Tempere and J. T. Devreese - *Weak coupling many-polaron description of ultracold bosonic impurities in a condensate* - The European physical journal Special topics **217**, 163 (2013).

- W. Casteels, J. Tempere and J. T. Devreese - *Bipolarons and multi-polarons consisting of impurity atoms in a Bose-Einstein condensate* - manuscript submitted to Phys. Rev. A.

8.2.2 Presentations

- Oral presentation at *Fysica 2010*; 23/04/2010; Utrecht, Netherlands.

- Poster presentation at *Tweedaagse van de Theoretische en Mathematische Fysica*; 28/05/2010 - 29/05/2010; Oostduinkerke, Belgium.

- Poster presentation at DPG Physics School on *Quantum Gases in Dilute Atomic Vapour;* 28/03/2011 - 01/04/2011; Physikzentrum Bad Honnef, Germany.

- Participation to the young speaker contest at *BPS Meeting 2011*; 25/05/2011; Namur, Belgium.

- Participation to the gong show at *Tweedaagse van de Theoretische en Mathematische Fy-sica*; 27/05/2011 - 28/05/2011; Oostduinkerke, Belgium.

- Poster presentation at *26th International Conference on Low Temperature Physics*; 10/08/2011 - 17/08/2011; Beijing, China.

- Poster presentation at workshop: *Many-Body Quantum Dynamics in Closed Systems*; 07/09/2011 - 09/09/2011; Barcelona, Spain.

- Poster presentation at MUARC & MPAGS Summer School: *Quantum Matter: Foundations and new trends*; 18/09/2011 - 22/09/2011; Granada; Spain.

- Participation in the poster contest at *BPS Meeting 2012*; 30/05/2012; Brussel, Belgium.

- Poster presentation at workshop: *Theory of Quantum Gases and Quantum Coherence*; 05/06/2012 - 08/06/2012; Lyon, France.
- Invited oral presentation (by Prof. Dr. Artur Widera) at the lab *Quantum Physics with Single Atoms and Quantum Gases*; 21/06/2012; Technische Universität Kaiserslautern, Germany.
- Poster presentation at Workshop: *FINESS 2013*; 16/02/2013 - 20/02/2013; Queenstown, New Zealand.
- Poster presentation at *Tweedaagse van de Theoretische en Mathematische Fysica*; 8/04/2013 - 9/04/2013; Oostduinkerke, Belgium.

Nederlandse samenvatting

In deze thesis onderzoeken we de eigenschappen van onzuiverheden in een Bose-Einstein condensaat. Met een Bose-Einstein condensaat wordt de toestand aangeduid waarin een bosonisch gas zich bevindt bij zeer lage temperaturen en waarbij een macroscopisch aantal bosonen zich in de grondtoestand bevinden. De onzuiverheid is dan een atoom dat onderscheidbaar is van de bosonen. De microscopische beschrijving van een Bose-Einstein condensaat gebeurt aan de hand van de Bogoliubov benadering. Indien deze van toepassing is bestaat er een afbeelding van de Hamiltoniaan van onzuiverheden in een condensaat op de Fröhlich polaron Hamiltoniaan. Het polaron is gekend uit de vaste stof fysica waar het een elektron in een geladen rooster beschrijft. De lading van het elektron induceert een lokale verplaatsing van het rooster, welke beschreven kan worden aan de hand van roostertrillingen of fononen. Het polaron is dan het quasideeltje dat bestaat uit het elektron en de omringende wolk fononen. In de context van de ultrakoude gassen bestaat het polaron uit de onzuiverheid tezamen met een omringende wolk Bogoliubov excitaties. Deze zijn de elementaire excitaties van het condensaat en kunnen beschouwd worden als het analogon van de fononen in vaste stof systemen. De idee is dan dat theoretische methoden die zijn uitgewerkt in het kader van vaste stof fysica kunnen toegepast worden op het ultrakoud atomair systeem. Het uiteindelijke doel is deze werkwijze terug te koppelen en door experimenten met ultra koude gassen iets bij te leren over het vaste stof polaron en in het bijzonder over de eigenschappen bij sterke koppeling waarover er nog geen theoretisch consensus bestaat.

In een verkennende studie, uitgevoerd in het kader van mijn master thesis, heb ik de eigenschappen van de grondtoestand van één onzuiverheid in een condensaat bestudeerd. Dit toonde aan dat, net zoals voor het vaste stof polaron, er verschillende regimes zijn als functie van de polaronische koppelingsparameter α. Bij zwakke koppeling is er sprake van een quasi vrij polaron en bij sterke koppeling spreekt men van een zelf-gelokaliseerd polaron. Met zelf-gelokaliseerd wordt bedoeld dat de onzuiverheid een gebonden toestand vormt in de potentiaal die gecreëerd wordt door de omgeving als reactie op de aanwezigheid van de onzuiverheid zelf. Het voordeel van het gebruik van ultra koude gassen is dat men α kan variëren als functie van een extern magnetisch veld met behulp van een Feshbach resonantie. Dit staat in contrast met het vaste stof polaron waarbij de koppelingsparameter een materiaalconstante is. Dit toont het potentieel aan om het regime bij sterke koppeling experimenteel te realiseren met een onzuiverheid in een condensaat.

Aangezien de discrepanties in het sterke koppelingsregime gerelateerd zijn aan de dynamische eigenschappen van het polaron hebben we de dynamische respons voor een onzuiverheid in een condensaat uitgewerkt in hoofdstuk 2. Aangezien we een

neutrale onzuiverheid beschouwen kunnen we geen gebruik maken van de optische absorptie, zoals het geval is bij het vaste stof polaron, om de respons te beschouwen. We tonen aan dat Bragg spectroscopie een aangewezen experimentele techniek is. Verder vinden we dezelfde karakteristieken in de spectra als voor het vaste stof polaron, met in het bijzonder de gerelaxeerde geëxciteerde toestand (RES). Deze toestand komt enkel voor bij sterke koppeling en komt overeen met een excitatie van de onzuiverheid in de zelf geïnduceerde potentiaal. Aangezien dit resulteert in een nieuwe, geëxciteerde golffunctie voor de onzuiverheid zal de zelf geïnduceerde potentiaal tevens verschillen van die van de grondtoestand, hij is met andere woorden gerelaxeerd aan de toestand van de onzuiverheid. Vanwege de eerder complexe aard van deze respons berekeningen werken we in hoofdstuk 3 een conceptueel eenvoudigere beschrijving van het sterke koppeling regime uit. Dit laat een eenvoudige afschatting toe van de locatie van de excitaties in het spectrum bij sterke koppeling, welke handig kan zijn voor de interpretatie van experimenten.

Tot aan hoofdstuk 3 beschouwden we steeds één onzuiverheid, in hoofdstuk 4 onderzoeken we wat er gebeurt indien we enkele interagerende onzuiverheden beschouwen. Voor twee onzuiverheden gebruiken we een theorie die toepasbaar is bij arbitraire koppeling en we vinden dat er bij voldoende sterke koppeling een gebonden toestand wordt gevormd, beter gekend onder de naam bipolaron. We presenteren tevens een sterke koppeling beschrijving en vergelijken de resultaten van de twee raamwerken. De beschrijving bij sterke koppeling breiden we nog uit naar meerdere onzuiverheden en dit resulteert in de voorspelling van de vorming van multi-polaronen bij sterke koppeling.

Al het voorgaande speelt zich af in 3 dimensies, in hoofdstuk 5 bekijken we het geval van gereduceerde dimensies. We vinden dat de polaronische eigenschappen meer uitgesproken worden en dat de amplitudes van de respons karakteristieken groter worden naarmate de dimensie wordt verlaagd. Dit suggereert dat een eventuele experimentele detectie van polaron-effecten makkelijker zou zijn in gereduceerde dimensies. Aangezien een ideaal laag-dimensionaal systeem niet bestaat is er voor deze systemen een extra parameter die experimenteel beïnvloedbaar is: de sterkte van de opsluiting. Het blijkt dat de polaronische koppelingsparameter bij gereduceerde dimensies een functie is van deze sterkte. Dit betekent ook dat het beschouwen van gereduceerde dimensies een extra werktuig met zich meebrengt dat gebruikt kan worden om het sterke koppelingsregime te realiseren.

In hoofdstuk 6 beschouwen we meerdere onzuiverheden in een condensaat bij zwakke polaronische koppeling. Dit is experimenteel relevant aangezien er verwacht wordt dat zonder het gebruik van een Feshbach resonantie het systeem zich in het regime van zwakke polaronische koppeling zal bevinden. Voor dit systeem berekenen we de effectieve massa van de polaronen en de respons van het systeem op Bragg spectroscopie, waarin we veel-deeltjes effecten ontwaren. Het blijkt dat er verschillende definities mogelijk zijn voor de effectieve massa die enkel overeen stemmen in de limiet voor één onzuiverheid of voor een hoge dichtheid aan onzuiverheden. In deze laatste limiet verdwijnen alle polaron gerelateerde effecten van zodra de gemiddelde afstand tussen de onzuiverheden vergelijkbaar wordt met de grootte van het polaron.

In hoofdstuk 7 focussen we op de mogelijkheid van een ion als onzuiverheid. Van-

wege de lading is de interactie met de bosonen veel sterker en kan de gebruikelijke beschrijving voor interacties tussen neutrale deeltjes niet toegepast worden. Hiertoe introduceren we een pseudopotentiaal die een cut-off bij korte afstand bevat. De waarde van deze cut-off is experimenteel echter niet uniek te bepalen waardoor een kwantitatieve analyse van het systeem niet mogelijk is. Vanwege deze sterke interactie is het mogelijk dat er een dusdanig grote depletie rond het ion ontstaat waardoor de Bogoliubov benadering in het gedrang komt. We onderzoeken de geschikte waardes voor de verschillende parameters om polaronische karakteristieken te kunnen observeren.

Bibliography

[1] R. Feynman, Simulating physics with computers, International Journal of Theoretical Physics 21 (1982) 467–488.

[2] I. Bloch, J. Dalibard, W. Zwerger, Many-body physics with ultracold gases, Rev. Mod. Phys. 80 (2008) 885–964.

[3] C. J. Pethick, H. Smith, Bose-Einstein Condensation in Dilute Gases, Cambridge University Press, 2004.

[4] L. Pitaevskii, S. Stringari, Bose-Einstein Condensation, Clarendom Press, Oxford, 2003.

[5] H. T. C. Stoof, K. B. Gubbels, D. B. M. Dickerscheid, Ultracold Quantum Fields, Springer, 2009.

[6] A. Einstein, Sitzber. Kgl. Preuss. Akad. Wiss. 261 (1925) 3.

[7] S. N. Bose, Plancks gesetz und lichtquantenhypothese, Zeitschrift für Physik A Hadrons and Nuclei 26 (1924) 178–181.

[8] M. H. Anderson, J. R. Ensher, M. R. Matthews, C. E. Wieman, E. A. Cornell, Observation of Bose-Einstein condensation in a dilute atomic vapor, Science 269 (5221) (1995) 198–201.

[9] K. B. Davis, M. O. Mewes, M. R. Andrews, N. J. van Druten, D. S. Durfee, D. M. Kurn, W. Ketterle, Bose-Einstein condensation in a gas of sodium atoms, Phys. Rev. Lett. 75 (1995) 3969–3973.

[10] C. C. Bradley, C. A. Sackett, J. J. Tollett, R. G. Hulet, Evidence of Bose-Einstein condensation in an atomic gas with attractive interactions, Phys. Rev. Lett. 75 (1995) 1687–1690.

[11] S. Inouye, M. R. Andrews, J. Stenger, H. J. Miesner, D. M. Stamper-Kurn, W. Ketterle, Observation of Feshbach resonances in a Bose-Einstein condensate, Nature 392 (6672) (1998) 151–154.

[12] I. Bloch, Ultracold quantum gases in optical lattices, Nature Physics 1 (1) (2005) 23–30.

[13] Y. Nishida, S. Tan, Universal Fermi gases in mixed dimensions, Phys. Rev. Lett. 101 (2008) 170401.

[14] V. Peano, M. Thorwart, C. Mora, R. Egger, Confinement-induced resonances for a two-component ultracold atom gas in arbitrary quasi-one-dimensional traps, New Journal of Physics 7 (1) (2005) 192.

[15] T. Bergeman, M. G. Moore, M. Olshanii, Atom-atom scattering under cylindrical harmonic confinement: Numerical and analytic studies of the confinement induced resonance, Phys. Rev. Lett. 91 (2003) 163201.

[16] M. Olshanii, Atomic scattering in the presence of an external confinement and a gas of impenetrable bosons, Phys. Rev. Lett. 81 (1998) 938–941.

[17] D. S. Petrov, G. V. Shlyapnikov, Interatomic collisions in a tightly confined Bose gas, Phys. Rev. A 64 (2001) 012706.

[18] E. Haller, M. J. Mark, R. Hart, J. G. Danzl, L. Reichsöllner, V. Melezhik, P. Schmelcher, H.-C. Nägerl, Confinement-induced resonances in low-dimensional quantum systems, Phys. Rev. Lett. 104 (2010) 153203.

[19] H. Moritz, T. Stöferle, K. Günter, M. Köhl, T. Esslinger, Confinement induced molecules in a 1D Fermi gas, Phys. Rev. Lett. 94 (2005) 210401.

[20] E. Haller, M. Gustavsson, M. J. Mark, J. G. Danzl, R. Hart, G. Pupillo, H.-C. Nägerl, Realization of an excited, strongly correlated quantum gas phase, Science 325 (5945) (2009) 1224–1227.

[21] G. Lamporesi, J. Catani, G. Barontini, Y. Nishida, M. Inguscio, F. Minardi, Scattering in mixed dimensions with ultracold gases, Phys. Rev. Lett. 104 (2010) 153202.

[22] B. Fröhlich, M. Feld, E. Vogt, M. Koschorreck, W. Zwerger, M. Köhl, Radio-frequency spectroscopy of a strongly interacting two-dimensional Fermi gas, Phys. Rev. Lett. 106 (2011) 105301.

[23] O. Penrose, L. Onsager, Bose-Einstein condensation and liquid helium, Phys. Rev. 104 (1956) 576–584.

[24] N. N. Bogoliubov, J. Phys. (USSR) 11 (1947) 23.

[25] W. Casteels, Master-thesis: *Grondtoestandseigenschappen van een polaron in een Bose-Einstein condensaat* - promotor: J. Tempere (2009).

[26] J. Steinhauer, R. Ozeri, N. Katz, N. Davidson, Excitation spectrum of a Bose-Einstein condensate, Phys. Rev. Lett. 88 (2002) 120407.

[27] A. S. Alexandrov, J. T. Devreese, Advances in Polaron Physics, Springer, 2009.

[28] A. Alexandrov, Polarons in Advanced Materials, Springer, 2007.

[29] J. T. Devreese, Lectures on Fröhlich polarons from 3D to 0D - including detailed theoretical derivations, ArXiv e-prints: 1012.4576.

[30] J. T. Devreese, "moles agitat mentem. ontwikkelingen in de fysica van de vaste stof". rede uitgesproken bij de aanvaarding van het ambt van buitengewoon hoogleraar in de fysica van de vaste stof, in het bijzonder de theorie van de vaste stof, bij de afdeling der technische natuurkunde aan de technische hogeschool eindhoven (1979).

[31] L. D. Landau, Phys. Z. Sowjetunion 3 (1933) 664.

[32] H. Fröhlich, Electrons in lattice fields, Advances in Physics 3 (11) (1954) 325–361.

[33] G. D. Mahan, J. J. Hopfield, Piezoelectric polaron effects in CdS, Phys. Rev. Lett. 12 (1964) 241–243.

[34] F. M. Peeters, J. T. Devreese, Acoustical polaron in three dimensions: The ground-state energy and the self-trapping transition, Phys. Rev. B 32 (1985) 3515–3521.

[35] V. B. Shikin, Y. P. Monarkha, J. Low. Temp. Phys. 16 (1974) 193.

[36] S. A. Jackson, P. M. Platzman, Polaronic aspects of two-dimensional electrons on films of liquid He, Phys. Rev. B 24 (1981) 499–502.

[37] G. E. Marques, N. Studart, Polaronic state of electrons on the surface of liquid-helium films: A self-consistent treatment, Phys. Rev. B 39 (1989) 4133–4139.

[38] J. Tempere, S. N. Klimin, I. F. Silvera, J. T. Devreese, Wigner lattice of ripplopolarons in a multielectron bubble in helium, Eur. Phys. J. 32 (2003) 329.

[39] F. M. Peeters, S. A. Jackson, Frequency-dependent response of an electron on a liquid-helium film, Phys. Rev. B 31 (1985) 7098–7108.

[40] J. Tempere, I. F. Silvera, J. T. Devreese, Properties of the spherical 2d electron system in a multielectron bubble in liquid helium, Physica E: Low-dimensional systems and nanostructures 22 (2004) 771.

[41] B. I. Lundqvist, Single-particle spectrum of the degenerate electron gas, Physik der Kondensierten Materie 6 (1967) 193.

[42] B. I. Lundqvist, Single-particle spectrum of the degenerate electron gas, Physik der Kondensierten Materie 7 (1968) 117.

[43] B. I. Lundqvist, Single-particle spectrum of the degenerate electron gas, Physik der Kondensierten Materie 6 (1967) 206.

[44] L. Hedin, B. I. Lundqvist, S. Lundqvist, Solid State Comm. 5 (1967) 237.

[45] L. Hedin, Many-body effects in soft x-ray emission in metals, Solid State Comm. 5 (1967) 451.

[46] A. J. Glick, P. Longe, Phys. Rev. Lett. 15 (1965) 589.

[47] B. Lundqvist, Single-particle spectrum of the degenerate electron gas, Physik der kondensierten Materie 6 (1967) 193–205.

[48] V. Sa-yakanit, M. Nithisoontorn, W. Sritrakool, Path-integral theory of the plasmaron, Physica Scripta 32 (4) (1985) 334.

[49] Y. Toyozawa, Theory of the electronic polaron and ionization of a trapped electron by an exciton, Prog. Theor. Phys. 12 (1954) 421.

[50] A. B. Kunz, J. T. Devreese, C. T. C., The role of the electronic polaron in the soft x ray absorption of the lithium halides, J. Phys. C: Solid State Phys. 5 (1972) 3259.

[51] J. T. Devreese, A. B. Kunz, C. T. C., A resonance of the electronic polaron appearing in the optical absoprtion of alkali halides, Solid State Comm. 11 (1972) 673.

[52] T. D. Lee, F. E. Low, D. Pines, The motion of slow electrons in a polar crystal, Phys. Rev. 90 (1953) 297–302.

[53] N. N. Bogolubov, S. V. Tyablikov, Zh. Eksp. i Teor. Fiz. 19 (1949) 256.

[54] L. D. Landau, S. I. Pekar, Zh. Eksper. Teor. Fiz. 18 (1948) 419.

[55] R. P. Feynman, Slow electrons in a polar crystal, Phys. Rev. 97 (1955) 660–665.

[56] N. V. Prokof'ev, B. V. Svistunov, Polaron problem by diagrammatic quantum Monte Carlo, Phys. Rev. Lett. 81 (1998) 2514–2517.

[57] A. S. Mishchenko, N. V. Prokof'ev, A. Sakamoto, B. V. Svistunov, Diagrammatic quantum Monte Carlo study of the Fröhlich polaron, Phys. Rev. B 62 (2000) 6317–6336.

[58] V. Gurevich, I. Lang, Y. Firsov, Sov. Phys. Solid State 4 (1962) 918.

[59] E. Kartheuser, R. Evrard, J. Devreese, Mechanism of absorption of light by free continuum polarons, Phys. Rev. Lett. 22 (1969) 94–97.

[60] R. P. Feynman, R. W. Hellwarth, C. K. Iddings, P. M. Platzman, Mobility of slow electrons in a polar crystal, Phys. Rev. 127 (1962) 1004–1017.

[61] J. Devreese, J. De Sitter, M. Goovaerts, Optical absorption of polarons in the Feynman-Hellwarth-Iddings-Platzman approximation, Phys. Rev. B 5 (1972) 2367–2381.

[62] A. S. Mishchenko, N. Nagaosa, N. V. Prokof'ev, A. Sakamoto, B. V. Svistunov, Optical conductivity of the Fröhlich polaron, Phys. Rev. Lett. 91 (2003) 236401.

[63] G. De Filippis, V. Cataudella, A. S. Mishchenko, C. A. Perroni, J. T. Devreese, Validity of the Franck-Condon principle in the optical spectroscopy: Optical conductivity of the Fröhlich polaron, Phys. Rev. Lett. 96 (2006) 136405.

[64] D. Emin, Formation, motion, and high-temperature superconductivity of large bipolarons, Phys. Rev. Lett. 62 (1989) 1544–1547.

[65] A. S. Alexandrov, Unconventional pairing symmetry of layered superconductors caused by acoustic phonons, Phys. Rev. B 77 (2008) 094502.

[66] A. S. Alexandrov, Theory of Superconductuvity: From Weak to Strong Coupling, IOP publishing, 2003.

[67] F. M. Peeters, W. Xiaoguang, J. T. Devreese, Ground-state energy of a polaron in n dimensions, Phys. Rev. B 33 (1986) 3926–3934.

[68] W. Xiaoguang, F. M. Peeters, J. T. Devreese, Exact and approximate results for the ground-state energy of a Fröhlich polaron in two dimensions, Phys. Rev. B 31 (1985) 3420–3426.

[69] F. M. Peeters, J. T. Devreese, Scaling relations between the two- and three-dimensional polarons for static and dynamical properties, Phys. Rev. B 36 (1987) 4442–4445.

[70] F. C. Brown, in Polarons and Excitons, edited by C. G. Kuper and G. D. Whitfield, p. 323-355, Plenum Press, New York, 1963.

[71] J. W. Hodby, G. P. Russell, F. M. Peeters, J. T. Devreese, D. M. Larsen, Cyclotron resonance of polarons in the silver halides: AgBr and AgCl, Phys. Rev. Lett. 58 (1987) 1471–1474.

[72] G. Verbist, F. M. Peeters, J. T. Devreese, Large bipolarons in two and three dimensions, Phys. Rev. B 43 (1991) 2712–2720.

[73] M. A. Smondyrev, G. Verbist, F. M. Peeters, J. T. Devreese, Stability of multipolaron matter, Phys. Rev. B 47 (1993) 2596–2601.

[74] C. Perroni, G. Iadonisi, V. Mukhomorov, Formation of polaron clusters, The European Physical Journal B - Condensed Matter and Complex Systems 41 (2004) 163–170.

[75] L. F. Lemmens, F. Brosens, J. T. Devreese, On the ground state energy of a gas of interacting polarons, physica status solidi (b) 82 (2) (1977) 439–447.

[76] J. Tempere, J. T. Devreese, Optical absorption of an interacting many-polaron gas, Phys. Rev. B 64 (2001) 104504.

[77] J. Tempere, J. T. Devreese, Sum rule for the optical absorption of an interacting many-polaron gas, European Physical Journal B 20 (2001) 27–33.

[78] F. Brosens, S. N. Klimin, J. T. Devreese, Variational path-integral treatment of a translation invariant many-polaron system, Phys. Rev. B 71 (2005) 214301.

[79] F. Bassani, M. Geddo, G. Iadonisi, D. Ninno, Variational calculations of bipolaron binding energies, Phys. Rev. B 43 (1991) 5296–5306.

[80] H. Bei-Bing, W. Shao-Long, Polaron in Bose-Einstein-condensation system, Chinese Physics Letters 26 (8) (2009) 080302.

[81] A. Novikov, M. Ovchinnikov, A diagrammatic calculation of the energy spectrum of quantum impurity in degenerate Bose-Einstein condensate, Journal of Physics A: Mathematical and Theoretical 42 (13) (2009) 135301.

[82] D. K. K. Lee, J. M. F. Gunn, Polarons and Bose decondensation: A self-trapping approach, Phys. Rev. B 46 (1992) 301–307.

[83] F. M. Cucchietti, E. Timmermans, Strong-coupling polarons in dilute gas Bose-Einstein condensates, Phys. Rev. Lett. 96 (2006) 210401.

[84] R. M. Kalas, D. Blume, Interaction-induced localization of an impurity in a trapped Bose-Einstein condensate, Phys. Rev. A 73 (2006) 043608.

[85] K. Sacha, E. Timmermans, Self-localized impurities embedded in a one-dimensional Bose-Einstein condensate and their quantum fluctuations, Phys. Rev. A 73 (2006) 063604.

[86] D. C. Roberts, S. Rica, Impurity crystal in a Bose-Einstein condensate, Phys. Rev. Lett. 102 (2009) 025301.

[87] S. Rica, D. C. Roberts, Induced interaction and crystallization of self-localized impurity fields in a Bose-Einstein condensate, Phys. Rev. A 80 (2009) 013609.

[88] D. H. Santamore, E. Timmermans, Multi-impurity polarons in a dilute Bose-Einstein condensate, New Journal of Physics 13 (10) (2011) 103029.

[89] J. Tempere, W. Casteels, M. K. Oberthaler, S. Knoop, E. Timmermans, J. T. Devreese, Feynman path-integral treatment of the BEC-impurity polaron, Phys. Rev. B 80 (2009) 184504.

[90] A. Novikov, M. Ovchinnikov, Variational approach to the ground state of an impurity in a Bose-Einstein condensate, Journal of Physics B: Atomic, Molecular and Optical Physics 43 (10) (2010) 105301.

[91] R. P. Feynman, Statistical Mechanics: A Set Of Lectures, Addison-Wesley Publ. Co., Reading, MA, 1990.

[92] H. Kleinert, Path Integrals in Quantum Mechanics, Statistics, Polymer Physics, and Financial Markets, World Scientific, Singapore, 2009.

[93] T. Schuster, Feshbach resonances and periodic potentials in ultracold Bose-Fermi mixtures, PhD thesis - University of Heidelberg (2012).

[94] S. Knoop, T. Schuster, R. Scelle, A. Trautmann, J. Appmeier, M. K. Oberthaler, E. Tiesinga, E. Tiemann, Feshbach spectroscopy and analysis of the interaction potentials of ultracold sodium, Phys. Rev. A 83 (2011) 042704.

[95] T. Schuster, R. Scelle, A. Trautmann, S. Knoop, M. K. Oberthaler, M. M. Haverhals, M. R. Goosen, S. J. J. M. F. Kokkelmans, E. Tiemann, Feshbach spectroscopy and scattering properties of ultracold Li + Na mixtures, Phys. Rev. A 85 (2012) 042721.

[96] N. Spethmann, F. Kindermann, S. John, C. Weber, D. Meschede, A. Widera, Inserting single Cs atoms into an ultracold Rb gas, Applied Physics B: Lasers and Optics 106 (2012) 513–519.

[97] N. Spethmann, F. Kindermann, S. John, C. Weber, D. Meschede, A. Widera, Dynamics of single neutral impurity atoms immersed in an ultracold gas, Phys. Rev. Lett. 109 (2012) 235301.

[98] E. G. M. van Kempen, S. J. J. M. F. Kokkelmans, D. J. Heinzen, B. J. Verhaar, Interisotope determination of ultracold rubidium interactions from three high-precision experiments, Phys. Rev. Lett. 88 (2002) 093201.

[99] T. Takekoshi, M. Debatin, R. Rameshan, F. Ferlaino, R. Grimm, H.-C. Nägerl, C. R. Le Sueur, J. M. Hutson, P. S. Julienne, S. Kotochigova, E. Tiemann, Towards the production of ultracold ground-state RbCs molecules: Feshbach resonances, weakly bound states, and the coupled-channel model, Phys. Rev. A 85 (2012) 032506.

[100] C. Zipkes, S. Palzer, C. Sias, M. Köhl, A trapped single ion inside a Bose-Einstein condensate., Nature 464 (7287) (2010) 388–91.

[101] S. Schmid, A. Härter, J. H. Denschlag, Dynamics of a cold trapped ion in a Bose-Einstein condensate, Phys. Rev. Lett. 105 (2010) 133202.

[102] S. Schmid, A. Harter, A. Frisch, S. Hoinka, J. H. Denschlag, An apparatus for immersing trapped ions into an ultracold gas of neutral atoms, Review of Scientific Instruments 83 (5) (2012) 053108.

[103] J. Catani, G. Lamporesi, D. Naik, M. Gring, M. Inguscio, F. Minardi, A. Kantian, T. Giamarchi, Quantum dynamics of impurities in a one-dimensional Bose gas, Phys. Rev. A 85 (2012) 023623.

[104] J. W. Park, C.-H. Wu, I. Santiago, T. G. Tiecke, S. Will, P. Ahmadi, M. W. Zwierlein, Quantum degenerate Bose-Fermi mixture of chemically different atomic species with widely tunable interactions, Phys. Rev. A 85 (2012) 051602.

[105] M. Repp, R. Pires, J. Ulmanis, R. Heck, E. D. Kuhnle, M. Weidemüller, E. Tiemann, Observation of interspecies ^{6}Li-^{133}Cs Feshbach resonances, Phys. Rev. A 87 (2013) 010701.

[106] T. Holstein, Studies of polaron motion: Part ii. the small polaron, Annals of Physics 8 (3) (1959) 343 – 389.

[107] M. Bruderer, A. Klein, S. R. Clark, D. Jaksch, Polaron physics in optical lattices, Phys. Rev. A 76 (2007) 011605.

[108] M. Bruderer, A. Klein, S. R. Clark, D. Jaksch, Transport of strong-coupling polarons in optical lattices, New Journal of Physics 10 (3) (2008) 033015.

[109] A. Privitera, W. Hofstetter, Polaronic slowing of fermionic impurities in lattice Bose-Fermi mixtures, Phys. Rev. A 82 (2010) 063614.

[110] A. Klein, M. Bruderer, S. R. Clark, D. Jaksch, Dynamics, dephasing and clustering of impurity atoms in Bose-Einstein condensates, New Journal of Physics 9 (11) (2007) 411.

[111] S. Will, T. Best, S. Braun, U. Schneider, I. Bloch, Coherent interaction of a single fermion with a small bosonic field, Phys. Rev. Lett. 106 (2011) 115305.

[112] B. Gadway, D. Pertot, R. Reimann, D. Schneble, Superfluidity of interacting bosonic mixtures in optical lattices, Phys. Rev. Lett. 105 (2010) 045303.

[113] J. Catani, L. De Sarlo, G. Barontini, F. Minardi, M. Inguscio, Degenerate Bose-Bose mixture in a three-dimensional optical lattice, Phys. Rev. A 77 (2008) 011603.

[114] F. Herrera, K. W. Madison, R. V. Krems, M. Berciu, Investigating polaron transitions with polar molecules, ArXiv e-prints: 1212.6212.

[115] A. J. Heeger, S. Kivelson, J. R. Schrieffer, W. P. Su, Solitons in conducting polymers, Rev. Mod. Phys. 60 (1988) 781–850.

[116] A. Schirotzek, C.-H. Wu, A. Sommer, M. W. Zwierlein, Observation of fermi polarons in a tunable fermi liquid of ultracold atoms, Phys. Rev. Lett. 102 (2009) 230402.

[117] S. Nascimbène, N. Navon, K. J. Jiang, L. Tarruell, M. Teichmann, J. McKeever, F. Chevy, C. Salomon, Collective oscillations of an imbalanced Fermi gas: Axial compression modes and polaron effective mass, Phys. Rev. Lett. 103 (2009) 170402.

[118] C. Kohstall, M. Zaccanti, M. Jag, A. Trenkwalder, P. Massignan, G. M. Bruun, F. Schreck, R. Grimm, Metastability and coherence of repulsive polarons in a strongly interacting Fermi mixture, Nature 485 (2012) 615.

[119] K. V. Houcke, F. Werner, E. Kozik, N. Prokof'ev, B. Svistunov, M. J. H. Ku, A. T. Sommer, L. W. Cheuk, A. Schirotzek, M. W. Zwierlein, Feynman diagrams versus Fermi-gas Feynman emulator, Nature Physics 8 (5) (2012) 366–370.

[120] A. J. Daley, P. O. Fedichev, P. Zoller, Single-atom cooling by superfluid immersion: A nondestructive method for qubits, Phys. Rev. A 69 (2004) 022306.

[121] A. Griessner, A. J. Daley, S. R. Clark, D. Jaksch, P. Zoller, Dark-state cooling of atoms by superfluid immersion, Phys. Rev. Lett. 97 (2006) 220403.

[122] A. Griessner, A. J. Daley, S. R. Clark, D. Jaksch, P. Zoller, Dissipative dynamics of atomic Hubbard models coupled to a phonon bath: dark state cooling of atoms within a Bloch band of an optical lattice, New Journal of Physics 9 (2) (2007) 44.

[123] A. Micheli, A. J. Daley, D. Jaksch, P. Zoller, Single atom transistor in a 1D optical lattice, Phys. Rev. Lett. 93 (2004) 140408.

[124] H. T. Ng, S. Bose, Single-atom-aided probe of the decoherence of a Bose-Einstein condensate, Phys. Rev. A 78 (2008) 023610.

[125] A. Recati, P. O. Fedichev, W. Zwerger, J. von Delft, P. Zoller, Atomic quantum dots coupled to a reservoir of a superfluid Bose-Einstein condensate, Phys. Rev. Lett. 94 (2005) 040404.

[126] A. Härter, A. Krükow, A. Brunner, W. Schnitzler, S. Schmid, J. H. Denschlag, Single ion as a three-body reaction center in an ultracold atomic gas, Phys. Rev. Lett. 109 (2012) 123201.

[127] F. M. Peeters, J. T. Devreese, Impedance function of large polarons: An alternative derivation of the Feynman-Hellwarth-Iddings-Platzman theory, Phys. Rev. B 28 (1983) 6051–6060.

[128] J. T. Devreese, L. F. Lemmens, J. Van Royen, Sum rule leading to a relation between the effective mass and the optical absorption of free polarons, Phys. Rev. B 15 (1977) 1212–1214.

[129] D. M. Stamper-Kurn, A. P. Chikkatur, A. Görlitz, S. Inouye, S. Gupta, D. E. Pritchard, W. Ketterle, Excitation of phonons in a Bose-Einstein condensate by light scattering, Phys. Rev. Lett. 83 (1999) 2876–2879.

[130] H. Mori, Transport, collective motion, and brownian motion, Prog. Theor. Phys. 33 (1965) 423–455.

[131] H. Mori, A continued-fraction representation of the time-correlation functions, Prog. Theor. Phys. 34 (1965) 399–416.

[132] M. Ichiyanagi, Projection operators in the theory of two-time green functions, Journal of the Physical Society of Japan 32 (3) (1972) 604–609.

[133] F. M. Peeters, J. T. Devreese, Nonlinear conductivity in polar semiconductors: Alternative derivation of the Thornber-Feynman theory, Phys. Rev. B 23 (1981) 1936–1946.

[134] G. D. Mahan, Many-Particle Physics, 2nd Edition, Plenum, New York, N.Y., 1993.

[135] J. L. M. van Mechelen, D. van der Marel, C. Grimaldi, A. B. Kuzmenko, N. P. Armitage, N. Reyren, H. Hagemann, I. I. Mazin, Electron-phonon interaction and charge carrier mass enhancement in $SrTiO_3$, Phys. Rev. Lett. 100 (2008) 226403.

[136] J. T. Devreese, S. N. Klimin, J. L. M. van Mechelen, D. van der Marel, Many-body large polaron optical conductivity in $SrTi_{1-x}Nb_xO_3$, Phys. Rev. B 81 (2010) 125119.

[137] W. Huybrechts, J. D. Sitter, J. Devreese, Temperature dependence of the optical absorption of free polarons, Solid State Communications 13 (2) (1973) 163 – 166.

[138] F. M. Peeters, J. T. Devreese, Acoustical polaron in three dimensions: The impedance function, Phys. Rev. B 35 (1987) 3745–3752.

[139] L. Van Hove, Correlations in space and time and Born approximation scattering in systems of interacting particles, Phys. Rev. 95 (1954) 249–262.

[140] J. Devreese, R. Evrard, On the Feynman polaron, Physics Letters 23 (3) (1966) 196 – 198.

[141] S. Pekar, Untersuchungen über die Elektronentheorie der Kristalle, Akademie-Verlag, 1954.

[142] N. N. Bogoliubov, Ukr. Matem. Zh. 2 (1950) 3.

[143] S. I. Pekar, Untersuchungen über die elektronentheorie der kristalle, Berlin, Akademie Verslag (1951).

[144] N. N. Bogoliubov, Ukr. Matem. Zh. 2 (1950) 3, in Advances in Theoretical Physics, Ed. by E. Caianiello (World Sci., Singapore, 1991), pp. 1–18.

[145] R. Evrard, On the excited states of the polaron, Physics Letters 14 (4) (1965) 295 – 296.

[146] P. Vansant, M. A. Smondyrev, F. M. Peeters, J. T. Devreese, Exact equations for bipolarons in the strong-coupling limit, Journal of Physics A: Mathematical and General 27 (23) (1994) 7925.

[147] M. Bruderer, W. Bao, D. Jaksch, Self-trapping of impurities in Bose-Einstein condensates: Strong attractive and repulsive coupling, EPL (Europhysics Letters) 82 (3) (2008) 30004.

[148] L. Viverit, C. J. Pethick, H. Smith, Zero-temperature phase diagram of binary boson-fermion mixtures, Phys. Rev. A 61 (2000) 053605.

[149] M. J. Bijlsma, B. A. Heringa, H. T. C. Stoof, Phonon exchange in dilute Fermi-Bose mixtures: Tailoring the Fermi-Fermi interaction, Phys. Rev. A 61 (2000) 053601.

[150] E. Kochetov, M. Smondyrev, Fröhlich multipolarons, Theoretical and Mathematical Physics 85 (1990) 1062–1072.

[151] C. Perroni, G. Iadonisi, V. Mukhomorov, Formation of polaron clusters, The European Physical Journal B - Condensed Matter and Complex Systems 41 (2004) 163–170.

[152] R. L. Frank, E. H. Lieb, R. Seiringer, L. E. Thomas, Bipolaron and n-polaron binding energies, Phys. Rev. Lett. 104 (2010) 210402.

[153] J. T. Devreese, A. S. Alexandrov, Fröhlich polaron and bipolaron: recent developments, Reports on Progress in Physics 72 (6) (2009) 066501.

[154] A. S. Alexandrov, N. F. Mott, Bipolarons, Reports on Progress in Physics 57 (12) (1994) 1197.

[155] W. Colson, A. Fetter, Mixtures of Bose liquids at finite temperature, Journal of Low Temperature Physics 33 (1978) 231–242.

[156] H.-J. Miesner, D. M. Stamper-Kurn, J. Stenger, S. Inouye, A. P. Chikkatur, W. Ketterle, Observation of metastable states in spinor Bose-Einstein condensates, Phys. Rev. Lett. 82 (1999) 2228–2231.

[157] P. Ao, S. T. Chui, Binary Bose-Einstein condensate mixtures in weakly and strongly segregated phases, Phys. Rev. A 58 (1998) 4836–4840.

[158] E. Timmermans, Phase separation of Bose-Einstein condensates, Phys. Rev. Lett. 81 (1998) 5718–5721.

[159] P. C. Hohenberg, Existence of long-range order in one and two dimensions, Phys. Rev. 158 (1967) 383–386.

[160] N. D. Mermin, H. Wagner, Absence of ferromagnetism or antiferromagnetism in one- or two-dimensional isotropic Heisenberg models, Phys. Rev. Lett. 17 (1966) 1133–1136.

[161] D. S. Petrov, G. V. Shlyapnikov, J. T. M. Walraven, Regimes of quantum degeneracy in trapped 1D gases, Phys. Rev. Lett. 85 (2000) 3745–3749.

[162] D. S. Petrov, M. Holzmann, G. V. Shlyapnikov, Bose-Einstein condensation in quasi-2D trapped gases, Phys. Rev. Lett. 84 (2000) 2551–2555.

[163] T. D. Schultz, Slow electrons in polar crystals: Self-energy, mass, and mobility, Phys. Rev. 116 (1959) 526–543.

[164] C. J. Myatt, E. A. Burt, R. W. Ghrist, E. A. Cornell, C. E. Wieman, Production of two overlapping Bose-Einstein condensates by sympathetic cooling, Phys. Rev. Lett. 78 (1997) 586–589.

[165] D. M. Stamper-Kurn, M. R. Andrews, A. P. Chikkatur, S. Inouye, H.-J. Miesner, J. Stenger, W. Ketterle, Optical confinement of a Bose-Einstein condensate, Phys. Rev. Lett. 80 (1998) 2027–2030.

[166] G. Modugno, M. Modugno, F. Riboli, G. Roati, M. Inguscio, Two atomic species superfluid, Phys. Rev. Lett. 89 (2002) 190404.

[167] D. Pines, Many Body Problem, Benjamin, New York, 1962.

[168] X. Wu, F. M. Peeters, J. T. Devreese, Effect of screening on the optical absorption of a two-dimensional electron gas in GaAs-$Al_xGa_{1-x}As$ heterostructures, Phys. Rev. B 34 (1986) 2621–2626.

[169] F. Zambelli, L. Pitaevskii, D. M. Stamper-Kurn, S. Stringari, Dynamic structure factor and momentum distribution of a trapped Bose gas, Phys. Rev. A 61 (2000) 063608.

[170] C. Schneider, M. Enderlein, T. Huber, T. Schaetz, Optical trapping of an ion, Nature Photonics 4 (11) (2010) 772–775.

[171] R. Côté, A. Dalgarno, Ultracold atom-ion collisions, Phys. Rev. A 62 (2000) 012709.

[172] Z. Idziaszek, T. Calarco, P. S. Julienne, A. Simoni, Quantum theory of ultracold atom-ion collisions, Phys. Rev. A 79 (2009) 010702.

[173] A. T. Grier, M. Cetina, F. Oručević, V. Vuletić, Observation of cold collisions between trapped ions and trapped atoms, Phys. Rev. Lett. 102 (2009) 223201.

[174] H. Doerk, Z. Idziaszek, T. Calarco, Atom-ion quantum gate, Phys. Rev. A 81 (2010) 012708.

[175] J. Goold, H. Doerk, Z. Idziaszek, T. Calarco, T. Busch, Ion-induced density bubble in a strongly correlated one-dimensional gas, Phys. Rev. A 81 (2010) 041601.

[176] P. Massignan, C. J. Pethick, H. Smith, Static properties of positive ions in atomic Bose-Einstein condensates, Phys. Rev. A 71 (2005) 023606.

[177] J. J. Sakurai, Modern Quantum Mechanics, Addison Wesley, 1993.

[178] R. Côté, V. Kharchenko, M. D. Lukin, Mesoscopic molecular ions in Bose-Einstein condensates, Phys. Rev. Lett. 89 (2002) 093001.

[179] Y. Sherkunov, B. Muzykantskii, N. d'Ambrumenil, B. D. Simons, Probing ultracold Fermi atoms with a single ion, Phys. Rev. A 79 (2009) 023604.